EXISTENCE AND STABILITY OF VORTICES AND VORTEX ARRAYS

Thesis by

Allen Conrad Robinson

In Partial Fulfillment of the Requirements

for the Degree of

Doctor of Philosophy

Applied Mathematics

California Institute of Technology

Pasadena, California

1984

(Submitted June 8, 1983)

ACKNOWLEDGEMENT

I wish to thank my advisor, Dr. Philip G. Saffman, for his guidance and support during the development of the work included in this thesis. His confidence and interest in my work has been greatly appreciated.

I thank my wife, Kaye Lynn, for her unwavering faith in me and for her tireless efforts on behalf of our family. I appreciate also my parents for their support and encouragement.

I acknowledge the financial support received at Caltech from Graduate Teaching and Research Assistantships as well as the Earle C. Anthony Graduate Fellowship and Achievement Rewards for College Scientists Fellowships. I extend appreciation to NASA Lewis, D.O.E. Office of Basic Energy Sciences and the O.N.R Fluid Dynamics Branch for providing summer and graduate research assistantship support. I am grateful for the use of the Caltech computing facilities and in particular of the Fluid Mechanics VAX 11/750 in the Applied Mathematics department. I also acknowledge the use of the CYBER 205 through grants from the Control Data Corporation.

ABSTRACT

The stability to three-dimensional disturbances of three classical steady vortex configurations in an incompressible inviscid fluid is studied in the limit of small vortex cross-sectional area and long axial disturbance wavelength. The configurations examined are the single infinite vortex row, the Kármán vortex street of staggered vortices and the symmetric vortex street. It is shown that the single row is most unstable to a two-dimensional disturbance, while the Kármán vortex street is most unstable to a three-dimensional disturbance over a significant range of street spacing ratios. The symmetric vortex street is found to be most unstable to three-dimensional or two-dimensional symmetric disturbances depending on the spacing ratio of the street. Short remarks are made concerning the relevance of the calculations to the observed instabilities in free shear layer, wake and boundary layer type flows.

The three-dimensional linear stability of a steady rectilinear vortex of elliptical cross-section existing in an irrotational straining field is studied numerically in the case of finite strain. It is shown that the instability predicted for weak strain persists for finite strain and that the weak strain results continue to be quantitatively valid for finite strain. Parametric dependence of the growth rates of the unstable modes on the strain and the axial disturbance wavelength is discussed. It is also shown that a three-dimensional instability is always more unstable than a two-dimensional instability in the range of parameters of most interest.

The radially symmetric Burgers' vortex is an example of a solution to the Navier-Stokes equations in which the intensification of vorticity due to vortex stretching is balanced by the diffusion of vorticity through viscosity. We present

analytical solutions obtained from a perturbation analysis as well as numerical computations of non-symmetric Burgers' vortices in which the radial flow field in a plane perpendicular to the vorticity is non-symmetric. We also demonstrate the linear stability of the symmetric Burgers' vortex to a restricted class of two-dimensional perturbations.

TABLE OF CONTENTS

1. Overview

In the study of the motion of homogenous incompressible fluids the vorticity, the curl of the velocity field, takes a prominent place. Many fascinating, important and often commonplace phenomena can be described in terms of localized concentrations of vorticity. The tornado, the bathtub vortex and the smoke ring shot from a Fourth of July cannon are all examples of vortical flow. The singing of telephone wires in the wind is due to the period shedding of vortices. The frequency of arrivals and departures at international airports is limited by the time required for large tip vortices shed from jumbo jets to no longer pose a danger to smaller aircraft.

The concept of vortices and vortex interactions in fluid mechanics is useful because in a homogenous incompressible fluid, the velocity field can be given in terms of an integral of a Green's function times the vorticity distribution. If the vorticity is localized or, in particular, singular, then the total flow field may be described economically in terms of the vorticity distribution. For an inviscid fluid, provided only conservative forces are acting, the dynamics of the motion are given by the statement that the vorticity moves with the fluid. It is often convenient to think of the flow field in a Lagrangian sense in which the vorticity moves according to the velocity which it induces.

Numerous review articles on the subject of the vortex motion in fluid dynamics have appeared over the past decade (Widnall, 1975; Saffman & Baker, 1979; Leonard, 1980; Saffman, 1981a, 1981b; Aref, 1983). Methods used to understand real fluid phenomenon using the concept of vortex motion can be divided into two broad categories. The first is characterized by the search for steady states followed by an analysis of stability. The use of the computer is not excluded in this group and indeed many interesting results would not have become possible

without the availability of large fast computers. The second approach is to study the dynamics of the flow directly by following the motion of discrete vortex elements (Leonard, 1980). Both avenues are of use in understanding more fully the complexities of vortex motion. Our contributions herein will be limited to the first approach.

In section 2 we discuss the three-dimensional stability of some classical steady configurations of rectilinear vortices. We consider the single infinite row of vortices which is a model for the mixing layer, the staggered double row of vortices or Kármán vortex street which may result from the periodic shedding of vortices from a bluff body, and the symmetric double row of vortices which is a model for the boundary layer provided only symmetric disturbances are allowed. The results of section 2 are limited to the case of large vortex separation and long axial disturbance wavelength with respect to the vortex core size. The modes of instability discussed in this section relate primarily to those modes which result from the mutual interaction of the vortices.

We study futher in section 3 the three-dimensional instability of a steady uniform vortex in an irrotational strain for finite values of the strain. The steady solution is known in closed form and we study the modes of instability through the numerical calculation of growth rates of normal modes of the linearized equations of motion. These computations have greatest relevance to those modes of instability of finite area steady vortex configurations in which the vortices are still well separated and for which the wavelength of the disturbance is on the order of the diameter of the vortex.

The results of section 2 and 3 have most applicability to large scale vortical structures in fluid flow where the dynamics can be modeled by the inviscid equations of motion. Section 4 represents some contributions which add to the state

of knowledge of the interaction between vorticity and viscosity when these effects are comparable. We present theoretical calculations via perturbation theory indicating the existence of Burgers' type vortices embedded in a non-symmetric irrotational straining field in which vortex stretching and resulting amplification are balanced by the diffusion of vorticity through the action of viscosity and show that the perturbation procedure may be continued indefinitely in principle. We present numerical solutions extending these perturbation results into a larger region of the parameter space. In addition, we show analytically that the symmetric Burgers' vortex is linearly stable with respect to a restricted two-dimensional class of disturbances.

2. Three-dimensional Stability of Vortex Arrays

2.1 Introduction

The linear stability to two-dimensional disturbances of a single infinite row of co-rotating line vortices and of the symmetric and staggered double rows of contra-rotating vortices in a perfect fluid was first treated by Kármán (1911), Kármán (1912) and Kármán & Rubach (1912). Lamb (1932) gives a careful exposition of much of the analysis. It is found that all configurations are unstable to infinitesimal two-dimensional disturbances except for a single configuration of the staggered vortex street in which the street spacing ratio (the distance between the rows divided by the separation of vortices in the same row) is 0.281. In particular, the staggered street, known as the Kármán vortex street, has attracted much attention (Rosenhead 1953; Wille 1960). The observations of coherent structures in the turbulent mixing layer has stimulated during the last decade much study of the single infinite row.

The subject of vortex interaction and stability is currently of great interest and the correct interpretation of vortex stability calculations with respect to experimental data is uncertain (Saffman 1981). An understanding of the linear stability of the above mentioned vortex configurations in an inviscid fluid to not only two-dimensional disturbances but also three-dimensional disturbances, including the effects of significant finite vortex cross-sectional area, would be of much value in interpreting the observed phenomena in real flows, and we propose to document quantitative results for the three-dimensional linear stability of the single row of vortices, the Kármán vortex street and the symmetric double row of vortices. The results will be limited, however, in the present section to the case of large vortex separation and long axial wavelength disturbances where the distance between the vortices and the wavelength of the three-

dimensional motion is referred to the radius of the cores. The evolution of the arrays to three-dimensional disturbances of arbitrary size can then be analyzed using the Biot-Savart law to compute the induced motion of the vortices and the cutoff approximation to compute the self-induced velocity of the individual vortices. The behavior of infinitesimal disturbances is obtained by linearizing the equations of motions about the steady state and then Fourier analysing in both the vortex axial direction and the row direction to reduce the linear stability equations to a finite system. The configuration is unstable to disturbances of a given axial and row wavelength if there exist exponentially growing solutions and stable (that is, neutrally stable) if there exist only oscillatory solutions to the reduced system. It should be noted that the wavelength in the row direction need not be an integral multiple of the vortex separation which is the spatial period of the undisturbed array.

Schlayer (1928) and Rosenhead (1930) have discussed the stability of the Kármán vortex street in this limit to three-dimensional disturbances. Schlayer formulates the problem completely but only gives qualitative results. Rosenhead's treatment is incomplete as it neglects the influence of transverse disturbance wavelength except for the stabilizing effect of the self-induction of a single vortex. Also, both authors introduce the cutoff approximation as an ad hoc assumption (there is, incidentally, no discussion of three-dimensional vortex stability in Lamb (1932)). Moreover, the complexity of the algebraic expressions and the labor required to evaluate them by hand limited the results to a few cases. One of our purposes here is to give further data for this flow. Formally consistent asymptotic expansions have now been given to justify the cutoff approximation and find the higher order corrections (Moore & Saffman 1972) and the stability to three-dimensional disturbances of several other vortex configurations have been documented in the literature. Widnall (1975) and

Saffman & Baker (1979) have reviewed much of this work. In addition to the work of Schlayer and Rosenhead on rectilinear vortex configurations, Gopal (1963) and Crow (1970) studied the case of a pair of contra-rotating vortices and Jimenez (1975) examined the co-rotating pair.

Although the effects of finite area are not treated in this section, it is appropriate to mention what has been achieved in this connection. With regard to the effect of vortex separations comparable to the size of the vortices, Saffman & Szeto (1981) have shown there is little effect on the two-dimensional stability of a single row. On the other hand Christiansen & Zabusky (1973) give suggestive numerical evidence and Saffman & Schatzman (1982a) show from linear stability calculations that giving the vortices finite area in a Kármán vortex street can stabililize the vortices to two-dimensional disturbances. See Saffman (1982) for a review.

For disturbances with axial wavelength comparable to the diameter of the vortex it has been shown that a rectilinear vortex may become unstable (Widnall, Bliss & Tsai 1974; Widnall 1975; Moore & Saffman 1975). This parametric instability may occur when the vortex is subject to a straining field if it happens that the frequencies of two normal modes coincide in such a way as to allow a standing wave to occur; the external field may then cause the vortex to become unstable. A similar instability is allowed by the cutoff theory outside its range of validity and although we shall at times show this instability in subsequent stability diagrams, it is to be understood that the axial wavenumber, width and magnitude of the instability are to be taken *only in a qualitative sense* as an indication of the phenomena as the instability may or may not be real depending on the internal structure of the vortex filament. A case where the cutoff prediction is spurious is given by Moore & Saffman (1974).

Pierrehumbert (1980, see also Pierrehumbert & Widnall 1982), has examined the stability to three-dimensional disturbances of the Stuart (1967) solution of the Euler equations which describes a single infinite row of continuous vortices, the flow varying from a hyperbolic tangent shear layer profile to a single infinite row of point vortices according to the value of a single parameter. Two types of disturbances are considered, one in which all the vortices are deformed in exactly the same manner and one in which the wavelength of the disturbance in the row direction is twice the separation and neighboring vortices move in an antisymmetrical way. The former gives rise to the short axial wavelength parametric instability, which cannot be calculated properly by the Biot-Savart induction law. The latter agrees reasonably in the long wavelength limit with the calculations of the present section.

Our calculations of the long wavelength instability of well separated vortex arrays are restricted to the cooperative modes of instability which depend primarily on the mutual induction. It is expected that the results will, however, be at least qualitatively informative for arrays containing vortices of significant area and determine when two-dimensional or three-dimensional disturbances are likely to be the more important. Also, the parametric dependence of stability characteristics relative to arbitrary row-wise wavelength is easily determined; that is, there is no restriction on the allowed subharmonic disturbance. The mathematical formulation of the problem is given in section 2.2. The results for the single row are described in section 2.3, the results for the Kármán vortex street are contained in section 2.4, and section 2.5 describes the case of the symmetrical double row. A summary and comparison of the three cases is given in section 2.6.

2.2 Analysis

Our analysis, which leads up to a finite dimensional eigenvalue problem, follows in the spirit of the previous work of Crow (1970) and Lamb (1932). We give details for the symmetric double row since the results for the single row and staggered double row follow immediately. The symmetric double row consists of two straight rows of vortices with the axis of each vortex aligned with the $\mathbf{k}$ or z direction. The rows are aligned in the $\mathbf{i}$ or x direction. The first row is assumed to lie in the plane $y=0$ with each vortex having circulation Γ. The second row lies in the plane $y=-h$ with each vortex having circulation $-\Gamma$. The vortices in each row are separated by a distance l. See figure 2.2.1 for a sketch of all configurations. A parametric representation of the position of each element of each vortex filament is given by

$$\mathbf{R}_m = (ml + Ut + x_m(\rho_m,t))\,\mathbf{i} + y_m(\rho_m,t)\,\mathbf{j} + (\rho_m + z(\rho_m,t))\,\mathbf{k} \qquad (2.2.1)$$

$$\mathbf{R}_n = (nl + Ut + x_n(\rho_n,t))\,\mathbf{i} + (-h + y_n(\rho_n,t))\,\mathbf{j} + (\rho_n + z(\rho_n,t))\,\mathbf{k} \qquad (2.2.2)$$

where the subscript m denotes a vortex on the first row and n a vortex on the second row and these subscripts range over all integral values. The Lagrangian variable, ρ, takes on values in $-\infty < \rho < +\infty$. U denotes the induced velocity of the undisturbed vortex street. For a vortex m on the first row the velocity field is given by

$$\mathbf{U}_m(\mathbf{R}_m) = \sum_p \frac{\Gamma}{4\pi} \int_{[c]_{p=m}} \frac{(\mathbf{R}'_p - \mathbf{R}_m) \wedge d\mathbf{R}'_p}{|\mathbf{R}'_p - \mathbf{R}_m|^3}$$

$$- \sum_q \frac{\Gamma}{4\pi} \int \frac{(\mathbf{R}'_q - \mathbf{R}_m) \wedge d\mathbf{R}'_q}{|\mathbf{R}'_q - \mathbf{R}_m|^3} \qquad (2.2.3)$$

where the summation is over all integral values of p and q. We take as a convention that summation in the dummy variable p refers to contributions from

vortices on the first row and for contribution from the second row we sum in the variable q. The symbol $[c]_{p=m}$ indicates that a cutoff length c is implemented on each side of the singularity in the integrand for $p=m$. The equations of motion are then

$$\frac{\partial x_m}{\partial t} + U = u_m$$

$$\frac{\partial y_m}{\partial t} = v_m \tag{2.2.4}$$

$$\frac{\partial z_m}{\partial t} = w_m$$

where $\mathbf{U}_m(\mathbf{R}_m) = u_m\,\mathbf{i} + v_m\,\mathbf{j} + w_m\,\mathbf{k}$. For points on the lower row similar equations are obtained. The equations are linearized to first order in $\partial x/\partial \rho, x/l, x/h$ for all x on both the first and second rows and similarly for each y and z. Upon doing this zeroeth order terms are satisfied identically. An infinite dimensional autonomous linear system in x_m, y_m, and z_m, and x_n, y_n, and z_n results. Now setting

$$x_m=\hat{x}_m e^{ik\rho_m},\ y_m=\hat{y}_m e^{ik\rho_m},\ z_m=\hat{z}_m e^{ik\rho_m}$$

$$x_n=\hat{x}_n e^{ik\rho_n},\ y_n=\hat{y}_n e^{ik\rho_n},\ z_n=\hat{z}_n e^{ik\rho_n} \tag{2.2.5}$$

we specify a sinusoidal disturbance of wavenumber $k = 2\pi/\lambda$ in the axial or spanwise direction at each vortex position on both the first and second rows. A general disturbance could be represented by a Fourier superposition of solutions. The analysis is somewhat involved but straightforward and the following equations for points on the first row are obtained.

$$\frac{\partial \hat{x}_m}{\partial t} = -\frac{\Gamma}{2\pi}\sum_p{}' \frac{\hat{y}_m - \psi_p\,\hat{y}_p}{l_{pm}^2} + \frac{\Gamma}{2\pi} k^2\,\omega(kc)\,\hat{y}_m$$

$$+\frac{\Gamma}{2\pi}\sum_q \frac{(l_{qm}^2 - h^2)\,\hat{y}_m - (l_{qm}^2\,\psi_q - h^2\,\chi_q)\,\hat{y}_q}{L_{qm}^4} \qquad (2.2.6)$$

$$+\frac{\Gamma}{2\pi}\sum_q \frac{l_{qm}\,h\,(2\hat{x}_m - (\chi_q + \psi_q)\,\hat{x}_q)}{L_{qm}^4}$$

$$\frac{\partial \hat{y}_m}{\partial t} = -\frac{\Gamma}{2\pi}\sum_p{}' \frac{\hat{x}_m - \chi_p\,\hat{x}_p}{l_{pm}^2} - \frac{\Gamma}{2\pi} k^2\,\omega(kc)\,\hat{x}_m$$

$$+\frac{\Gamma}{2\pi}\sum_q \frac{(l_{qm}^2 - h^2)\,\hat{x}_m - (l_{qm}^2\,\chi_q - h^2\,\psi_q)\,\hat{x}_q}{L_{qm}^4} \qquad (2.2.7)$$

$$-\frac{\Gamma}{2\pi}\sum_q \frac{l_{qm}\,h\,(2\hat{y}_m - (\chi_q + \psi_q)\,\hat{y}_q)}{L_{qm}^4}$$

$$\frac{\partial \hat{z}_m}{\partial t} = -\frac{\Gamma}{2\pi}\sum_q \frac{i\,h\,k}{L_{qm}^2}\chi_q\,\hat{x}_q \qquad (2.2.8)$$

where

$$\chi(\xi) = \xi\,K_1(\xi)$$

$$\psi(\xi) = \xi^2\,K_0(\xi) + \xi\,K_1(\xi) \qquad (2.2.9)$$

$$\omega(\xi) = \frac{1}{2}\left[\frac{\cos\xi - 1}{\xi^2} + \frac{\sin\xi}{\xi} - Ci(\xi)\right]$$

The functions χ and ψ are Crow's first and second mutual induction functions respectively and ω is his self-induction function. K_0, K_1 and Ci are modified Bessel functions of the second kind and the integral cosine function, respectively. It is easily shown that both χ and ψ have a value of 1.0 at $\xi = 0.0$. The functions go to zero exponentially for large arguments and are essentially negli-

gible for ξ greater that 5.0. A plot of χ and ψ are given in figure 2.2.2. The axial wavenumber k is assumed from here on to be non-negative to avoid constant repetition of absolute value signs. The subcripts on ψ and χ indicate that the function arguments are $|l_{pm}|\,k$ and $L_{qm}\,k$ for subscripts p and q respectively where $l_{pm} = (p - m)l$ and $L_{qm}^2 = l_{qm}^2 + h^2$ with $l_{qm} = (q - m)l$. The equations have been put into a form such that in the limit $k \to 0.0$ the stability equations of Lamb for the two-dimensional case are obtained.

The cutoff length, c, is chosen from the formula (Moore & Saffman 1972)

$$\begin{aligned} c &= \tfrac{1}{2} a e^{\frac{1}{4}} f \\ f &= \exp\left(\frac{1}{4} - \frac{4\pi^2}{\Gamma^2}\int_0^a v^2 a'\,da'\right) \end{aligned} \tag{2.2.10}$$

where v represents the distribution of swirl velocity in the core and we have assumed no axial velocity in the core. For uniform vorticity $f = 1$ and all results presented in this paper have assumed $f = 1$. Since the asymptotic theory using the cutoff method is accurate only to $O(ka)^2$, the function ω is replaced by the leading order terms giving

$$\omega(kc) \approx \tfrac{1}{2}\left[\ln\frac{2}{kaf} - \gamma + \frac{1}{4}\right] = \vartheta(ka) \tag{2.2.11}$$

where $\gamma = 0.5772...$ is Euler's constant.

It may now be noted that the $\hat{x}$ and $\hat{y}$ equations decouple from the $\hat{z}$ equations and that for considerations of stability it is sufficient to work with only the coupled set. The rest of the analysis follows precisely as given in Lamb for these modified equations. We now specify disturbances on the first row by $\hat{x}_m = a_1 e^{im\varphi}$, and $\hat{y}_m = b_1 e^{im\varphi}$, and for disturbances on the second row by $\hat{x}_n = a_2 e^{in\varphi}$, and $\hat{y}_n = b_2 e^{in\varphi}$ where $-\pi \le \varphi \le \pi$. The stability equations for the first row are

$$\begin{aligned} \frac{2\pi l^2}{\Gamma}\frac{da_1}{dt} &= -(A-\eta)\,b_1 - B\,a_2 - C\,b_2 \\ \frac{2\pi l^2}{\Gamma}\frac{db_1}{dt} &= -(\tilde{A}+\eta)\,a_1 - \tilde{C}\,a_2 + \tilde{B}\,b_2 \end{aligned} \tag{2.2.12}$$

where $\eta = (kl)^2\,\vartheta(ka)$ and for the symmetric double row

$$A = \sum_p{}' \frac{1-\psi(|p|kl)\,e^{ip\varphi}}{p^2} - \sum_q \frac{q^2-\kappa^2}{(q^2+\kappa^2)^2}$$

$$= \frac{\pi^2}{3} - 2\sum_{p=1}^{\infty}\frac{\psi(pkl)\cos(p\varphi)}{p^2} + \frac{\pi^2}{\sinh^2(\kappa\pi)} \tag{2.2.13}$$

$$B = \sum_q \frac{2q\kappa}{(q^2+\kappa^2)^2}\left[\frac{\chi(\sqrt{q^2+\kappa^2}kl)+\psi(\sqrt{q^2+\kappa^2}kl)}{2}\right]e^{iq\varphi}$$

$$= 2i\sum_{q=1}^{\infty}\frac{2q\kappa}{(q^2+\kappa^2)^2}\left[\frac{\chi(\sqrt{q^2+\kappa^2}kl)+\psi(\sqrt{q^2+\kappa^2}kl)}{2}\right]\sin(q\varphi) \tag{2.2.14}$$

$$C = \sum_q \frac{q^2\psi(\sqrt{q^2+\kappa^2}kl)-\kappa^2\chi(\sqrt{q^2+\kappa^2}kl)}{(q^2+\kappa^2)^2}e^{iq\varphi}$$

$$= -\frac{\chi(\kappa kl)}{\kappa^2} + 2\sum_{q=1}^{\infty}\frac{q^2\psi(\sqrt{q^2+\kappa^2}kl)-\kappa^2\chi(\sqrt{q^2+\kappa^2}kl)}{(q^2+\kappa^2)^2}\cos(q\varphi) \tag{2.2.15}$$

where $\kappa = h/l$ is the ratio of the distance between the rows, h, and the separation of vortices on a single row, l. $\tilde{A}$, $\tilde{B}$, and $\tilde{C}$ are found by interchanging the symbols χ and ψ in the above equations.

The corresponding equations for the lower row are found by reversing the signs of Γ and κ and interchanging the subscripts 1 and 2. Thus

$$\begin{aligned}
\frac{2\pi l^2}{\Gamma}\frac{da_2}{dt} &= (A-\eta)\,b_2 - B\,a_1 + C\,b_1 \\
\frac{2\pi l^2}{\Gamma}\frac{db_2}{dt} &= (\tilde{A}+\eta)\,a_2 + \tilde{C}\,a_1 + \tilde{B}\,b_1
\end{aligned} \tag{2.2.16}$$

We now look at symmetric and anti-symmetric modes with respect to a plane midway between the two parallel rows.

$$a_S = a_1 + a_2, \quad b_S = b_1 - b_2$$

$$a_A = a_1 - a_2, \quad b_A = b_1 + b_2 \tag{2.2.17}$$

Introducing disturbances proportional to $e^{\sigma t}$, the eigenvalue problem reduces to

$$\begin{aligned}
\hat{\sigma}_l\, a_S &= -B\,a_S - (A - C - \eta)\,b_S \\
\hat{\sigma}_l\, b_S &= -(\tilde{A} + \tilde{C} + \eta)\,a_S - \tilde{B}\,b_S
\end{aligned}$$

$$\begin{aligned}
\hat{\sigma}_l\, a_A &= +B\,a_A - (A + C - \eta)\,b_A \\
\hat{\sigma}_l\, b_A &= -(\tilde{A} - \tilde{C} + \eta)\,a_A + \tilde{B}\,b_A
\end{aligned} \tag{2.2.18}$$

where $\hat{\sigma}_l = 2\pi l^2\sigma/\Gamma$ is the non-dimensional growth rate based on constant l and Γ. This transformation reduces the determination of linear stability or instability to a question of the character of roots of quadratic equations. Since $B = \tilde{B}$, the solution of the equations is especially simple so that we have

$$\hat{\sigma}_l^S = -B \pm \sqrt{(A-C-\eta)(\tilde{A}+\tilde{C}+\eta)}$$

$$\hat{\sigma}_l^A = +B \pm \sqrt{(A+C-\eta)(\tilde{A}-\tilde{C}+\eta)} \tag{2.2.19}$$

Since B is pure imaginary the stability of the configuration is determined only by the sign of the products under the radical. If the product is negative the system is neutrally stable, if positive the system is unstable.

The variable φ must be allowed to vary continuously in the range $-\pi \le \varphi \le \pi$. However, since negative values of φ simply give the complex conjugate eigenfunctions of those with φ positive, it is sufficient to consider values of φ only in the

range $0 \leq \varphi \leq \pi$. Now φ / l may be thought of as the wavenumber of the disturbance in the row direction so that $2\pi l / \varphi = \mu l$ is the wavelength in the row direction with $2 \leq \mu \leq \infty$. Thus $\mu = 2.0$ implies a repetition every two vortices, $\mu = 4.0$ a repetition every four vortices, and $\mu = \infty$ implies that all the vortices on a single row when viewed in an $x-y$ plane cross-section are displaced in the same direction. It is important to realize that $\mu = \infty$ implies a simple translation of the whole row as a unit only for the case $kl = 0.0$. That is, the magnitude and sign of the two-dimensional displacements in a given $x-y$ plane will vary with z for finite values of the axial wavelength, λ.

In the symmetric mode $a_1 = a_2$, and $b_1 = -b_2$. This mode can therefore be thought of as a row of vortices near a wall with the second row representing an image system. In the anti-symmetric mode, $a_1 = -a_2$ and $b_1 = b_2$ so that one may visualize in a given $x-y$ plane each pair of vortices (separated by h in the y direction) being displaced in opposite x-directions about their common $y-z$ plane but equally displaced in the y-direction.

The subscript l on $\hat{\sigma}_l^S$ and $\hat{\sigma}_l^A$ refers to the way σ is non-dimensionalized. A subscript l means we base σ on constant l and Γ. Changes in $\kappa = h / l$ then refer to changes in h alone. It is equally feasible to non-dimensionalize on h and Γ so that changes in κ refer to changes in l. In this case $\kappa = 0.0$ corresponds to an isolated pair of translating vortices. It is clear that $\hat{\sigma}_h = \kappa^2 \hat{\sigma}_l$ where in the computation of $\hat{\sigma}_l$ we replace kl by kh / κ.

We now pass easily to the case of the staggered double row of vortices or the Kármán vortex street. The disturbances on the first row are given by $\hat{x}_m = a_1 e^{im\varphi}$, and $\hat{y}_m = b_1 e^{im\varphi}$, and on the second row by $\hat{x}_n = a_2 e^{i(n+\frac{1}{2})\varphi}$, and $\hat{x}_n = b_2 e^{i(n+\frac{1}{2})\varphi}$ where $-\pi \leq \varphi \leq \pi$. The corresponding stability equations are exactly the same if we replace q by $(q+\frac{1}{2})$ in equations 2.2.13 to 2.2.15. Thus

$$A = \sum_p{}' \frac{1 - \psi(|p|kl)\, e^{ip\varphi}}{p^2} - \sum_q \frac{(q+\tfrac{1}{2})^2 - \kappa^2}{((q+\tfrac{1}{2})^2 + \kappa^2)^2}$$

$$= \frac{\pi^2}{3} - 2\sum_{p=1}^{\infty} \frac{\psi(pkl)\cos(p\varphi)}{p^2} - \frac{\pi^2}{\cosh^2(\kappa\pi)} \qquad (2.2.20)$$

$$B = \sum_q \frac{2(q+\tfrac{1}{2})\kappa}{((q+\tfrac{1}{2})^2 + \kappa^2)^2}\left[\frac{\chi(\sqrt{(q+\tfrac{1}{2})^2+\kappa^2}kl) + \psi(\sqrt{(q+\tfrac{1}{2})^2+\kappa^2}kl)}{2}\right] e^{i(q+\frac{1}{2})\varphi} \qquad (2.2.21)$$

$$= 2i\sum_{q=0}^{\infty} \frac{2(q+\tfrac{1}{2})\kappa}{((q+\tfrac{1}{2})^2 + \kappa^2)^2}\left[\frac{\chi(\sqrt{(q+\tfrac{1}{2})^2+\kappa^2}kl) + \psi(\sqrt{(q+\tfrac{1}{2})^2+\kappa^2}kl)}{2}\right] \sin((q+\tfrac{1}{2})\varphi)$$

$$C = \sum_q \frac{(q+\tfrac{1}{2})^2\psi(\sqrt{(q+\tfrac{1}{2})^2+\kappa^2}kl) - \kappa^2\chi(\sqrt{(q+\tfrac{1}{2})^2+\kappa^2}kl)}{((q+\tfrac{1}{2})^2 + \kappa^2)^2} e^{i(q+\frac{1}{2})\varphi} \qquad (2.2.22)$$

$$= 2\sum_{q=0}^{\infty} \frac{(q+\tfrac{1}{2})^2\psi(\sqrt{(q+\tfrac{1}{2})^2+\kappa^2}kl) - \kappa^2\chi(\sqrt{(q+\tfrac{1}{2})^2+\kappa^2}kl)}{((q+\tfrac{1}{2})^2 + \kappa^2)^2} \cos((q+\tfrac{1}{2})\varphi)$$

with $\tilde{A}$, $\tilde{B}$ and $\tilde{C}$ again found by interchanging the symbols ψ and χ. As before, it is sufficient for stability considerations to consider φ in the range $0 \le \varphi \le \pi$ or $2 \le \mu \le \infty$ for both the symmetric and anti-symmetric modes. The geometrical meaning of each mode can be clarified by assuming a very long row-wise disturbance wavelength. The symmetric mode in any $x-y$ cross-section would then appear only as a change in the y-dimension of the street without changing the relative row-wise alignment of the street. The anti-symmetric mode on the other hand would appear in the same section to cause a relative change in the spacing in the x-direction between vortices on the first and second rows of the street.

The case of the single row of vortices is easily obtained from the above by dropping all quantities relating to the second row. Thus

$$\frac{2\pi l^2}{\Gamma}\frac{da_1}{dt} = -(A - \eta)\, b_1$$
$$\frac{2\pi l^2}{\Gamma}\frac{db_1}{dt} = -(\tilde{A} + \eta)\, a_1 \qquad (2.2.23)$$

so that

$$\hat{\sigma}_l = \pm \sqrt{(A-\eta)(\tilde{A}+\eta)}$$
$$A = \sum_p{}' \frac{1-\psi(|p|kl)e^{ip\varphi}}{p^2} = \frac{\pi^2}{3} - 2\sum_{p=1}^{\infty} \frac{\psi(pkl)}{p^2}\cos(p\varphi) \qquad (2.2.24)$$

It is again sufficient to consider only the range $2 \leq \mu \leq \infty$ for considerations of stability.

The next sections will be devoted to a description of the stability diagrams computed from the above formula. When the growth rate is based on constant l, it is convenient to introduce the notation $\alpha_l + i\,\beta_l = \hat{\sigma}_l 2/\pi^2$. Then α_l represents the real part of the eigenvalue with this growth rate non-dimensionalized on constant l and Γ. The factor $2/\pi^2$ normalizes the maximum growth rate of the single infinite row to the value 1. We define α_h in a similar manner as the real part of $\hat{\sigma}_h$.

2.3 Single Row

The single infinite row of co-rotating vortices is, of course, always unstable to pure two-dimensional disturbances. The most unstable mode is the pairing instability whereby adjacent vortices are displaced in opposite directions. This mode corresponds to μ=2.0. As $\mu \to \infty$, this maximum growth rate decreases to zero. Figure 2.3.1 shows that as $l/\lambda = kl/2\pi$ increases, the growth rates fall rapidly to zero. This is due to the self-induced straining field counteracting the induced strain of the other vortices. As l/λ increases the functions χ and ψ fall quickly to zero so that mutual interaction effects are soon negligible and only the zeroeth order strain from the other vortices and the self-induced strain contribute to the stability equations. For small axial wavelengths, as the self-induced strain goes to zero, the vortex becomes unstable to the straining field of the other vortices in the row. Figure 2.3.1 is for $a/l = 0.1$ This value of a/l was chosen in order to include the indication of the short transverse wavelength

parametric instability in the diagram. We stress again that the instability shown is only representative of a phenomenon which occurs only when the internal structure of the vortex allows. For smaller vortex area a much larger l/λ is required to obtain the value $ka = 1.44$ which is the zero of the self-induction function. The effect of smaller a/l on the long axial wavelength instability is to decrease the width of the unstable region near $l/\lambda = 0.0$. No qualitative features are changed as shown in figure 2.3.2.

The stability diagrams shown are consistent with well known observed behavior in the mixing layer whereby vortices which form from the Kelvin-Helmholtz instability are observed to undergo a pairing interaction (Roshko 1976). It is seen in the stability diagrams that three-dimensional disturbances have a smaller growth rate than the pure two-dimensional pairing mode. This may in part account for the continued strong two-dimensional character of the mixing layer as it develops through a pairing process.

2.4 Staggered Double Row or Kármán Vortex Street

The staggered double row of vortices which appears in the wake of many different objects over a wide range of Reynolds numbers has long been an enigma to both theoreticians and experimenters alike. Kármán, in his original papers, predicted two values of the spacing ratio for the staggered vortex street. In his first paper he allowed perturbations to only a pair of vortices. The value of the street spacing ratio then obtained by requiring neutral stability to infinitesimal two-dimensional disturbances was $\cosh\kappa\pi = \sqrt{3}$ or $\kappa = 0.365$. In subsequent papers, by allowing two-dimensional perturbations to all of the vortices in the two rows the value of $\cosh\kappa\pi = \sqrt{2}$ or $\kappa = 0.281$ was obtained. Both of these values will appear in the subsequent investigation. It is now known of course that the street is unstable to two-dimensional finite amplitude distur-

bances (Schmieden 1936; Kochin 1939; Domm 1956). Indeed there are questions about the relevance of the stability calculations to the appearance of the street at all (Saffman & Schatzman 1982b).

Upon introducing disturbances in the spanwise or axial direction one finds the stability characteristics to depend significantly on the axial wavelength. Figures 2.4.1 to 2.4.3 give important features of the stability diagrams for the anti-symmetric mode. In figure 2.4.1 for $\mu = 4.0$ a long axial wavelength instability is always observed at some value of l / λ even though a pure two-dimensional mode may be stable. The neutrally stable saddle point moves down to the κ axis as $\mu \to 2.0$ and the small region of stability below the saddle point disappears. The saddle point lies at a value $\kappa = 0.281$ when $\mu = 2.0$. This situation is shown in figure 2.4.2. For larger values of μ the saddle point moves toward the lower right hand corner of the diagram and the growth rates to the right of the saddle decrease to zero. On the other hand as $\mu \to \infty$, even though strictly two-dimensional modes become neutrally stable, the large growth rates for three-dimensional modes to the left of the saddle point increase in magnitude as shown in figure 2.4.3.

The symmetric mode exhibits much simpler characteristics. Figure 2.4.4 shows the growth rate curves for $\mu = 4.0$. Note the region of neutral stability to long wavelength axial disturbances. For $\mu \to 2.0$ this region decreases to a single point, $\kappa = 0.281$ as shown in figure 2.4.2. As $\mu \to \infty$ the stable region grows until for $\mu = \infty$ all long wavelength axial modes are stable.

In figures 2.4.5 to 2.4.7 we plot the maximum over l / λ and μ of the growth rates as well as the values of these parameters at which the maximum occurs. The maximum growth rate occurs for the anti-symmetric mode and $\mu = \infty$ for κ less than a value between 0.3 and 0.4. For larger values of κ the dominant insta-

bility is a two-dimensional mode with μ = 2.0. The precise value of κ at which the characteristics of the dominant mode change is dependent on a/l and increases slightly with decreasing a/l. Figure 2.4.8 shows the relative size of the maximum growth rates for the $\mu = \infty$ and $\mu = 0$ long axial wavelength modes.

As l/λ increases the functions χ and ψ rapidly approach zero so that the effect of the displacement of the other vortices has little to do with the stability of the given vortex filament. The growth rate then becomes essentially a function of κ and the self-induction function. At a value of l/λ such that the parametric instability is possible the magnitude of this instability is a function of κ. The point of zero growth rate, as can be seen from equations 2.2.20 and 2.2.22, approaches the value of κ given by $\cosh\kappa\pi=\sqrt{3}$ for large l/λ. This is essentially the value of the spacing ratio at which the straining field due only to the zeroeth order fields of the other vortices is negligible. As mentioned before this is the value of the spacing ratio first proposed by Kármán (1911). This is also the value at which two-dimensional vortices of small size change from being elongated in the tranverse direction to being longer in the streamwise direction (Saffman & Schatzman 1981). The growth rate for the short wavelength instability, computed by neglecting exponentially small terms in l/λ, is shown by the dotted line in figures 2.4.5 to 2.4.7.

As in the case of the single row smaller values of a/l have the effect of decreasing the width in l/λ of the unstable region near l/λ = 0.0 and also of increasing the magnitude of the $\mu = \infty$ growth rate. The short wavelength instabilities also occur at correspondingly larger values of l/λ. It is interesting to note that both long and short axial wavelength modes have maximum growth rates that are smallest for values of κ from about 0.3 to 0.4. For κ less than about 0.3, the dominant long wavelength axial mode is a three-dimensional mode with $\mu = \infty$. Whether this mode or the short wavelength mode has a larger

growth rate depends on the precise value of a/l. For very small a/l the long wavelength mode is dominant. When κ is greater than about 0.4, the two-dimensional $\mu = 2.0$ instability is dominant.

The effect of significant vortex area has still an undetermined effect on the three-dimensional stability of the vortex street. As mentioned earlier larger vortex area will stabilize the street to two-dimensional disturbances for a small interval about $\kappa = 0.281$. Whether significant finite area will reduce and/or eliminate the instability for a three-dimensional disturbance is unknown but seems possible. There is no doubt however that the third dimension is of great importance in discussing the stability of the Kármán vortex street and must be a part of any consistent theory for its existence and evolution.

2.5 Symmetric Vortex Street

It is instructive to view the case of the symmetric vortex street in terms of constant h. Thus changes in κ refer to changes in l and we now plot Re $\hat{\sigma}_h = \alpha_h$. For $\kappa = 0.0$ we find the results of Gopal and Crow for a pair of co-rotating line vortices. Figure 2.5.1 gives growth rate diagrams for the symmetric mode. It is observed that for long axial wavelengths the configuration is always unstable. For values of κ less than one, the most unstable mode has a finite wavelength in the axial direction. For larger κ, a pure two-dimensional mode is most unstable. It is seen that the most unstable modes are at $\mu = 2.0$, ie. the pairing mode. As κ increases the magnitude of the growth rate also grows as the induced velocity of more vortices becomes effective. However, for μ near ∞ the growth rate no longer increases but rather decreases with increasing κ as seen in figure 2.5.2. For short axial wavelengths, no corresponding region of relatively small growth rate such as in the case of the Kármán vortex street is found. This is easily seen from the stability equations for kl large.

For the anti-symmetric mode, figure 2.5.3 shows that the most unstable configuration is always the two-dimensional pairing mode for long axial wavelengths. Larger μ only serves to decrease the growth rates until for $\mu = \infty$ the instability is reduced to nought for any value of κ. The short axial wavelength instability has the same characteristics as the symmetric mode.

Figures 2.5.4 and 2.5.5 give growth rates for the symmetric mode if we base the growth rate on l instead of h. In this case we cannot allow κ to become too small as the growth rates are based on l and become infinite as h/l goes to zero. The three-dimensional $\mu = 2.0$ mode is most unstable. It is only for larger values of κ that the dominant instability approaches a pure two-dimensional mode. Increasing the wavelength in the row direction serves only to decrease the magnitude of the growth rate and in general, except for very long axial wavelengths, this decrease is slight as in figure 2.5.5.

For the anti-symmetric mode, figure 2.5.6 indicates that the long axial wavelength instability is present but not as strong as the symmetric mode instability. It is seen that a change in κ has a minor effect and that the characteristics of the long axial wavelength instability are very much like the single vortex row. The dominant growth rate is for a two-dimensional, pairing instability.

For both the symmetric and anti-symmetric modes the short axial wavelength instability is always present and the growth rate increases monotonically with decreasing κ. In the case of the symmetric mode for $a/l = 0.1$ and κ small, the long and short axial wavelength growth rate curves merge to give a bimodal curve such as seen in figures 2.5.4 and 2.5.5.

The symmetric mode models the effect of a wall on a single row of vortices as the second row represents an image system of vortices. It is clear from the figures that the symmetric mode is always unstable. Not only are two-

dimensional disturbances unstable, but also, depending on the value of κ, there may be a three-dimensional disturbance which has a larger growth rate. Moreover, the row-wise wavelength for the maximum instability is the $\mu = 2.0$ or pairing type instability. This suggests that provided a real flow may be modeled initially by a system of vortices of the type considered, one would expect a strong instability to develop.

2.6 Relative Instability of the Configurations

It is now of interest to compare the magnitudes of the maximum growth rates for the three different configuration over various values of κ for the long wavelength instability. We consider only the symmetric mode for the symmetric double row but both the symmetric and anti-symmetric mode for the staggered double row. In the case of the staggered double row the maximum always occurs for the anti-symmetric mode although when $\mu = 2.0$ this maximum is also attained for the symmetric mode.

Figures 2.6.1 to 2.6.3 show the maximum growth rates for the staggered and symmetric double rows as well as the values of l/λ and $1/\mu$ at which the maximums occur. The single row corresponds to the $\kappa \to \infty$ limit and we see that the $\mu = 2.0$, two-dimensional, pairing instability is the dominant instability. The most obvious feature of the graphs is that the growth rate of the symmetric double row is always the largest of the three, while except for a region near $\kappa = 0.0$ the staggered double row has the smallest growth rate. The symmetric double row is most unstable always for the $\mu = 2.0$ mode with the corresponding value of λ decreasing with decreasing κ. On the other hand the staggered double row is most unstable at the values $\mu = 2.0$ and $l/\lambda = 0.0$ for all κ greater than about 0.3 to 0.4. For smaller values of κ the most unstable mode switches to a $\mu = \infty$ mode with l/λ of the maximum increasing slightly as κ decreases.

The dependence of the diagram on a/l is very weak. A smaller value of a/l has the effect of increasing the magnitude of the three-dimensional mode for the staggered double row as well as the value of κ at which the two-dimensional mode becomes dominant. The value l/λ for a dominant three-dimensional mode decreases with decreasing a/l for both array configurations.

These results indicate that provided κ is not too large, the fastest growing symmetric disturbances to the symmetric double row, which is a model for the boundary layer, are three-dimensional, and have larger growth rates than those of the staggered double row and the single row. These configurations are models for the wake and the mixing layer, respectively. The mixing layer model indicates maximum instability for a two-dimensional pairing mode. The wake model, on the other hand, indicates that the wake is most unstable to a three-dimensional disturbance for small values of the street spacing ratio while for larger values of the spacing ratio, a two-dimensional pairing mode is most unstable. The third dimension is thus seen to be a signicant factor in discussing the stability of configurations of finite area vortices and ought not to be neglected when discussing the stability of real two-dimensional flows which may be modeled by inviscid vortex filaments.

3. Three-dimensional Stability of a Uniform Vortex in a Straining Field

3.1 Introduction

The three-dimensional stability of the vortex arrays described in section 2 serves to illuminate the effect of axial disturbances on the modes of instability which depend primarily on the mutual induction of the vortices as this instability is modified by the effect of the self-induced straining field of each vortex. The analysis is valid only for axial disturbance wavelengths and vortex separations which are large compared with the diameter of the vortices. It is now of interest to examine those modes of instability which depend primarily on the structure of a vortex core interacting with the induced straining field of the other vortices.

A popular method for analyzing the properties of steady configurations of finite area two-dimensional vortices is through use of top hat vorticity distributions, that is, the vorticity is either zero or a constant. The velocity field can then be written economically in terms of an integral equation over the boundary of the vortex and the problem is reduced from a two-dimensional formulation to a one-dimensional formulation. Saffman & Szeto (1981) and Pierrehumbert & Widnall (1981), studied the single vortex row using this vorticity distribution. A pair of rectilinear contra-rotating vortices was studied by Pierrehumbert (1980) and discussed further by Saffman & Tanveer (1982). Saffman & Schatzman (1981, 1982a) studied the Kármán vortex street using this distribution. An especially significant exact solution was given by Moore & Saffman (1971) where they showed that a uniform vortex of elliptical cross-section can exist as a steady state in a straining field at infinity. This steady solution was used subsequently by Saffman & Szeto (1981) to compute the properties of the single infinite row of finite area uniform vortices by assuming that the orientation and shape of each

vortex in the array is given by the exact solution for a uniform vortex in an irrotational straining field. In this model the irrotational strain seen by one vortex in the array is computed by summing the contribution of all the other vortices in the array. The model solution gave very good agreement with the exact solution found by solving an integro-differential equation for the boundary of the vortices. It is to be expected that other steady configurations of finite area vortices would also be approximated well by the elliptical vortex model.

The above considerations indicate that an important step in the study of the three-dimensional instabilities of finite area steady vortex arrays for axial wavelengths on the order of the vortex core would be a study of the three-dimensional stability of the solution found by Moore and Saffman. It is expected that the results of this analysis will be useful in discussing the three-dimensional instabilities of well-separated vortex arrays and will be especially significant when the mutual interaction effects become small for axial disturbance wavelengths on the order of the vortex core as was discussed in section 2. The primary mechanism for instability of the steady flow will then be the interaction of the vortex core with the primary induced straining field of the other vortices.

It is our purpose here to study for finite values of the strain the three-dimensional linear instability of the Moore-Saffman vortex predicted for weak strain by the arguments of Widnall, Bliss & Tsai (1974) and demonstrated by the perturbation analysis of Moore & Saffman (1975) and Tsai & Widnall (1976). This analysis has been further extended to explain successfully the observed instability of vortex rings (Widnall & Tsai 1977; Saffman 1978). Tsai & Widnall (1976) gave numerical results for the Moore-Saffman vortex in weak strain. We wish to extend that analysis numerically for finite values of the strain in order to determine the persistence and extent of this parametric instability as well as higher

order effects. The growth rates of the instabilities will be given as a function of of two-parameters: the wavelength of the disturbance in the axial direction and the magnitude of the external strain. The strain is simply related to the ratio of the major and minor axes and often it will be convenient to give our results in terms of this ratio. We discuss respectively in sections 3.2 to 3.7 the properties of the exact steady solution, the known linearized stability results for special cases, the formulation of the linearized stability equations and boundary conditions, the numerical method and the results of the computations.

3.2 The Steady State

Moore and Saffman (1971) showed that a steady or stationary solution of the equations of motion for an inviscid incompressible flow in which a rectilinear vortex with uniform vorticity, ω_0, aligned along the axis, exists in an irrotational straining field at infinity. Although the actual two- dimensional dynamical equations of motion have now been given by Kida (1981) for elliptical deformations, our interest lies in the three-dimensional instabilities of the steady vortex. We shall now describe the analytic form of this steady solution. The equations which the flow satisfies are:

$$\nabla^2\Psi = \begin{Bmatrix} 0 & \text{outside E} \\ -\omega_0 & \text{inside E} \end{Bmatrix} \tag{3.2.1}$$

where

$$\Psi \sim \frac{1}{2} e\,(x^2 - y^2) \quad \text{as} \quad |x^2 + y^2| \to \infty$$

$$\frac{\partial \Psi}{\partial n} \text{ continuous across E}$$

$$\Psi = \text{constant on E}$$

where E denotes the boundary of the ellipse, Ψ is the streamfunction and e denotes the values the irrotational strain. The solution to the interior equation is,

$$\Psi = -\tfrac{1}{2}\Omega ab\left(\frac{x^2}{a^2} + \frac{y^2}{b^2} - 1\right), \quad \Omega = \frac{\omega_0 ab}{a^2+b^2} \tag{3.2.2}$$

where a and b are the semi-major and semi-minor axes of the ellipse, respectively. Matching the solution to the irrotational outer flow on the boundary of the ellipse gives a requirement on the shape of the ellipse. If $\theta = a/b$ then

$$\frac{e}{\omega_0} = \frac{\theta(\theta-1)}{(\theta^2+1)(\theta+1)} \tag{3.2.3}$$

The strain as a function of θ has a single maximum, $e/\omega_0 \cong 0.15$ at $\theta_{cr} \cong 2.9$. For $e/\omega_0 \lesssim 0.15$ there are two possible steady solutions, one more elongated than the other, and none for e/ω_0 greater than this value.

It will be convenient to give the interior flow field in terms of its representation in elliptic cylinder coordinates with $x = c\cosh\xi\cos\eta$ and $y = c\sinh\xi\sin\eta$ where c is the semi-focal.length. We have

$$hU_\xi = \frac{\partial\Psi}{\partial\eta} = \frac{\omega_0 c^2}{4}(1 - f(\theta)\cosh 2\xi)\sin 2\eta \tag{3.2.4}$$

$$hU_\eta = -\frac{\partial\Psi}{\partial\xi} = \frac{\omega_0 c^2}{4}(1 - f(\theta)\cos 2\eta)\sinh 2\xi \tag{3.2.5}$$

where $f(\theta) = (\theta^2 - 1)/(\theta^2 + 1)$, h is the line element in elliptic cylinder coordinates and U_ξ and V_η are velocities in the ξ and η directions, respectively. The line element is the same for both coordinates, depends on both ξ and η, and is given by $h^2 = \frac{1}{2}c^2(\cosh 2\xi - \cos 2\eta)$. Note that hU_ξ and hU_η are smooth functions of the coordinates ξ and η. This is true in general. That is, suppose in Cartesian coordinates we have a vector function

$$\mathbf{U} = U_x(x,y,z)\,\mathbf{i} + U_y(x,y,z)\,\mathbf{j} + U_z(x,y,z)\,\mathbf{k} \tag{3.2.6}$$

where U_x, U_y and U_z are all smooth functions of x, y and z with convergent Taylor series. If we write this vector in terms of elliptic cylinder coordinates then

$$\begin{aligned}\mathbf{U} = {} & (U_x \sinh\xi\cos\eta + U_y \cosh\xi\sin\eta)(c/h)\hat{\xi} \\ & + (U_y \sinh\xi\cos\eta - U_x \cosh\xi\sin\eta)(c/h)\hat{\eta} \\ & + U_z\hat{z}\end{aligned} \tag{3.2.7}$$

Thus hU_ξ and hU_η are smooth functions of ξ and η. It should perhaps be emphasized that the velocities are not related to functions of the complex variable $\xi + i\eta$ as in inviscid irrotational flow theory.

3.3 Linearized Stability - Limiting Cases

We describe briefly here the results that have already been given for the stability of the Moore-Saffman vortex to both two and three dimensional disturbances. These results are limited to the boundaries of the parameter space which we wish to study. In their original paper Moore and Saffman computed the stability of the vortex to two-dimensional disturbances characterized by a mode number $m > 0$ giving the angular dependence in elliptic cylinder coordinates. In this special case the growth rate σ is given by the formula

$$\frac{\sigma^2}{\omega_0^2} = \left\{ \left(\frac{2m\theta}{\theta^2+1} \right)^2 - \left(\frac{\theta-1}{\theta+1} \right)^{2m} \right\} \tag{3.3.1}$$

and in the case $m = 1$ we have

$$\frac{\sigma^2}{\omega_0^2} = \frac{\theta^2(\theta-1)^2}{(\theta+1)^2(\theta^2+1)^2} = \frac{e^2}{\omega_0^2} > 0 \tag{3.3.2}$$

Thus the $m = 1$ mode is always unstable and corresponds to a translation of the ellipse parallel to the outward principal axis of strain. For $m > 1$ the flow is stable for $\theta < \theta_{cr}$. The vortex is thus structurally stable to two-dimensional

disturbances provided $\theta < \theta_{cr}$. Moore and Saffman also computed the effect of long-axial wavelength three-dimensional disturbances on the $m = 1$ mode and concluded that the effect is to reduce the growth rate of the instability. This is exactly the stabilizing effect of the self-induction discussed in section 2 and is predicted by the cutoff theory.

The other limiting case for which analytical results are known is for $\theta \cong 1.0$. or a nearly circular or circular vortex. The $\theta \equiv 1.0$ case was discussed many years ago by Kelvin (1880). For disturbances proportional to $\exp(\sigma t + im\varphi)$ the dispersion relation giving $\sigma(k,m)$ which he found for waves on a rectilinear uniform circular vortex can be given as follows

$$\frac{J'_{|m|}(g)}{gJ_{|m|}(g)} + \frac{m}{g^2\gamma} = -\frac{K'_{|m|}(ka)}{kaK_{|m|}(ka)} \tag{3.3.3}$$

where m is the angular mode number in cylindrical polar coordinates, k is the axial wavenumber, a is the radius of the vortex, $g^2 = (ka)^2\,(1-\gamma^2)/\gamma^2$, with $\gamma = m/2 - i\sigma/\omega_0$. The function J is the Bessel function of the first kind and K is the modified Bessel function of the second kind. All roots are pure imaginary giving the frequency of oscillations of the unstrained vortex. The roots arise from solutions with γ in (-1,1) so that $-i\sigma/\omega_0 = \mathrm{Im}(\sigma/\omega_0)$ lies in $(-1-m/2,\ 1-m/2)$. There are an infinite number of roots for each m and k.

Figure 3.3.1 shows a plot of some of the $|m| = 1$ roots as a function of ka. Tsai & Widnall (1976) studied the effect of weak strain on the eigenvalues at the crossing points of the eigenvalues shown in the figure. They found that at some of these points the eigenvalues would become unstable and gave numerical results from the perturbation theory for the change in the eigenvalues and the width in k of the region of instability. The results of Tsai and Widnall are significant as they allow precise checks to be made on the numerical method used to calculate the modes of instability for finite values of the strain.

3.4 Linearized Stability Equations

The stability of the Moore-Saffman vortex will be studied by finding normal modes of the linearized equations. As the flow inside the vortex is rotational we cannot say that the resulting normal modes will be irrotational and the interior flow must be described by the Euler equations. Outside the vortex the flow is irrotational and thus according to Kelvin's theorem the perturbed motion will be irrotational also. We can describe the exterior flow by a velocity potential satisfying Laplace's equation. We have also boundary conditions matching the interior to the exterior flow. The fact that vortex lines on the boundary of the vortex move with the fluid gives a condition on normal velocity. Continuity of tangential velocity on the boundary of the vortex insures continuity of the pressure. The linearized boundary conditions are derived by expansion about the undisturbed boundary of the exact non-linear boundary condition satisfied on the *disturbed boundary*. The choice of coordinate system is thus crucial to the simplicity of the analytical statement of the linearized boundary condition as well as its numerical implementation. Since the boundary of the vortex is an ellipse it is natural to use elliptic cylinder coordinates.

It is convenient to use an elliptic cylinder coordinate system not only in the exterior but also in the interior of the ellipse. This makes implementation of the boundary conditions on the surface of the vortex extremely simple at the cost of introducing a singularity at $|x| = c$ in the coordinate system in the interior of the ellipse. However, this poses little difficulty as will be shown. The Eulerian equation of motion in elliptic cylinder coordinates can be derived from standard relations for orthogonal curvilinear coordinates (Batchelor, 1967). They are

$$\frac{1}{h^2}\left\{\frac{\partial}{\partial\xi}(hu_\xi)+\frac{\partial}{\partial\eta}(hu_\eta)\right\}+\frac{\partial\bar{u}_z}{\partial z}=0 \tag{3.4.1}$$

$$\frac{\partial u_\xi}{\partial t}+\frac{u_\xi}{h}\frac{\partial u_\xi}{\partial\xi}+\frac{u_\eta}{h}\frac{\partial u_\xi}{\partial\eta}+\bar{u}_z\frac{\partial u_\xi}{\partial z}+\frac{u_\xi u_\eta}{h^2}\frac{\partial h}{\partial\eta}-\frac{u_\eta^2}{h^2}\frac{\partial h}{\partial\xi}=-\frac{1}{h}\frac{\partial\bar{p}}{\partial\xi}$$

$$\frac{\partial u_\eta}{\partial t}+\frac{u_\xi}{h}\frac{\partial u_\eta}{\partial\xi}+\frac{u_\eta}{h}\frac{\partial u_\eta}{\partial\eta}+\bar{u}_z\frac{\partial u_\eta}{\partial z}+\frac{u_\xi u_\eta}{h^2}\frac{\partial h}{\partial\xi}-\frac{u_\xi^2}{h^2}\frac{\partial h}{\partial\eta}=-\frac{1}{h}\frac{\partial\bar{p}}{\partial\eta}$$

$$\frac{\partial\bar{u}_z}{\partial t}+\frac{u_\xi}{h}\frac{\partial\bar{u}_z}{\partial\xi}+\frac{u_\eta}{h}\frac{\partial\bar{u}_z}{\partial\eta}+\bar{u}_z\frac{\partial\bar{u}_z}{\partial z}=-\frac{\partial\bar{p}}{\partial z} \tag{3.4.2}$$

The first equation represents the condition of incompressibility and the other three are the Eulerian equations of motion with the constant density set to unity. The velocity in the subscripted coordinate directions and the pressure are, respectively, u_ξ, u_η, $\bar{u}_z$ and $\bar{p}$. It is now convenient for numerical purposes to rewrite the equations so that the dependent variables are smooth functions of ξ and η. To this end we set $\bar{u}_1 = hu_\xi$ and $\bar{u}_2 = hu_\eta$ and, for convenience of notation, $x_1 = \xi$ and $x_2 = \eta$. This allows the use of the summation convention for the indices 1 and 2. The resulting equations are

$$\frac{1}{h^2}\frac{\partial\bar{u}_j}{\partial x_j}+\frac{\partial\bar{u}_z}{\partial z}=0 \tag{3.4.3}$$

$$\frac{\partial\bar{u}_i}{\partial t}+\frac{\bar{u}_j}{h^2}\frac{\partial\bar{u}_i}{\partial x_j}+\bar{u}_z\frac{\partial\bar{u}_i}{\partial z}+\frac{\bar{u}_j^2}{2}\frac{\partial}{\partial x_i}\left(\frac{1}{h^2}\right)=-\frac{\partial\bar{p}}{\partial x_i}, \quad i=1,2 \tag{3.4.4}$$

$$\frac{\partial\bar{u}_z}{\partial t}+\frac{\bar{u}_j}{h^2}\frac{\partial\bar{u}_z}{\partial x_j}+\bar{u}_z\frac{\partial\bar{u}_z}{\partial z}=-\frac{\partial\bar{p}}{\partial z} \tag{3.4.5}$$

We now look for normal modes of the linearized equations by taking perturbations of the following form,

$$\begin{aligned}\bar{u}_n &= U_n(x_1,x_2) + u_n(x_1,x_2)e^{\sigma t + ikz}, \quad n = 1,2\\ \bar{u}_z &= \qquad\qquad u_z(x_1,x_2)e^{\sigma t + ikz}\\ \bar{p} &= P(x_1,x_2) \quad + p(x_1,x_2)e^{\sigma t + ikz}\end{aligned} \tag{3.4.6}$$

The steady state velocity and pressure are represented by capitalized quantities. The steady state velocities are given in equations 3.2.4 and 3.2.5. Inserting (3.4.6) into the equations and dropping all terms of second order in the perturbations we obtain a set of linear equations for the perturbations u_1, u_2, u_z and p. Solving for u_z in the continuity equation (3.4.3), we can eliminate u_z explicitly by substitution into the third equation of motion (3.4.5). This gives an expression for p which we can then eliminate through the first two equations of motion (3.4.4). The resulting system is a set of coupled linear equations for u_1 and u_2. They can be simply expressed as follows,

$$\left\{A_{ij} - k^2(C_{ij} + D_{ij})\right\}u_j = \sigma\left\{k^2\delta_{ij} - B_{ij}\right\}u_j, \quad i = 1,2 \tag{3.4.7}$$

where

$$A_{ij}(\cdot) = \frac{\partial}{\partial x_i}\left\{\frac{U_m}{h^2}\frac{\partial}{\partial x_m}\left[\frac{1}{h^2}\frac{\partial(\cdot)}{\partial x_j}\right]\right\}, \quad B_{ij}(\cdot) = \frac{\partial}{\partial x_i}\left[\frac{1}{h^2}\frac{\partial(\cdot)}{\partial x_j}\right]$$

$$C_{ij}(\cdot) = \left\{\frac{\partial}{\partial x_i}\left[\frac{1}{h^2}U_j\right] + (i-j)\omega_0\right\}(\cdot), \quad D_{ij}(\cdot) = \delta_{ij}\frac{U_m}{h^2}\frac{\partial(\cdot)}{\partial m}$$

The above constitute the linear stability equations for the interior flow.

The exterior irrotational flow is described by a velocity potential, $\bar{\varphi}$, satisfying Laplace's equation. Proceeding as before we let $\bar{\varphi} = \Phi(x_1,x_2) + \varphi(x_1,x_2)e^{\sigma t + ikz}$. The perturbation φ satisfies

$$\frac{1}{h^2}\left[\frac{\partial^2\varphi}{\partial x_n^2}\right] - k^2\varphi = 0 \tag{3.4.8}$$

and the solutions of this equation via the method of separation of variables are

products of Mathieu functions.

3.5 Boundary Conditions

We describe here the boundary conditions to be satisfied by the normal modes if we express the solution in elliptic cylinder coordinates. It is clear that all dependent variables must be 2π periodic in $x_2 = \eta$, the angular coordinate. In the radial coordinate, $\xi = x_1$, the situation is more complicated. At $\xi = 0$, we must require that the velocity be smooth in a nonsingular coordinate system. From equation 3.2.7 we see that

$$\begin{aligned} \bar{u}_m(\xi,\eta) &= -\bar{u}_m(-\xi,-\eta)\,, \quad m = 1,2 \\ \bar{u}_z(\xi,\eta) &= \bar{u}_z(-\xi,-\eta) \end{aligned} \tag{3.5.1}$$

This implies the following relations at $\xi = 0$

$$\begin{aligned} \frac{\partial^n \bar{u}_m}{\partial \xi^n}(0,\eta) &= (-1)^{n+1}\frac{\partial^n \bar{u}_m}{\partial \xi^n}(0,-\eta), \quad m = 1,2 \\ \frac{\partial^n \bar{u}_z}{\partial \xi^n}(0,\eta) &= (-1)^n \frac{\partial^n \bar{u}_z}{\partial \xi^n}(0,-\eta) \end{aligned} \tag{3.5.2}$$

for all non-negative integers n. Since the steady flow satisfies these relations and the relations are linear, the perturbations must also satisfy them.

The linearized boundary conditions at the surface of the vortex require some care as the exact boundary conditions giving the motion of the vortex are non-linear. We parametrize the surface of the vortex by

$$\xi = \xi_0 + F(\eta)e^{\sigma t + ikz} \tag{3.5.3}$$

where F is a small quantity. The kinematic condition giving the motion of the boundary of the vortex is then

$$\frac{D}{Dt}(\xi - \xi_0 - F(\eta)e^{\sigma t + ikz}) = 0 \quad \text{at } \xi = \xi_0 + F(\eta)e^{\sigma t + ikz} \tag{3.5.4}$$

We also have the dynamic boundary condition for continuity of tangential velo-

city on the disturbed boundary. Substitution of the assumed form of the velocities and expanding in small quantities about ξ_0 gives the following conditions at ξ_0. (See Moore & Saffman, 1971).

$$\frac{\partial \varphi}{\partial \xi} = \sigma h^2 F + \Omega \frac{\partial}{\partial \eta}(h^2 F) \tag{3.5.5}$$

$$u_1 = \sigma h^2 F + \Omega \frac{\partial}{\partial \eta}(h^2 F) \tag{3.5.6}$$

$$\frac{\partial \varphi}{\partial \eta} - u_2 = h^2 F \tag{3.5.7}$$

$$\frac{\partial^2 \varphi}{\partial \xi^2} - \frac{\partial u_1}{\partial \xi} = - \frac{\partial}{\partial \eta}(h^2 F) \tag{3.5.8}$$

The first three conditions are exactly the equations derived by Moore and Saffman for the two-dimensional stability problem. The last condition requires continuity of axial perturbation velocity through the continuity equation. That these are the correct linearized boundary conditions for the full three-dimensional stability problem is clear since there is no steady axial flow in the vortex to link at first order with the perturbation quantities.

In the exterior region we require the perturbation velocity to decay exponentially as $x^2 + y^2 \to \infty$. The appropriate solutions to the reduced equation 3.4.8 are products of Mathieu functions, $Ke_n(\xi;q)ce_n(\eta;-q)$ and $Ko_n(\xi;q)se_n(\eta;-q)$, where we have used the notation of Abramowitz & Stegun (1972) and the parameter $q = (ck)^2/4$.

3.6 Numerical Method

The computation of the eigenvalues is accomplished by means of a straightforward collocation scheme similar to the kind recommended by Boyd (1978) for eigenvalue problems of our type and used with success for example by Pierrehumbert & Widnall (1982) in their calculations.

An examination of the coefficients in the linearized equations 3.4.7 and 3.4.8 shows that the only η dependence is through either $\cos 2\eta$ or $\sin 2\eta$. This indicates that the normal modes must separate into π and 2π periodic solutions just as in the standard analysis of the periodic solutions of Mathieu's equation. We will study only 2π periodic unstable modes and, of these, specifically the ones which corresponds to the zero crossings of the eigenvalues in the case of the circular vortex. These angular modes have azimuthal dependence $|m| = 1$ in equation 3.3.3. There are several reasons to limit the computations to this restricted subcase. First of all, as noted in section 3.3, there exists an infinite number of pure imaginary roots for each m and k in the unstrained case. For the 2π-periodic case we may have a pair of physically distinguishable modes with the same frequency provided that the angular mode numbers are (m_1, m_2) = (1,-1),(1,3),(-1,-3),(3,5), etc.. This is seen from the discussion of the location of the roots given in section 3.3. For the π-periodic case we have similarly (m_1,m_2) = (0,2),(0,-2),(2,4),(-2,-4), etc.. There is an infinite number of such crossing points for each pair (m_1,m_2). Moore & Saffman (1975) give a good discussion of why such crossing points may become unstable at infinitesimal strain. They showed that under assumptions satisfied by the Moore-Saffman vortex, the zero-crossing eigenvalues of the $|m| = 1$ modes would become unstable. For eigenvalues which cross at non-zero values the effect of strain may or may not be destabilizing. Tsai & Widnall (1976) gave specific results for the (m_1,m_2) = (1, -1) case as in figure 3.3.1. They found however that the growth rates of the instabilities for the eigenvalues at non-zero crossings were an order of magnitude smaller than the zero-crossing instabilities. In the (m_1,m_2) = (0,2),(0,-2) cases the eigenvalues do not cross at zero frequency but do cross at non-zero frequencies so that these may also become unstable. Practical considerations dictate that some decision be made on the eigenmodes and eigenvalues to be calculated.

We expect only those modes with the least structure in both the azimuthal and radial directions and with the largest growth rates to be of physical relevance since presumably viscous effects come into play at the smaller scales. We thus make the plausible assumption that at finite strain the most important unstable modes continue to be the ones arising from the zero-crossings of the $|m| = 1$ modes at infinitesimal strain and that the instabilities which may arise from other resonances in both the 2π and π-periodic cases at non-zero crossing points of the eigenvalues are of less importance.

Recalling the conditions 3.5.2 on the interior solutions, we now represent the 2π periodic modes in the following form,

$$u_i = c^i_{mn} T_{2n+1}(\xi/\xi_0)\cos((2m+1)\eta) + d^i_{mn} T_{2n}(\xi/\xi_0)\sin((2m+1)\eta)\,, \quad i = 1,2$$

$$\varphi = c^3_m \frac{Ke_{2m+1}(\xi,q)}{Ke_{2m+1}(\xi_0,q)} ce_{2m+1}(\eta,-q) + d^3_m \frac{Ko_{2m+1}(\xi,q)}{Ko_{2m+1}(\xi_0,q)} se_{2m+1}(\eta,-q)$$

$$h^2 F = c^4_m \cos((2m+1)\eta) + d^4_m \sin((2m+1)\eta) \tag{3.6.1}$$

with the summation convention used for $m = 0,1,\ldots,N_A-1$ and $n = 0,1,\ldots,N_R-1$. T_m are Tchebyscheff polynomials. With this representation we now require that the interior equations (3.4.7) be satisfied at the points (ξ_i,η_j) where

$$\begin{aligned} \frac{\xi_i}{\xi_0} &= \cos\left[\frac{\pi}{4}\frac{2i-1}{N_R-1}\right], \quad i = 1,2,\ldots,N_R-1 \\ \eta_j &= \frac{\pi(j-1)}{2N_A}, \quad j = 1,2,\ldots,2N_A \end{aligned} \tag{3.6.2}$$

To accomplish this, the equations represented in compact form by (3.4.7) are fully expanded and the explicit singularities in the equations removed by multiplying through by h^8. We also require that the boundary conditions 3.5.5 to 3.5.8 be satisfied at the points η_j.

The above collocation scheme leads to a generalized eigenvalue problem for the growth rates σ and eigenvectors $\mathbf{x} = (c^1_{mn}, d^1_{mn}, c^2_{mn}, d^2_{mn}, c^3_m, d^3_m, c^4_m, d^4_m)^T$ of the form

$$\mathbf{Ax} = \sigma\mathbf{Bx} \tag{3.6.3}$$

with the matrices **A** and **B** coming from the collocation equations. The size of the system is $N = 4N_A(N_R+1)$. Eigenvalues of interest were computed initially using the Eispack QZ algorithm (Garbow, et. al. 1977) and the grading portion of the pre-processor described by Ward (1981). Since the desired eigenvalues are small, it was convenient to solve for $1/\sigma$ rather than σ. The QZ algorithm tends to produce the largest eigenvalues first so that in this way it was a simple matter to isolate the appropriate eigenvalues and eigenvectors. Once a single eigenvalue and eigenvector of interest was found then the parametric dependence on k and θ was determined by extending the system through the normalization condition $\mathbf{x}^T\mathbf{x} - 1 = 0$ and solving for both the eigenvalue and eigenvector via Newton's method. The accuracy of the computations was checked by increasing the number of modes in the truncated expansions and by comparision with limiting results. A useful rule of thumb which became apparent was that the accuracy of a given eigenvalue was on the order of the size of the coefficients of the higher order modes in the u_i expansions.

Some comment should be made concerning the computation of the Mathieu functions. The characteristic values as well as the functional values of the angular Mathieu functions were computed from their Fourier series representation using appropriate routines and/or modifications of the routines given by Clem (1969). See also Sale (1970). These routines are based on algorithms given by Blanch (1966). The radial Mathieu function can be calculated once the corresponding characteristic values for the periodic solutions are known. The

equation for the radial Mathieu function is

$$\frac{d^2y}{d\xi^2} - (\alpha + 2q\cosh 2\xi)y = 0 \tag{3.6.4}$$

where q is a positive parameter and α is the characteristic value from the angular equation. Making the change of variable $z = \sqrt{q}e^{\xi}$ the equation becomes

$$\frac{d^2y}{dz^2} + \frac{1}{z}\frac{dy}{dz} - \left[1 + \frac{\alpha}{z^2} + \frac{q^2}{z^4}\right]y = 0 \tag{3.6.5}$$

which shows the correspondence with the modified Bessel function. Now with the normalization which we have used in the representation 3.6.1 we shall need to know the values of $y'(\xi)/y$ and $y''(\xi)/y$ at $\xi = \xi_0$ in order to implement the boundary conditions. The second ratio is given directly from equation 3.6.4. The first ratio is equal to $zp(z)$ where $p(z) = y'(z)/y$ and p satisfies the corresponding Ricatti equation

$$\frac{dp}{dz} + p^2 + \frac{1}{z}p - (1 + \frac{\alpha}{z^2} + \frac{q^2}{z^4}) = 0 \tag{3.6.6}$$

for this ratio. An asymptotic analysis of the Ricatti equation as $z \to \infty$ gives the following behavior.

$$p \sim \sum_{n=0}^{\infty} A_n z^{-n}, \quad z \to +\infty \tag{3.6.7}$$

where

$$A_0 = -1, \; A_1 = -\tfrac{1}{2}, \; A_2 = -\tfrac{1}{2}(\alpha - \tfrac{1}{4}), \; A_3 = -A_2$$
$$A_4 = -\tfrac{1}{2}[\tfrac{3}{2}(\alpha - \tfrac{1}{4}) - \tfrac{1}{4}(\alpha - \tfrac{1}{4})^2 + q^2]$$

and

$$A_n = \frac{1}{2}\left[(2-n)A_{n-1} + 2\sum_{k=1}^{[n/2]} A_k A_{n-k}\right], \quad \text{n odd}$$

$$A_n = \frac{1}{2}\left[(2-n)A_{n-1} + 2\sum_{k=1}^{[(n-2)/2]} A_k A_{n-k} + A_{n/2}^2\right], \quad \text{n even}$$

There are actually two asymptotic solutions. The other solution has leading behavior +1 rather than −1. We choose the minus sign corresponding to the exponentially decaying solution in y. To compute the value of $p(z_0)$ we integrate backwards from some sufficiently large value, z_∞, using the starting value given by the asymptotics. A variable step Taylor's series routine was written especially to perform this integration. The number of terms in the asymptotic expansion and the value of z_∞ was chosen according to the usual optimal truncation rule (Bender & Orszag, 1978) and an error tolerance. This gave a very good estimate for $p(z_\infty)$. Although the desired solution is not asymptotically stable for z increasing, it is the stable solution for z decreasing and one would expect to find good results at z_0 even for a poor starting value provided $z_\infty \gg z_0$. The values computed by the routine were compared with tables of Bessel and Mathieu functions (Abramowitz & Stegun 1972; Wiltse & King 1958) and by a self-consistency check in which p' was computed numerically using the values of p output from the routine and then checked against the exact value. Excellent agreement was obtained over a wide range of parameter values.

The equations are non-dimensionalized in the following manner. The time scale is defined by the value of the vorticity in the undisturbed vortex and the length scale by the geometric mean of the semi-major and semi-minor axes. Then we have $\hat{\sigma} = \sigma/\omega_0$ and $\hat{k} = k\sqrt{ab}$. The value of ξ_0 is given by the formula $\xi_0 = \frac{1}{2}\log[(\theta+1)/(\theta-1)]$ and c^2/ab is equal to $(\theta^2-1)/\theta$. The quantities c and k appear in the equations only as a product squared which gives $q = (ck)^2/4 = \hat{k}^2(\theta^2-1)/(4\theta)$.

3.7 Results and Discussion

We now describe the results of the computation of the growth rate of the zero crossing eigenvalues as a function of the axial wavenumber and the axis-ratio. The eigenvalues σ are pure real in the cases to be described. Figure 3.7.1 shows the values of the growth rate as θ is increased from very near 1.0 to 2.9 which is the value at which the strain is maximized for a steady solution. Also shown are the values of the growth rate and the region of instability for each mode as predicted by the perturbation analysis of Tsai & Widnall (1976). It is seen that the numerical results match the perturbation results extremely well for small values of the strain. The effect of larger strain is weak relative to perturbation results but several interesting features are observed. Note that the value of the axial wavenumber of maximum instability decreases slightly with increasing strain for the modes with one and two internal radial nodes initiating at $\hat{k} = 2.5$ and 4.35, respectively. These modes are labeled σ_{11} and σ_{12} where the first subscript denotes the angular dependence and the second the number of radial nodes for the nearly circular case. These modes meet at $\theta \cong 1.4$ as the strain is increased. The growth rate curves then cross as seen in the figure for $\theta = 1.5$ and apparently also cross at larger θ although these details were not resolved. The σ_{11} maximum is always the largest. The σ_{10} and the σ_{11} growth rate curves also meet at about the value of the maximum strain. Notice in particular that the total range of unstable wave numbers is very large for large strain and that the magnitudes of the growth rates for a significant portion of the wavenumber space are quite comparable. This suggests the possibility that observed instabilities in real flows might be more sensitive to the properties of external disturbances than to the structure of the vortex.

The stabilizing effect of the self-induction for long axial wavelengths as is

predicted by the cutoff theory for the helical or σ_{10} mode is also seen in figure 3.7.1. The dotted lines indicated the growth rate predicted by the cutoff theory with

$$\hat{\sigma} = \left\{ \left(\frac{e}{\omega_0}\right)^2 - \left(\frac{\hat{k}^2}{4}[\ln(2/\hat{k}) - \gamma + .25]\right)^2 \right\}^{1/2} \tag{3.7.1}$$

where we have replaced the length scale for the radius of the vortex in the cutoff theory by the length scale, $\sqrt{ab}$. Note the excellent agreement for small values of the strain. As the strain is increased the most unstable long-wavelength mode is no longer purely two-dimensional but has a maximum at a finite value of the axial wavenumber. However this effect is quite small and the general characteristics predicted by the cutoff theory are retained for the long wavelength axial mode even for finite strain. This is a satisfying result relative to the computations outlined in section 2 since it indicates that the cutoff theory, which assumes circular vortices moving in external strain, gives the correct long-wavelength stability behavior for steady vortex configurations in which the size of the vortices relative to their separations need not be very small and the vortices may take on an elliptical steady shape.

We look now at the steady state for $\theta \geq 2.9$ and show the variation of the parametric instability with θ. The flow is now unstable to two-dimensional structural instabilities of π-periodic type but it is of interest to see how the growth rate for the three-dimensional disturbance varies as θ increases at least until the three-dimensional and the two-dimensional growth rates are comparable. Figure 3.7.2 shows for $\theta \geq \theta_{cr}$ the dependence of the σ_{10} and σ_{11} modes on θ. The most unstable long wavelength mode is seen to decrease in magnitude while still maintaining its three-dimensional character while the short-wavelength mode is seen to increase initially as θ increases above θ_{cr} and then decreases as θ is increased further. For $\theta = 4.0$ we can see from equation 3.3.1 with $m = 2$ that

the growth rate for the two-dimensional structural instability is $\sigma = 0.1776$ and is thus of the same order as the three-dimensional instability.

In summary we have shown that the effect of finite strain on the three-dimensional modes studied is to increase the growth rates above the values predicted by the perturbation theory while altering slightly the wavenumber of the most unstable modes. The effect of large deformation in the steady solution thus does not ameliorate the three-dimensional instability. For θ less than about 4.0 the three-dimensional instabilities have larger growth rates than the two-dimensional instabilities. It is also seen that the characteristics of the long-wavelength mode are not significantly affected by finite strain. This further justifies the use of the Biot-Savart formulation as a useful tool to analyze three-dimensional long wavelength instabilities of rectilinear vortex arrays.

4. Burgers' Vortices

4.1 Introduction

G. I. Taylor (1938) noted that one of the fundamental processes which controls the dissipation of energy in turbulence must be the interaction of the intensification of vorticity due to vortex stretching with the diffusion of vorticity through the action of viscosity. One exact solution of the Navier-Stokes equations which typifies this interaction was given by Burgers (1948). The Burgers' vortex is found by assuming a solution of the Navier-Stokes equations of the form

$$\begin{aligned} u_r &= -\alpha r + u(r,\theta,t) \\ u_\theta &= \qquad\quad v(r,\theta,t) \\ u_z &= 2\alpha z \end{aligned} \tag{4.1.1}$$

where we divide the velocity field into an irrotational and rotational part. Note that only the z component of vorticity is present. In vorticity-streamfunction formulation in cylindrical polar coordinates we have the equations of motion

$$\frac{\partial \omega}{\partial t} + (-\alpha r - \frac{1}{r}\frac{\partial \psi}{\partial \theta})\frac{\partial \omega}{\partial r} + \frac{1}{r}\frac{\partial \psi}{\partial r}\frac{\partial \omega}{\partial \theta} = 2\alpha\omega + \nu\nabla^2\omega \tag{4.1.2}$$

$$\nabla^2\psi = \omega\,, \quad u = -\frac{1}{r}\frac{\partial \psi}{\partial \theta}\,, \quad v = \frac{\partial \psi}{\partial r} \tag{4.1.3}$$

A solution independent of θ and t is the Burgers' vortex

$$\omega = \Omega\, e^{\frac{-\alpha r^2}{2\nu}} \tag{4.1.4}$$

$$u_\theta = \frac{\nu\Omega}{\alpha r}(1 - e^{\frac{-\alpha r^2}{2\nu}}) \tag{4.1.5}$$

The quantity Ω is arbitrary and is a measure of the strength of the vortex. We can also define a Reynolds number $R = \Omega/\alpha = \Gamma/(2\pi\nu)$ where Γ is the circulation.

4.2 Linearized Stability of Burgers' Vortex

The question of the global stability of Burgers' vortex has been discussed by Leibovich & Holmes (1981) who found that there is no finite viscosity for which the Burgers vortex is globally stable (from energy considerations) with respect to the admissible class of divergence free velocity fields. This does not imply that the vortex is unstable but only that energy arguments could not give an upper bound for the critical viscosity. The linearized stability of Burgers' vortex has apparently not been treated before and we wish in this section to make a few remarks on the stability of Burger's vortex to a restricted class of two-dimensional infinitesimal perturbations. The more important case of arbitrary three-dimensional infinitesimal perturbations is not treated.

It is a straightforward matter to compute the linearized normal mode equations for infinitesimal perturbations about the steady state (4.1.5). The non-dimensional equations for the perturbation quantities are

$$\begin{aligned} &L\omega + \mu\omega = inR[f\psi + \tfrac{1}{2}g\omega] \\ &M\psi = \omega \end{aligned} \tag{4.2.1}$$

where

$$\begin{aligned} &L(\cdot) \equiv \frac{1}{r}\frac{d}{dr}(r\frac{d}{dr}(\cdot)) - \frac{n^2}{r^2}(\cdot) + \frac{1}{r}\frac{d}{dr}(r^2(\cdot)) \\ &M(\cdot) \equiv \frac{1}{r}\frac{d}{dr}(r\frac{d}{dr}(\cdot)) - \frac{n^2}{r^2}(\cdot) \\ &f \equiv e^{-r^2/2}, \quad g \equiv \frac{1-e^{-r^2/2}}{(r^2/2)} \end{aligned} \tag{4.2.2}$$

where time is scaled on α^{-1} and lengths on $(\nu/\alpha)^{\frac{1}{2}}$. We have taken out the time and angular dependence through a factor $\exp(-\mu\alpha t + in\theta)$ in the vorticity and streamfunction.

For $n = 0$ there is no angular dependence. Batchelor (1967) notes that in

this case it may be shown that an initial distribution of vorticity will approach the Burgers' vortex solution. One way to show this is to take the Hankel transform of the full equations of motion for the radially symmetric case. We define the Hankel transform pair by

$$\begin{aligned} \hat{\omega}(k) &= \int_0^\infty \omega(r) J_n(rk) r dr \\ \omega(r) &= \int_0^\infty \hat{\omega}(k) J_n(rk) k dk \end{aligned} \tag{4.2.3}$$

The equation of motion

$$\frac{\partial \omega}{\partial t} = \frac{\alpha}{r}\frac{\partial(\omega r^2)}{\partial r} + \nu\left(\frac{\partial^2 \omega}{\partial r^2} + \frac{1}{r}\frac{\partial \omega}{\partial r}\right) \tag{4.2.4}$$

becomes after the application of the Hankel transform of order zero

$$\frac{\partial \hat{\omega}}{\partial t} + \alpha k \frac{\partial \hat{\omega}}{\partial k} = -\nu k^2 \hat{\omega}. \tag{4.2.5}$$

This is now a first order wave equations in k and t for the transform $\hat{\omega}$ which we can solve by the method of characteristics. The solution is

$$\hat{\omega} = \hat{\omega}_0(ke^{-\alpha t}) e^{-\frac{\nu k^2}{2\alpha}(1-e^{-\alpha t})} \tag{4.2.6}$$

where $\hat{\omega}_0$ is the transform of the initial distribution of vorticity. As $t \to \infty$ the solution approaches the transform of Burgers' vortex.

For the more general two-dimensional stability problem, this suggests the use of the Hankel transform to find the eigenvalues μ of the operator L in equation 4.2.1. Knowledge of the eigenvalues and eigenfunctions will lead to a determination of the stability of the Burgers' vortex for small R via perturbation theory.

The use of the Hankel transform of order n can be used to find the exact solutions of the eigenvalue problem for $n \geq 1$ of

$$
\begin{aligned}
&Ly + \mu y = 0 \\
&y = O(r^n)\ ,\ r \to 0 \\
&y \sim Ar^{\mu} e^{-r^2/2}\ ,\ r \to \infty
\end{aligned}
\tag{4.2.7}
$$

The boundary conditions can be obtained from a local analysis about the origin and infinity. Note that the solutions for $n < 0$ are simply the complex conjugate eigenfunctions of those for n positive so that there is no loss of generality. Upon applying the appropriate Hankel transform, integrating the resulting ordinary differential equation once and inverting using standard tables, or by manipulation (in hindsight) of the equations, one obtains the solution with the required behavior at the origin,

$$y = r^n M[(\mu+n+2)/2\ ;\ n+1\ ;\ -r^2/2] \tag{4.2.8}$$

M is the regular confluent hypergeometric function in the notation of Abramowitz & Stegun (1972). The asymptotic behavior as $z \to -\infty$ is

$$
\begin{aligned}
M[a,b;z] = e^{i\pi a}\frac{\Gamma(b)}{\Gamma(b-a)}\frac{1}{z^a}\left\{\sum_{n=0}^{S-1}\frac{(a)_n(1+a-b)_n}{n!}(-z)^{-n} + O(|z|^{-S})\right\} \\
+ \frac{e^z z^{a-b}}{\Gamma(a)}\Gamma(b)\left\{\sum_{n=0}^{T-1}\frac{(b-a)_n(1-a)_n}{n!}(z)^{-n} + O(|z|^{-T})\right\}
\end{aligned}
\tag{4.2.9}
$$

where $(a)_n = (a)(a+1)\cdots(a+n-1)$. In our case $b = n+1 > 0$ so that $\Gamma(b)$ is never singular but $\Gamma(b-a)^{-1} = 0$ for $b-a = (n+1) - (\mu+n+2)/2 = -m$, $m = 0,1,2,....$ Thus $\mu = n + 2m$ for m a nonnegative integer gives the values of μ for which the behavior at infinity is exponential rather than algebraic. Then the eigenfunctions are

$$
\begin{aligned}
y &= r^n\ M[n+m+1\ ,\ n+1\ ;\ -r^2/2] \\
&= r^n\ e^{-r^2/2}\ M[-m\ ,\ n+1\ ;\ r^2/2] \\
&= r^n\ e^{-r^2/2}\ \frac{m!}{(n+1)_m}\ L_m^{(n)}(r^2/2)
\end{aligned}
\tag{4.2.10}
$$

where we have used Kummer's transformation to identify the solution in terms

of the generalized Laguerre polynomial $L_m^{(n)}$. A more convenient normalization for the eigenfunctions is

$$\omega_0(n,k) = 2^{-n/2}\, r^n\, e^{-r^2/2} L_k^{(n)}(r^2/2) \tag{4.2.11}$$

corresponding to the eigenvalues $\mu_0(n,k) = n + 2k$. For the case in which the circulation is zero or $R = 0$, the vortex is stable. The effect of non-zero circulation can be determined by perturbation theory for small R.

We assume a solution of the form

$$\begin{aligned} \psi &= \psi_0 + R\psi_1 + R^2\psi_2 + \cdots \\ \omega &= \omega_0 + R\omega_1 + R^2\omega_2 + \cdots \\ \mu &= \mu_0 + R\mu_1 + R^2\mu_2 + \cdots \end{aligned} \tag{4.2.12}$$

which results in the following set of equations for the perturbation quantities

$$R^0) \quad \begin{aligned} &L\omega_0 + \mu_0\omega_0 = 0 \\ &M\psi_0 = \omega_0 \end{aligned} \tag{4.2.13}$$

$$R^1) \quad \begin{aligned} &L\omega_1 + \mu_0\omega_1 = in(f\psi_0 + \tfrac{1}{2}g\omega_0) - \mu_1\omega_0 \\ &M\psi_1 = \omega_1 \end{aligned} \tag{4.2.14}$$

$$R^2) \quad \begin{aligned} &L\omega_2 + \mu_0\omega_2 = in(f\psi_1 + \tfrac{1}{2}g\omega_1) - \mu_1\omega_1 - \mu_2\omega_0 \\ &M\psi_1 = \omega_1 \end{aligned} \tag{4.2.15}$$

At each stage, once ω is found, then $\psi = M^{-1}\omega$. For $n \geq 1$ the solutions ψ_0 corresponding to ω_0 are

$$\psi_0(n,0) = -\frac{1}{2}\frac{(n-1)!}{z^{n/2}}(1 - e_{n-1}(z)e^{-z}) \tag{4.2.16}$$

$$\psi_0(n,k) = -\frac{1}{2k}\omega_0(n,k-1)\,, \quad k \geq 1 \tag{4.2.17}$$

where $z = r^2/2$ and $e_{n-1}(z)$ is the truncated exponential function. Now we can expand ω_1 and the right hand side of equation 4.2.14 in the eigenfunctions ω_0 because of the completeness of the Laguerre polynomials. The coefficients in the expansion can be determined by taking the inner product of equation 4.2.14

with $\omega_0(n,l)$ successively. The eigenvalue μ_1 is determined from the Fredholm alternative condition. We define the inner product

$$(u,v) = \int_0^\infty u\bar{v}e^{r^2/2}rdr \tag{4.2.18}$$

With this definition the operator L is self-adjoint so that the required solutions and alternative conditions can be given explicitly in terms of the ω_0 solutions. The R^1 solution is

$$\omega_1(n,k) = \sum_{l=0}^{\infty}{}' \frac{in}{2(k-l)N(k,l)}[F(n,k,l)+\tfrac{1}{2}G(n,k,l)]\omega_0(n,l)$$

$$\psi_1(n,k) = \sum_{l=0}^{\infty}{}' \frac{in}{2(k-l)N(k,l)}[F(n,k,l)+\tfrac{1}{2}G(n,k,l)]\psi_0(n,l) \tag{4.2.19}$$

$$\mu_1(n,k) = \frac{in}{N(k,l)}[F(n,k,l)+\tfrac{1}{2}G(n,k,l)]$$

where

$$F(n,k,l) = (f\,\psi_0(n,k)\,,\,\omega_0(n,l)) = -\frac{\Gamma(n+k+l)}{\Gamma(k+1)\Gamma(l+1)}2^{-(n+k+l+1)} \tag{4.2.20}$$

$$G(n,k,l) = (g\,\omega_0(n,k)\,,\,\omega_0(n,l)) \tag{4.2.21}$$

$$=(n-1)!\left[n + \min_{n}(k,l)\right] - \sum_{k'=0}^{k}\sum_{l'=0}^{l}\frac{\Gamma(n+k'+l')}{\Gamma(k'+1)\Gamma(l'+1)2^{k'+l'+n}}$$

$$N(n,k) = (\omega_0(n,k),\omega_0(n,k)) = \Gamma(n+k+1)/\Gamma(k+1) \tag{4.2.22}$$

Thus the real part of μ is not changed to first order since the shift in the eigenvalues is pure imaginary. We must then go to second order to compute the change in Reμ. The Fredholm alternative condition for μ_2 leads to

$$\mu_2(n,k) = -\frac{n^2}{2N(n,k)}\sum_{l=0}^{\infty}{}'\frac{1}{(k-l)N(k,l)}[F(n,k,l) + \tfrac{1}{2}G(n,k,l)]^2 \tag{4.2.23}$$

using the orthogonality of the eigenfunctions and the fact that F and G are

symmetric in k and l. For $k = 0$ we have $\mu_2 \geq 0$ so that the effect of the circulation on the smallest eigenvalue for any n is not destabilizing. For $k \geq 1$ we cannot see immediately from the formula the sign of μ_2 since we have both positive and negative terms in the summation. Table 4.2.1 gives some values of μ_2 for several values of n and k such that $n + 2k$ is small. It is seen that in all cases except $n = 1, k = 0$ the sign of μ_2 is positive so that the effect of circulation is to stabilize the vortex. In the special case $n = 1, k = 0$, we have μ_1 and μ_2 identically zero, and examination of the equations shows that this eigenvalue and eigenfunction are valid for all R.

It may seem to be a paradoxical result that the effect of a larger Reynolds' number is to stabilize the vortex via an increase in the decay rate of the normal modes. However, since the viscosity and the strain α have been used to fix the time and length scales, changes in R must be thought of in terms of changes in the magnitude of the vorticity or of the total circulation. Stewartson (1982) has noted that in the study of swirling viscous flows the effect of rotation is often a stabilizing factor. It appears that for two-dimensional perturbations of the Burgers' vortex solution the effect of rotation is similar and that at least for small circulation the Burgers' vortex is linearly stable to two-dimensional disturbances.

4.3 Non-symmetric Burgers' Vortices

We wish to discuss now the properties of the vorticity field which arises when the external irrotational strain is not axially symmetric. We assume the velocity field takes the form

$$\begin{aligned} \hat{u} &= -\alpha\tilde{x} + \tilde{u}(\tilde{x},\tilde{y}) \\ \hat{v} &= -\beta\tilde{y} + \tilde{v}(\tilde{x},\tilde{y}) \\ \hat{w} &= (\alpha+\beta)\tilde{z} \end{aligned} \tag{4.3.1}$$

so that we have irrotational exterior strain upon which is super-imposed a

rotational two-dimensional flow. In vorticity-stream function form the equations which are to be satisfied for a steady solution are

$$(-\alpha\tilde{x} + \tilde{u})\tilde{\omega}_{\tilde{x}} + (-\beta\tilde{y} + \tilde{v})\tilde{\omega}_{\tilde{y}} = (\alpha + \beta)\tilde{\omega} + \nu\tilde{\nabla}^2\tilde{\omega} \tag{4.3.2}$$

$$\tilde{\nabla}^2\tilde{\psi} = \tilde{\omega}, \quad \tilde{u} = -\frac{\partial\tilde{\psi}}{\partial\tilde{y}}, \quad \tilde{v} = \frac{\partial\tilde{\psi}}{\partial\tilde{x}} \tag{4.3.3}$$

where $\tilde{\omega}$ is the vorticity and $\tilde{\psi}$ is the streamfunction. The equations can be conveniently non-dimensionalized by scaling the time on $(\alpha + \beta)/2$ and lengths on $(2\nu/\alpha+\beta)^{\frac{1}{2}}$. In addition we scale the magnitude of the non-dimensional vorticity and streamfunction on the Reynold's number $R = \int\int\tilde{\omega}d\tilde{x}d\tilde{y}/(2\pi\nu)$ so that the circulation is constant in the scaled form and the Reynold's number enters as a parameter in the equations.

Our equations in these variable are

$$\omega_{xx} + \omega_{yy} + [(1+\varepsilon)x - R\,u]\omega_x + [(1-\varepsilon)y - R\,v]\omega_y + 2\omega = 0 \tag{4.3.4}$$

$$\nabla^2\psi = \omega, \quad u = -\frac{\partial\psi}{\partial y}, \quad v = \frac{\partial\psi}{\partial x} \tag{4.3.5}$$

where $\varepsilon = \frac{\alpha-\beta}{\alpha+\beta}$ and $\int\int\omega dxdy = 2\pi$. The existence of solutions of the above steady form of the Navier-Stokes equations is to be treated in this section. For the special case $R = 0$ the solution can be given in closed form as

$$\omega = \sqrt{1-\varepsilon^2}\exp\left\{-(1+\varepsilon)\frac{x^2}{2} - (1-\varepsilon)\frac{y^2}{2}\right\} \tag{4.3.6}$$

This solution is also valid for $\varepsilon = 0$ and any R. We wish to present the extension of these solutions for ε and R small and non-zero and show that the perturbation procedure can be extended indefinitely in principle. Solutions are also calculated numerically and matched with the perturbations results. These considerations lend support to our belief that solutions of the type described will exist for arbitrary $0 \leq \varepsilon < 1$ and $0 \leq R < \infty$. Symmetry considerations also give

solutions for negative values of the parameters. It must be noted that with the scaling we have used it is important to regard ε as a measure of the difference between α and β where these quantities have the same positive sign. Also since lengths scale with the viscosity, change in R should be considered as change in the circulation similar to the interpretation given in the previous section on the stability of Burgers' vortex. Other scalings are possible. For example, if α and β are of opposite signs and we wish their magnitudes to be comparable or equal, then other scalings would be appropriate and we might expect to find solutions similar to the Moore-Saffman vortex discussed in section 3.2. Other cases have yet to be studied however.

We propose at this point to calculate analytically the first few terms in a double series expansion of the solution for small ε and R and to show how this expansion could be continued indefinitely in principle. These results will provide insight as well as some check on the numerical results to follow. The equations to be solved in polar coordinates are

$$\mathbf{L}\,\omega = -\varepsilon r\cos 2\theta\,\frac{\partial\omega}{\partial r} + \varepsilon\sin 2\theta\frac{\partial\omega}{\partial\theta} - \frac{R}{r}\frac{\partial\psi}{\partial\theta}\frac{\partial\omega}{\partial r} + \frac{R}{r}\frac{\partial\psi}{\partial r}\frac{\partial\omega}{\partial\theta} \tag{4.3.7}$$

$$\nabla^2\psi = 0\,, \quad \mathbf{L}(\cdot) \equiv \nabla^2(\cdot) + \frac{1}{r}\frac{\partial}{\partial r}(r^2(\cdot))$$

If we now assume for ε, $R \ll 1$ an expansion of the form

$$\omega = \sum_{m=0}^{\infty}\sum_{n=0}^{\infty} \varepsilon^m\, R^n\, \omega^{mn} \tag{4.3.8}$$

and a similiar expansion for ψ, we get the following set of perturbation equations,

$$\mathbf{L}\,\omega^{mn} = -\cos 2\theta\, r\,\frac{\partial \omega}{\partial r}^{m-1,n} + \sin 2\theta\,\frac{\partial \omega}{\partial \theta}^{m-1,n} \tag{4.3.9}$$

$$-\frac{1}{r}\sum_{m'=0}^{m}\sum_{n'=0}^{n-1}\frac{\partial \psi}{\partial \theta}^{m-m',n-1-n'}\frac{\partial \omega}{\partial r}^{m',n'} + \frac{1}{r}\sum_{m'=0}^{m}\sum_{n'=0}^{n-1}\frac{\partial \psi}{\partial r}^{m-m',n-1-n'}\frac{\partial \omega}{\partial \theta}^{m',n'}$$

where negative superscripts indicate terms that are not present. We shall continue in the notation of section 4.2 with the exception that for the operators L and M we shall now explicitly show the dependence on n via a superscript n. We give now the solution of the perturbation equations 4.3.9 up to terms with $m + n = 2$. The solution to the homogeneous equation for the ω^{00} term is the Burgers' vortex

$$\omega_{00} = \omega_0(0,0) = e^{-r^2/2} \tag{4.3.10}$$

since there is only one eigenfunction with zero eigenvalue of all the operators L^n which result from a Fourier analysis in θ of the operator $\mathbf{L}$. Note that at this point we have imposed the circulation condition $\int\int \omega dx dy = 2\pi$. At subsequent orders we then impose the requirement of zero circulation. This can always be satisfied since we have an arbitrary constant at each stage from the zero eigenvalue eigenfunction. At the same time however we have a Fredholm alternative condition to be satisfied for a solution to exist at all. This condition is that the inhomogeneous terms should be orthogonal to ω^{00}. This is easily seen from equation 4.2.18 to be equivalent to the requirement that the forcing in (4.3.9) have zero total area. If we take a Fourier expansion in θ of the inhomogeneous terms then this requirement reduces to showing that

$$\int_0^\infty C_0(r)\, r dr = 0 \tag{4.3.11}$$

where $C_0(r)$ is the constant term in the expansion. We shall show that this condition will always be satisfied automatically at all orders.

Proceeding in the above described manner, we obtain the solution at the $m + n = 1$ order as

$$\omega^{10} = -\cos 2\theta\, \omega_0(2,0)\,, \quad \omega^{01} = 0 \tag{4.3.12}$$

Note that the ω^{m0} terms must give exactly the Taylor expansion of equation 4.3.6 and that the ω^{0n} term must be identically zero since ω^{00} is a solution for all R provided $\varepsilon = 0$. At the next order the only possible secular term is in the equation for ω^{20} where

$$\mathbf{L}\,\omega^{20} = \frac{1}{2r}\frac{d}{dr}[r^2\omega_0(2,0)] + \frac{1}{2}\cos 4\theta\,[r\,\frac{d}{dr}\omega_0(2,0) - 2\omega_0(2,0)]$$

$$= 2\omega_0(0,1) - 2\omega_0(0,2) - \cos 4\theta\,\omega_0(4,0) \tag{4.3.13}$$

The first form of the equation shows why it is obvious that the Fredholm condition is satisfied and the second form leads to a rapid solution of the equation. Thus

$$\omega^{20} = -\omega_0(0,1) + \frac{1}{2}\,\omega_0(0,2) + \frac{1}{4}\cos 4\theta\,\omega_0(4,0) \tag{4.3.14}$$

One may show that this solution satisfies the zero circulation condition from the normalization and that it matches the expansion of the exact solution (4.3.6). The other two equations at the same order have no possible secular terms and after some labor the solutions can be given by

$$\omega^{11} = -\sin 2\theta \sum_{k=0}^{\infty} \frac{\omega_0(2,k)}{2^{k+2}(k+1)^2(k+2)}\,, \quad \omega^{02} = 0 \tag{4.3.15}$$

which completes the exact perturbation calculations up to order $m + n = 2$.

We now describe why the alternative condition will always be satisfied at any order in which it may appear. Secular terms might arise in equation 4.3.9 from the first two terms on the right hand side provided $\omega^{m-1,n}$ has a nonzero coefficient for the $\cos 2\theta$ term in its Fourier expansion. But then it is clear that

we can combine the two secular terms from the products into a perfect derivative as in the first version of equation 4.3.13. Thus the Fredholm condition is satisfied for the first two forcing terms in (4.3.9). The other summation terms on the right hand side of (4.3.9) which arise from the non-linear terms in the original equation can also be matched up in a similar manner in such a way as to show that the only possible secular terms are perfect derivatives. The easiest way to see this is to take the complex form of the Fourier expansions for a typical product term. If

$$\omega^{ab} = \sum_{n=-\infty}^{\infty} C_n(r)\, e^{in\theta}, \quad \psi^{cd} = \sum_{n=-\infty}^{\infty} D_n(r)\, e^{-in\theta} \tag{4.3.16}$$

then the terms from corresponding products in the two summations on the right hand side of equation 4.3.9 give

$$-\frac{1}{r}\frac{\partial \psi^{cd}}{\partial \theta}\frac{\partial \omega^{ab}}{\partial r} + \frac{1}{r}\frac{\partial \psi^{cd}}{\partial r}\frac{\partial \omega^{ab}}{\partial \theta} = \sum_{n=-\infty}^{\infty} in\, \frac{1}{r}\frac{d}{dr}(C_n D_n) + \cdots \tag{4.3.17}$$

where we have not given the explicit form of terms with θ dependence. The alternative condition 4.3.11 will thus be satisfied provided each product $C_n D_n$ vanishes at zero and infinity. Since there is no $n = 0$ term in the summation in (4.3.17) this requirement holds since the C_n and D_n terms come from solutions of equations with operators L^n and M^n with $n > 0$. Thus, in principle, the expansion may be continued indefinitely.

We now give numerical results for non-zero ε and R and match these results with the small parameter solution presented above. The numerical solution is obtained by approximating the vorticity with a double series of sinc functions which leads to a non-linear systems of equations via straightforward collocation. Stenger (1981) recommends this approach for approximation of functions $f(x)$ which are analytic in a strip about the real line and which decay exponentially as $|x| \to \infty$. The function f is represented by a finite sum

$$f(x) \simeq \sum_{k=-N}^{+N} f(kh) S(k,h)(x) \tag{4.3.18}$$

where the sinc function is defined by

$$S(k,h)(x) = \frac{\sin \frac{\pi}{h}(x-kh)}{\frac{\pi}{h}(x-kh)} \tag{4.3.19}$$

Approximate formulas for integration and differentiation of f are

$$\int_{-\infty}^{+\infty} f(\xi) d\xi \simeq h \sum_{k} f(kh) \tag{4.3.20}$$

$$f^{(n)}(x) \simeq \sum_{k} h^{-n} \sum_{l} \delta_{lk}^{(n)} f(lh) S(k,h)(x) \tag{4.3.21}$$

where we sum from $-N$ to $+N$ and, in particular,

$$\delta_{mn}^{(1)} = \frac{(-1)^{n-m}}{n-m}(1-\delta_{mn}) \; ; \quad \delta_{mn}^{(2)} = -\frac{\pi^2}{3}\delta_{mn} - \frac{2(-1)^{n-m}}{(n-m)^2}(1-\delta_{mn}) \tag{4.3.22}$$

If $h = c / N^{1/2}$, then, for example, the error in (4.3.18),(4.3.20) and (4.3.21) may be shown to be $O(e^{-\gamma N^{1/2}})$ as $N \to \infty$ where both c and γ are positive constants.

Since in our problem the vorticity will decay exponentially we expect to be able to represent the vorticity distribution efficiently using a double series of sinc functions. We represent the vorticity by

$$\omega = \sum_{k=-M}^{+M} \sum_{l=-N}^{+N} \omega_{kl} S(k,h)(x) \; S(l,h)(y) \tag{4.3.23}$$

and plan to solve for the vorticity via Newton's method by collocation at the points (ih, jh), $-M \le i \le M$, $-N \le j \le N$ in equation 4.3.4. This will give a non-linear system for the vorticity at the collocation points provided we have an expression for the velocities u and v in terms of the ω_{ij} through the solution of the Poisson equation 4.3.5.

The approximate velocities u and v at each of the collocation points can be

computed by a weighted sum of the values of the vorticity at each of these points. We now give the derivation of the weights. It will be sufficient to compute the velocity induced by a single sinc function distribution of vorticity since the total velocity at a point can then be given by superposition. In terms of the Fourier transform of the vorticity distribution we have

$$u = -\frac{\partial \psi}{\partial y} = \frac{-i}{(2\pi)^2}\int\int \frac{\eta \hat{\omega}}{\xi^2 + \eta^2} e^{-i\xi x - i\eta y} d\xi d\eta \tag{4.3.24}$$

$$v = \frac{\partial \psi}{\partial x} = \frac{i}{(2\pi)^2}\int\int \frac{\xi \hat{\omega}}{\xi^2 + \eta^2} e^{-i\xi x - i\eta y} d\xi d\eta \tag{4.3.25}$$

where $\hat{\omega}$ is the transform of the vorticity. Now if $\omega = S(k,h)(x)\, S(l,h)(y)$ then since

$$\hat{S}(k,h)(\xi) = he^{i\xi kh}[H(\xi+\pi/h) - H(\xi-\pi/h)] \tag{4.3.26}$$

we derive the values of the velocities at the collocations points $x = k'h$ and $y = l'h$ as

$$u_{k'l'} = -\frac{h}{\pi} I_{l'-l,\,k'-k}\,, \quad v_{k'l'} = \frac{h}{\pi} I_{k'-k,\,l'-l} \tag{4.3.27}$$

where

$$I_{m,n} = \int_0^1 \int_0^1 \frac{\xi}{\xi^2 + \eta^2} \sin(m\pi\xi)\cos(n\pi\eta)\, d\xi d\eta \tag{4.3.28}$$

or, in a form more suitable for computation,

$$I_{m,n} = \int_0^1 \left[\frac{\sin^2((m\pi+n\pi x)/2)}{m\pi+n\pi x} + \frac{\sin^2((m\pi-n\pi x)/2)}{m\pi-n\pi x} \right] \frac{dx}{1+x^2}$$

$$+ \int_0^1 \left[\frac{\sin^2((m\pi x+n\pi)/2)}{m\pi x+n\pi} + \frac{\sin^2((m\pi x-n\pi)/2)}{m\pi x-n\pi} \right] \frac{x\,dx}{1+x^2} \tag{4.3.29}$$

The quantities $I_{m,n}$ can be calculated numerically and then stored for subsequent use. Several representative values of $I_{m,n}$ are given in table 4.3.1.

We can now give explicitly the equations which are to be solved numerically for the vorticity. We have

$$F_{ij} = h^{-2}\sum_k \delta^{(2)}_{ki}\omega_{kj} + h^{-2}\sum_l \delta^{(2)}_{lj}\omega_{il} + 2\omega_{ij} \tag{4.3.30}$$

$$+ \left[(1+\varepsilon)ih - R\, u_{ij}\right]\sum_k h^{-1}\delta^{(1)}_{ki}\,\omega_{kj} + \left[(1-\varepsilon)jh - R\, v_{ij}\right]\sum_l h^{-1}\delta^{(1)}_{lj}\omega_{il} = 0$$

where

$$u_{ij} = -\frac{h}{\pi}\sum_k \sum_l I_{j-l,i-k}\,\omega_{kl}\,, \quad v_{ij} = \frac{h}{\pi}\sum_k \sum_l I_{i-k,j-l}\,\omega_{kl} \tag{4.3.31}$$

and we sum over $-M \le k \le M$ and $-N \le l \le N$. Now we expect the Jacobian of this system to be singular as we have not specified the total circulation or the centroid of vorticity. An examination of the above equations shows if $F_{ij}(\omega_{pq}) = 0$, then $F_{-i,-j}(\omega_{-p,-q}) = 0$ also. Thus the equations are invariant under the transformation $p \to -p$ and $q \to -q$. If $\omega_{pq} = \omega_{-p,-q}$, then the equations for F_{ij} and $F_{-i,-j}$ are identical. By looking for solutions with this property the size of the system is reduced to $(2M+1)N+M+1$ unknowns. We still need to specify the total circulation. This is done by multiplying a somewhat arbitrary function $\tilde{g}$ times the circulation condition and adding this to the F equation so that the Jacobian $\partial G_{ij}/\partial\omega_{kl}$ is non-singular where

$$G_{ij} = F_{ij} + \tilde{g}(i,j)[h^2\sum_k\sum_l \omega_{kl} - 2\pi] \tag{4.3.32}$$

with $0 \le i \le M$ for $j = 0$, $-M \le i \le M$ for $1 \le j \le N$, and $\omega_{kl} = \omega_{-k,-l}$. The fractional part of $\pi(i+j+\pi)$ is an example of one such $\tilde{g}(i,j)$ which seemed to work well. The Jacobian of the system can be written down explicitly as well as the equations for the variation of G with R and ε. Newton's method with Euler continuation in R and/or ε was used to solve for the vorticity. By trial and error the value of h was chosen to be $1.5/M^{1/2}$ by comparing the computed solutions

with the exact solutions for $R = 0$ or $\varepsilon = 0$.

Figures 4.3.1 to 4.3.3 show contour plots of the vorticity for $\varepsilon = 0.5$ and $R = 0, 10, 100$. As R increases it is apparent that the elongated axis of the vorticity distribution rotates counter-clockwise. As R increases further the apparent elliptical cross-section tends more and more towards a circle. This is a typical behavior for any ε. Figure 4.3.4 shows the dependence on R and ε of the rotation angle, φ, which would be required for zero cross-moment of the vorticity distribution in a rotated (x',y') coordinate system. That is, if

$$\begin{aligned} \sigma_x^2 &= \int\int x^2\omega \, dxdy / 2\pi \\ \sigma_{xy} &= \int\int xy\,\omega \, dxdy / 2\pi \\ \sigma_y^2 &= \int\int y^2\omega \, dxdy / 2\pi \end{aligned} \tag{4.3.33}$$

and

$$\begin{aligned} x' &= \quad x\cos\varphi + y\sin\varphi \\ y' &= -x\sin\varphi + y\cos\varphi \end{aligned} \tag{4.3.34}$$

then for an appropriate choice of φ we have $\sigma_{x'y'} = 0$ where

$$\begin{aligned} \tan 2\varphi &= \frac{2\sigma_{xy}}{\sigma_x^2 - \sigma_y^2} \\ \sigma_{x'}^2 &= \cos^2\varphi\,\sigma_x^2 + \sin 2\varphi\,\sigma_{xy} + \sin^2\varphi\,\sigma_y^2 \\ \sigma_{y'}^2 &= \sin^2\varphi\,\sigma_x^2 - \sin 2\varphi\,\sigma_{xy} + \cos^2\varphi\,\sigma_y^2 \end{aligned} \tag{4.3.35}$$

The quantities φ, $\sigma_{x'}$, $\sigma_{y'}$ have no apparent special physical significance but are given here as a means to characterize the solutions. The value of φ depends strongly on R as φ tends from zero to an apparent asymptote of 45 degrees as R increases. The dependence on ε is very weak and increasing ε serves to decrease φ. The weak dependence on ε in φ appears also in the perturbation solution. We obtain after some calculation for $\varepsilon, R \ll 1$,

$$\sigma_x^2 \simeq 1 + \varepsilon + \varepsilon^2\,, \quad \sigma_{xy} \simeq -\varepsilon R/16\,, \quad \sigma_y^2 \simeq 1 - \varepsilon + \varepsilon^2 \tag{4.3.36}$$

$$\varphi \simeq R/16\,, \quad \sigma_{x'}^2 \simeq 1+\varepsilon+\varepsilon^2\,, \quad \sigma_{y'}^2 \simeq 1-\varepsilon+\varepsilon^2 \tag{4.3.37}$$

so that to the order of the perturbation calculation φ depends only on R. The predicted value of φ for small R and ε is shown in figure 4.3.4. Figure 4.3.5 shows the variation of $\sigma_{x'}$ and $\sigma_{y'}$ with R and ε. Note that for small R we observe the elongated distribution of equation 4.3.6. For large R in order to satisfy the dominant non-linear terms in the equation the velocity must become orthogonal to the gradient of the vorticity. This gives the approach to a circular shape seen for large R and corresponds to a dominance of inertial effects due to the large rotational velocity of the vortex.

As $\varepsilon \to 1$ the elongation of the vorticity distribution tends to infinity so that our numerical represention breaks down and we cannot compute with confidence in this region. The Newton's method seemed to converge to the solutions described above regardless of the initial distribution of vorticity. The starting solution was taken to be some point on the boundary of the parameter space where the solution was known in closed form. Figure 4.3.6 shows the region of the parameter space where solutions were computed. An Euler-Newton continuation scheme was begun at $R = 0$ at a given ε and continued using steps in R of 1.0 or 2.0. For $20 \le R \le 100$, steps of 5.0 were used. As mentioned previously, larger steps were easily possible but small steps were chosen for better graphical accuracy.

We have thus computed a new class of solutions of the Navier-Stokes equations which can be termed non-symmetric Burgers' vortices. These vortices depend on two parameters: the difference between the external two-dimensional strains, ε, and the Reynold's number, R. The parameter space was studied numerically in the rectangle $[0 \le \varepsilon \le .75, 0 \le R \le 100]$ for solutions with reflection symmetry about the origin. No bifurcation or turning points were

found although the formulation did not allow for symmetry breaking bifurcations. The numerical results agree well with the small parameter perturbation expansion. We conjecture that solutions of the type described exist for all ε and R as $\varepsilon \to 1$ and/or $R \to \infty$.

References

[1] ABRAMOWITZ, M. & STEGUN, I. A. 1972 *Handbook of Mathematical Functions*. Nat. Bur. Stand. Dover Pub., Inc.

[2] AREF, H. 1983 Integrable, chaotic, and turbulent vortex motion in two-dimensional flow. *Ann. Rev. Fluid Mech.*, **15**, 345-389.

[3] BATCHELOR, G. K. 1967 *An Introduction to Fluid Mechanics*. Cambridge University Press.

[4] BENDER, C. M. & ORSZAG, S. A. 1978 *Advanced Mathematical Methods for Scientists and Engineers*. McGraw-Hill, Inc.

[5] BLANCH, G. 1966 Numerical aspects of Mathieu eigenvalues. *Rend. Circ. Mat. Palermo (2)* **15**, 51-97.

[6] BOYD, J. P. 1978 Spectral and pseudospectral methods for eigenvalue and nonseparable boundary value problems. *Mon. Weather Rev.* **106**, 1192-1203.

[7] BURGERS, J. M. 1948 A mathematical model illustrating the theory of turbulence. *Adv. Appl. Mech.* **1**, 171-199.

[8] CHRISTIANSEN, J. P. & ZABUSKY, N. J. 1973 Instability, coalescence and fission of finite-area vortex structures. *J. Fluid Mech.* **61**, 219-243.

[9] CLEMM, D. S. 1969 Algorithm 352: Characteristic values and associated solutions of Mathieu's differential equation. *Comm. ACM* **12** (7), 399-407.

[10] CROW, S. C. 1970 Stability theory for a pair of trailing vortices. *A.I.A.A. J.* **8**, 2172-2179.

[11] DOMM, U. 1956 Über die Wirbelstraβen von geringster Instabilität. *Z. angew. Math. Mech.* **36**, 367-371.

[12] GARBOW, B. S., BOYLE, J. M., DONGARRA, J. J., & MOLER, C. B. 1977 *Matrix Eigensystem Routines*-EISPACK *Guide Extension*, Lecture Notes in Computer Science **51**, Springer-Verlag.

[13] GOPAL, E. S. R. 1963 Motion and stability of quantized vortices in a finite channel: Application to liquid helium II. *Ann. Phys.* **25**, 196-220.

[14] JIMENEZ, J. 1975 Stability of a pair of co-rotating vortices. *Phys. Fluids* **18**, 1580-1581.

[15] KÁRMÁN, T. VON 1911 Über den Mechanismus des Widerstands, den ein bewegter Körper in einer Flüssigkeit erfährt. *Göttinger Nachrichten, Math. Phys. Kl.*, 509-517.

[16] KÁRMÁN, T. VON 1912 Über den Mechanismus des Widerstands, den ein bewegter Körper in einer Flüssigkeit erfährt. *Göttinger Nachrichten, Math. Phys. Kl.*, 547-556.

[17] KÁRMÁN, T. VON & RUBACH, H.L. 1912 Über den Mechanismus des Flüssigkeits- und Luftwiderstands. *Phys. Zeitschr.* **13**, 49-59.

[18] LORD KELVIN. 1880 Vibrations of a columnar vortex. *Phil. Mag.* **10**, 155-168.

[19] KIDA, S. 1981 Motion of an elliptic vortex in a uniform shear flow. *J. Phys. Soc. Japan* **50** (10), 3517-3520.

[20] KOCHIN, N. J. 1939 On the instability of von Kármán's vortex street. *Compt. Rend. (Doklady) de l'Academie des Sciences de l'SSSR* **24**, 19-23.

[21] LAMB, H. 1932 *Hydrodynamics*. Cambridge University Press.

[22] LEIBOVICH, S. & HOLMES, P. H. 1981 Global stability of Burgers' vortex. *Phys. Fluids* **24**(3), 548-549.

[23] LEONARD, A. 1980 Vortex methods for flow simulation. *J. Comp. Phys.* **37**,

289-335.

[24] MOORE, D. W. & SAFFMAN, P. G. 1971 Structure of a line vortex in an imposed strain. *Aircraft Wake Turbulence* (ed. Olsen, Goldburg & Rogers), Plenum Press, 339-354.

[25] MOORE, D. W. & SAFFMAN, P. G. 1972 The motion of a vortex filament with axial flow. *Phil. Trans. R. Soc. Lond.* A. **272**, 403-429.

[26] MOORE, D. W. & SAFFMAN, P. G. 1974 A note on the stability of a vortex ring of small cross-section. *Proc. R. Soc. Lond.* A. **338**, 535-537.

[27] MOORE, D. W. & SAFFMAN, P. G. 1975 The instability of a straight vortex filament in a strain field. *Proc. R. Soc. Lond.* A. **346**, 413-425.

[28] PIERREHUMBERT, R. T. 1980 A family of steady, translating vortex pairs with distributed vorticity. *J. Fluid Mech.* **99**, 129-144.

[29] PIERREHUMBERT, R. T. 1980 The structure and stability of large vortices in an inviscid flow. M.I.T. Fluid Dynamics Lab. Rep. 80-1.

[30] PIERREHUMBERT, R. T. & WIDNALL, S. E. 1981 The structure of organized vortices in a free shear layer. *J. Fluid Mech.* **102**, 301-313.

[31] PIERREHUMBERT, R. T. & WIDNALL, S. E. 1982 The two- and three-dimensional instabilities of a spatially periodic shear layer. *J. Fluid Mech.* **114**, 59-82.

[32] ROSENHEAD, L. 1930 The spread of vorticity in the wake behind a cylinder. *Proc. R. Soc. Lond.* A. **127**, 590-612.

[33] ROSENHEAD, L. 1953 Vortex systems in wakes. *Adv. Appl. Mech.* **3**, 185-195.

[34] ROSHKO, A. 1976 Structure of turbulent shear flows: A new look. *A.I.A.A. J.* **14**, 1349-1357.

[35] SAFFMAN, P. G. 1978 The number of waves on unstable vortex rings. *J.Fluid*

Mech. **84**, 625-639.

[36] SAFFMAN, P. G. 1981a Dynamics of vorticity. *J. Fluid Mech.* **106**, 49-58.

[37] SAFFMAN, P. G. 1981b Vortex interactions and coherent structures in turbulence. *Transition and Turbulence*, Academic Press, 149-166.

[38] SAFFMAN, P. G. 1982 Structure and stability of streets of finite vortices. *Vortex Motion* (eds. Hornung & Müller) Friedr. Vieweg & Sohn, 142-156.

[39] SAFFMAN, P. G. & BAKER, G. R. 1979 Vortex interactions. *Ann. Rev. Fluid Mech.* **11**, 95-122.

[40] SAFFMAN, P. G. & SCHATZMAN, J. C. 1981 Properties of a vortex street of finite vortices. *SIAM J. Sci. Stat. Comp.* **2**, 285-295.

[41] SAFFMAN, P. G. & SCHATZMAN, J. C. 1982a Stability of a vortex street of finite vortices. *J. Fluid Mech.* **117**, 171-185.

[42] SAFFMAN, P. G. & SCHATZMAN, J. C. 1982b An inviscid model for the vortex street wake. *J. Fluid Mech.* **122**, 467-486.

[43] SAFFMAN, P. G. & SZETO, R. 1981 Structure of a linear array of uniform vortices. *Stud. Appl. Math.* **65**, 223-248.

[44] SAFFMAN, P. G. & TANVEER, S. 1982 The touching pair of equal and opposite uniform vortices. *Phys. Fluids* **25** (11), 1929-1930.

[45] SALE, A. H. J. 1970 Remark on algorithm 352 [S22]: Characteristic values and associated solutions of Mathieu's differential equation. *Comm. ACM* **13** (12), 750.

[46] SCHLAYER, K. 1928 Über die Stabilität der Kármánschen Wirbelstraße gegenüber beliebigen Störungen in drei Dimensionen. *Z. angew. Math. Mech.* **8**, 352-372.

[47] SCHMIEDEN, C. 1936 Zur Theorie der Kármánschen Wirbelstraße. *Ing. Arch.* **7**, 215-221.

[48] STENGER, F. 1981 Numerical methods based on Whittaker cardinal, or sinc functions. *SIAM Rev.* **23**(2), 165-224.

[49] STUART, J. T. 1967 On finite amplitude oscillations in laminar mixing layers. *J. Fluid Mech.* **29**, 417-440.

[50] STUARTSON, K. 1982 The stability of swirling flows at large Reynolds number when subjected to disturbances with large azimuthal wavenumber. *Phys. Fluids* **25**(11), 1953-1957.

[51] TAYLOR, G. I. 1938 Production and dissipation of vorticity in a turbulent fluid. *Proc. Roy. Soc. London* A. **164**, 15-23.

[52] TSAI, C-Y. & WIDNALL, S. E. 1976 The stability of short waves on a straight vortex filament in a weak externally imposed strain field. *J. Fluid Mech.* **73**, 721-733.

[53] WARD, R.C. 1981 Balancing the generalized eigenvalue problem. *SIAM J. Sci. Stat. Comp.* **2** (2), 141-152.

[54] WIDNALL, S. E. 1975 The structure and dynamics of vortex filaments. *Ann. Rev. Fluid Mech.* **7**, 141-165.

[55] WIDNALL, S. E., BLISS, D. B. & TSAI, C-Y. 1974 The instability of short waves on a vortex ring. *J. Fluid Mech.* **66**, 35-47.

[56] WIDNALL, S. E. & TSAI, C-Y. 1977 The instability of the thin vortex ring of constant vorticity. *Phil. Trans. R. Soc. Lond.* A. **287**, 273-305.

[57] WILLE, R. 1960 Kármán vortex streets. *Adv. Appl. Mech.* **6**, 273-287.

[58] WILTSE, J. C. & KING, M. J. 1958 Values of the Mathieu functions. The John

Hopkins Univ. Radiation Lab. Tech. Rep. AF-53, Baltimore, Md.

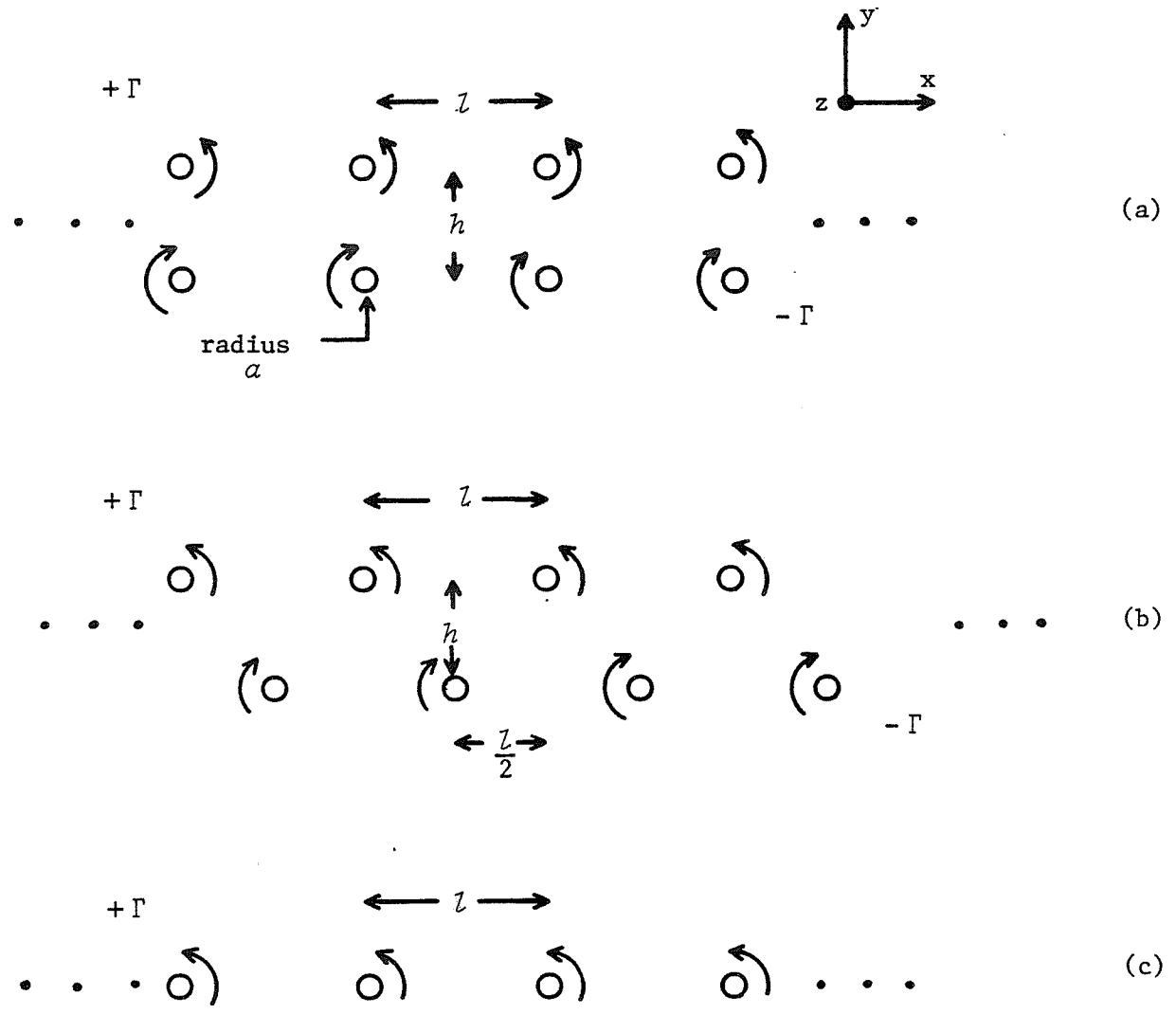

FIGURE 2.2.1 Steady vortex configurations (two-dimensional x-y plane cross section). (a) Symmetric double row. (b) Staggered double row or Kármán vortex street. (c) Single row.

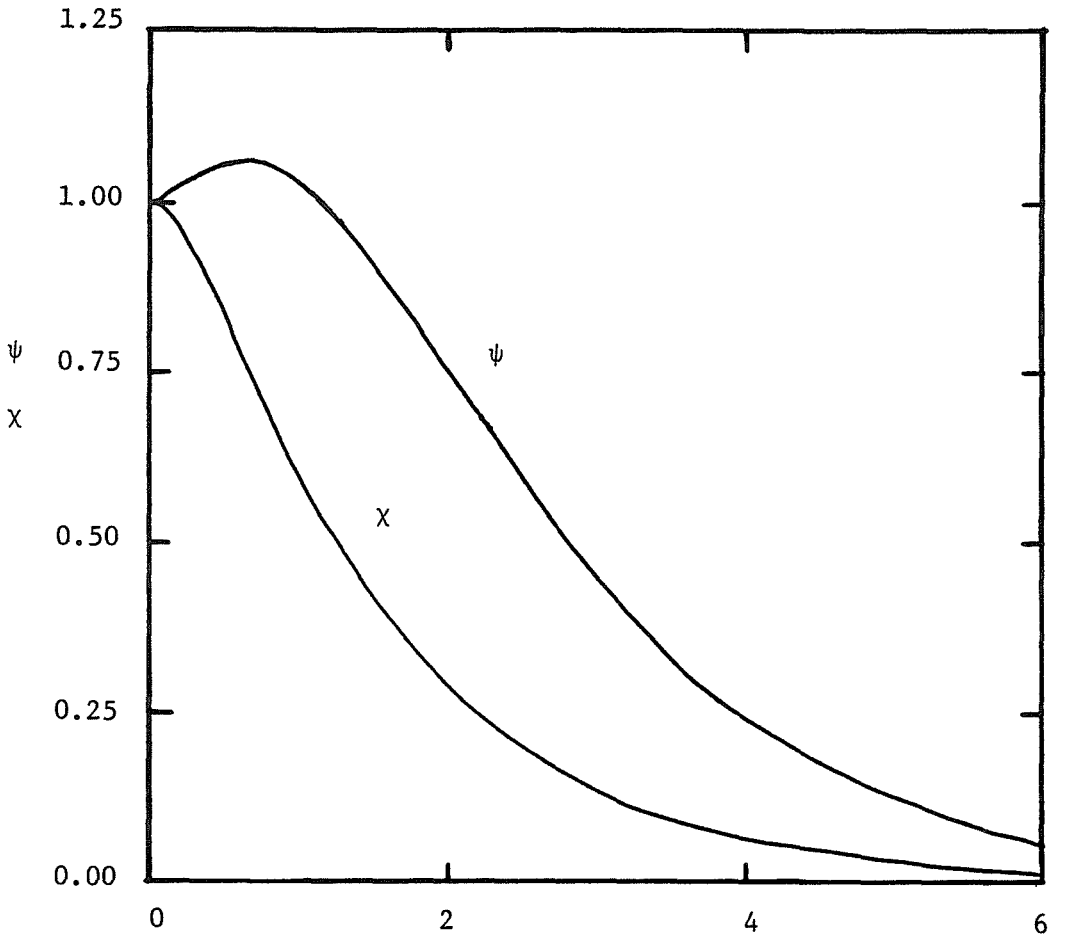

FIGURE 2.2.2 Mutual-induction functions χ and ψ (after Crow (1970)).

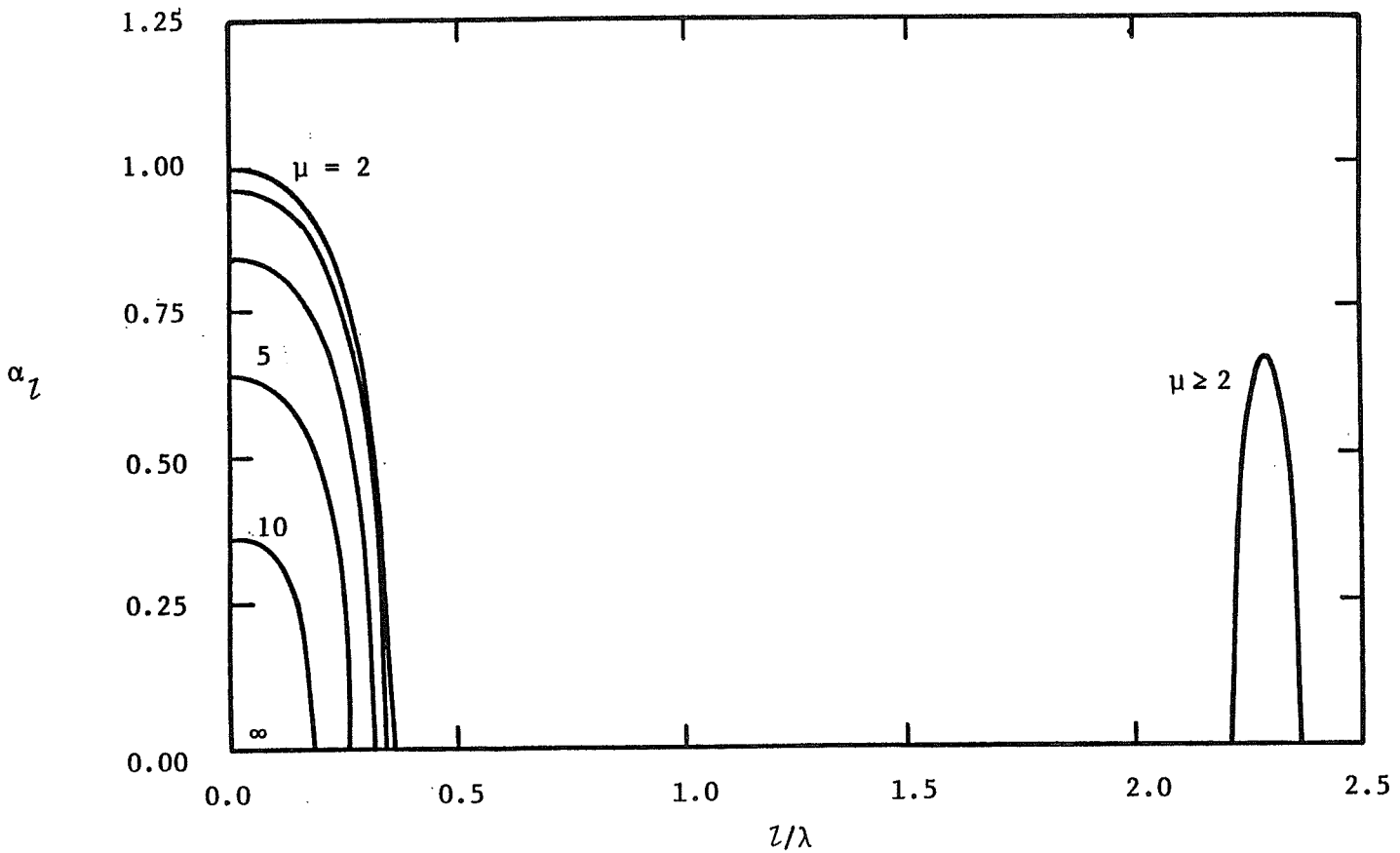

FIGURE 2.3.1 Plot of the growth rate α_l versus l/λ for various values of μ and $a/l = 0.1$ in the case of the single row.

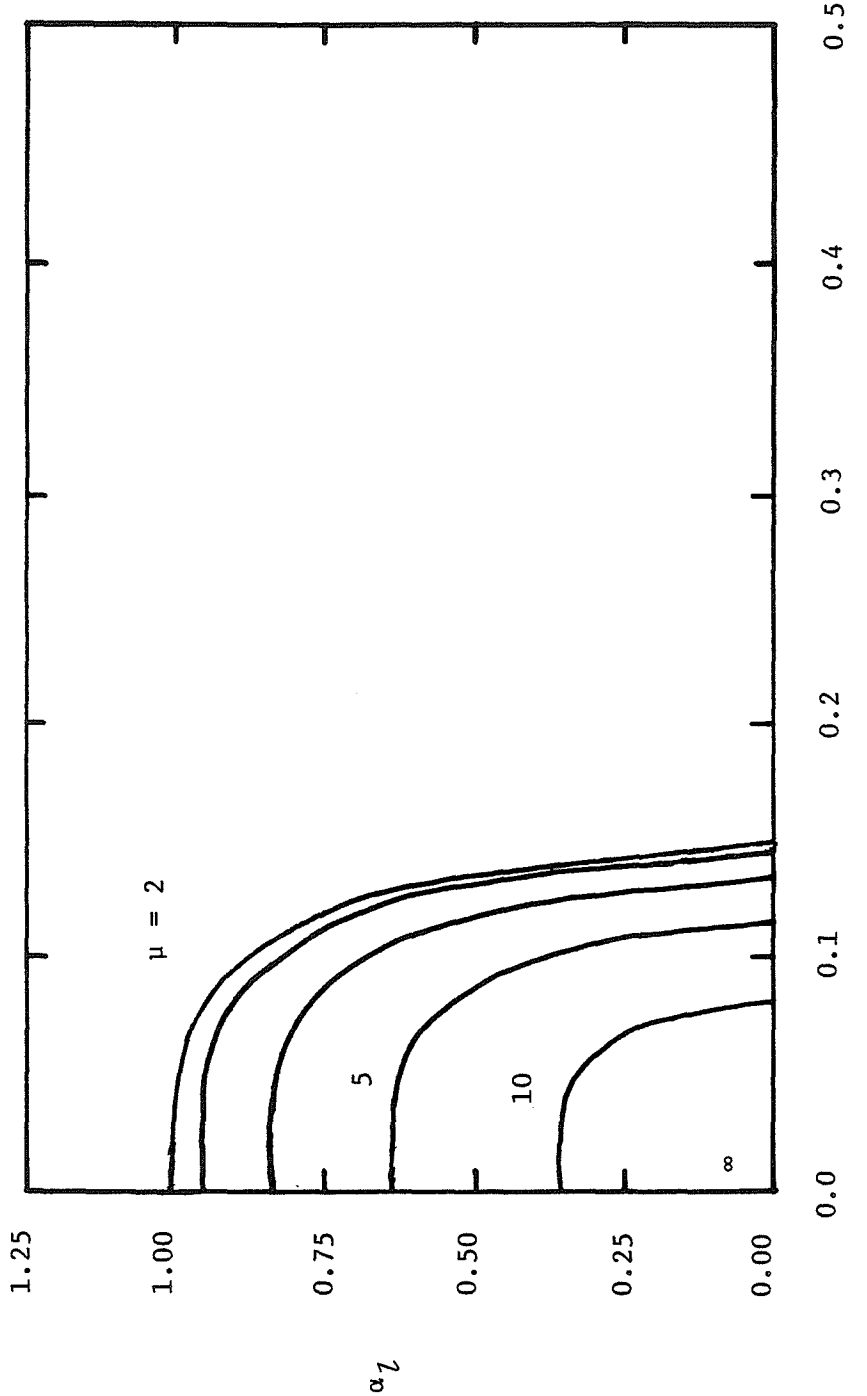

FIGURE 2.3.2 Plot of the growth rate α_ℓ versus ℓ/λ for various values of μ and $a/\ell = 10^{-5}$ in the case of the single row.

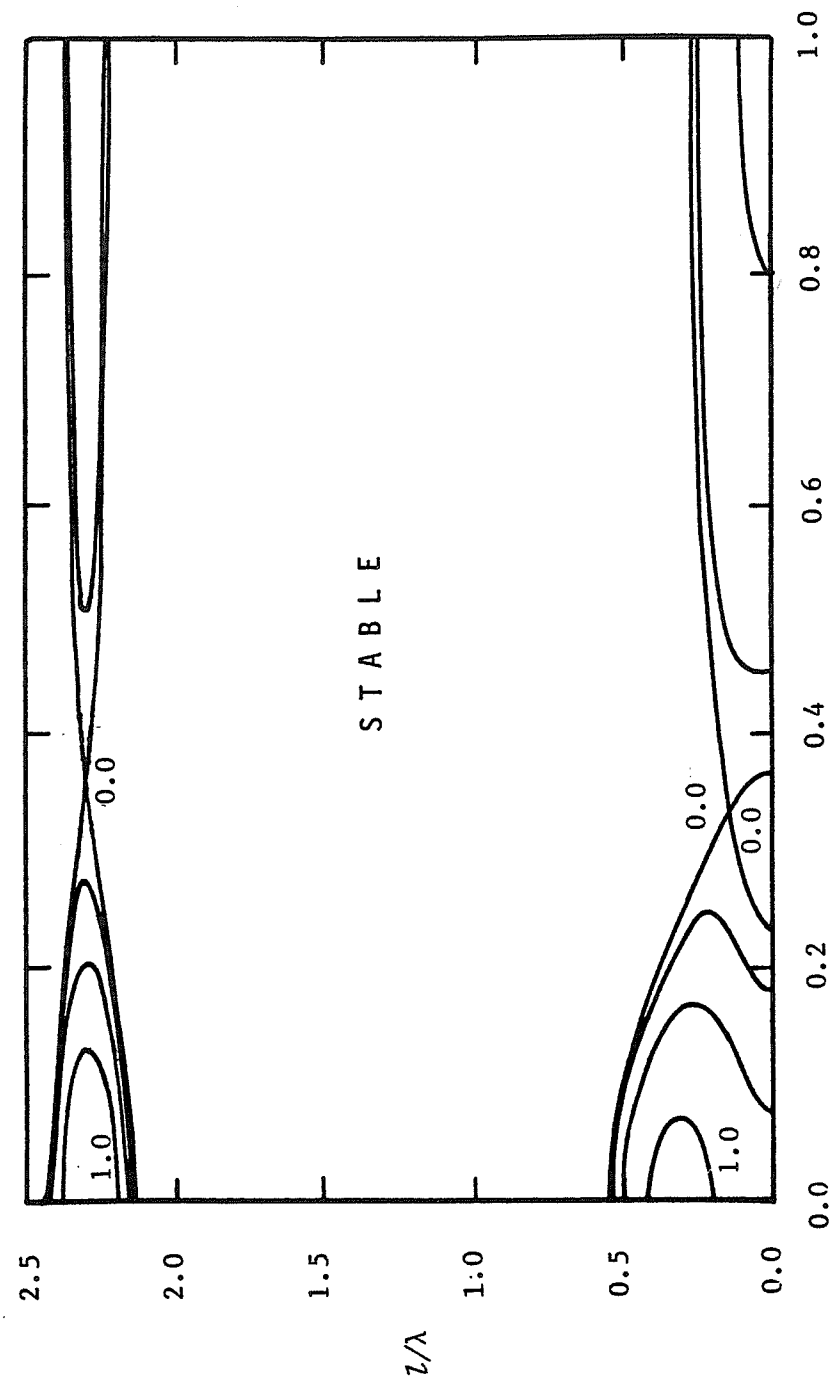

FIGURE 2.4.1 Contour plot of α_ℓ^A in κ and ℓ/λ for $\mu = 4.0$ and $a/\ell = 0.1$ in the case of the staggered double row.

FIGURE 2.4.2 Contour plot of α_ℓ^S (and α_ℓ^A) in κ and ℓ/λ for $\mu = 2.0$ and $a/\ell = 0.1$ in the case of the staggered double row.

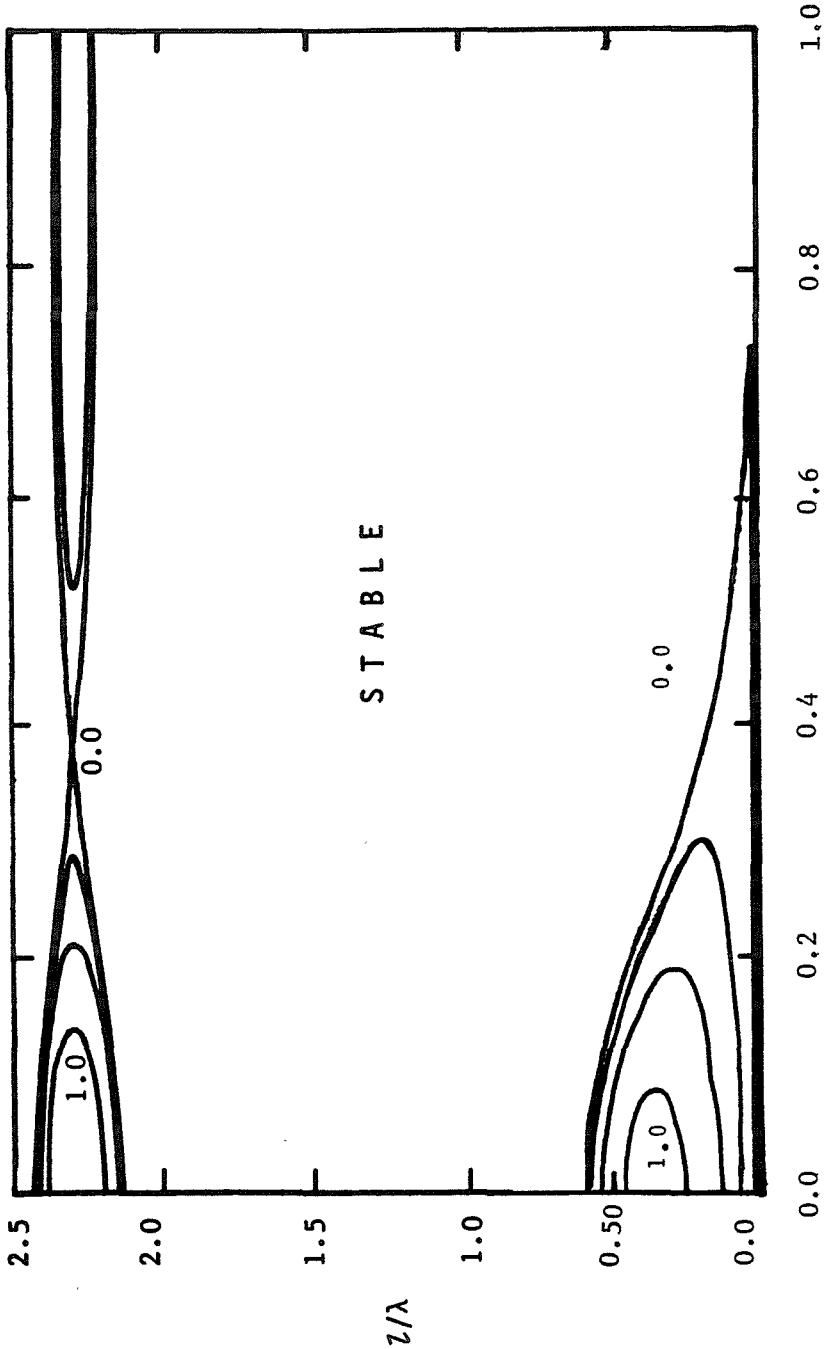

FIGURE 2.4.3 Contour plot of α_ℓ^A in κ and ℓ/λ for $\mu = \infty$ and $a/\ell = 0.1$ in the case of the staggered double row.

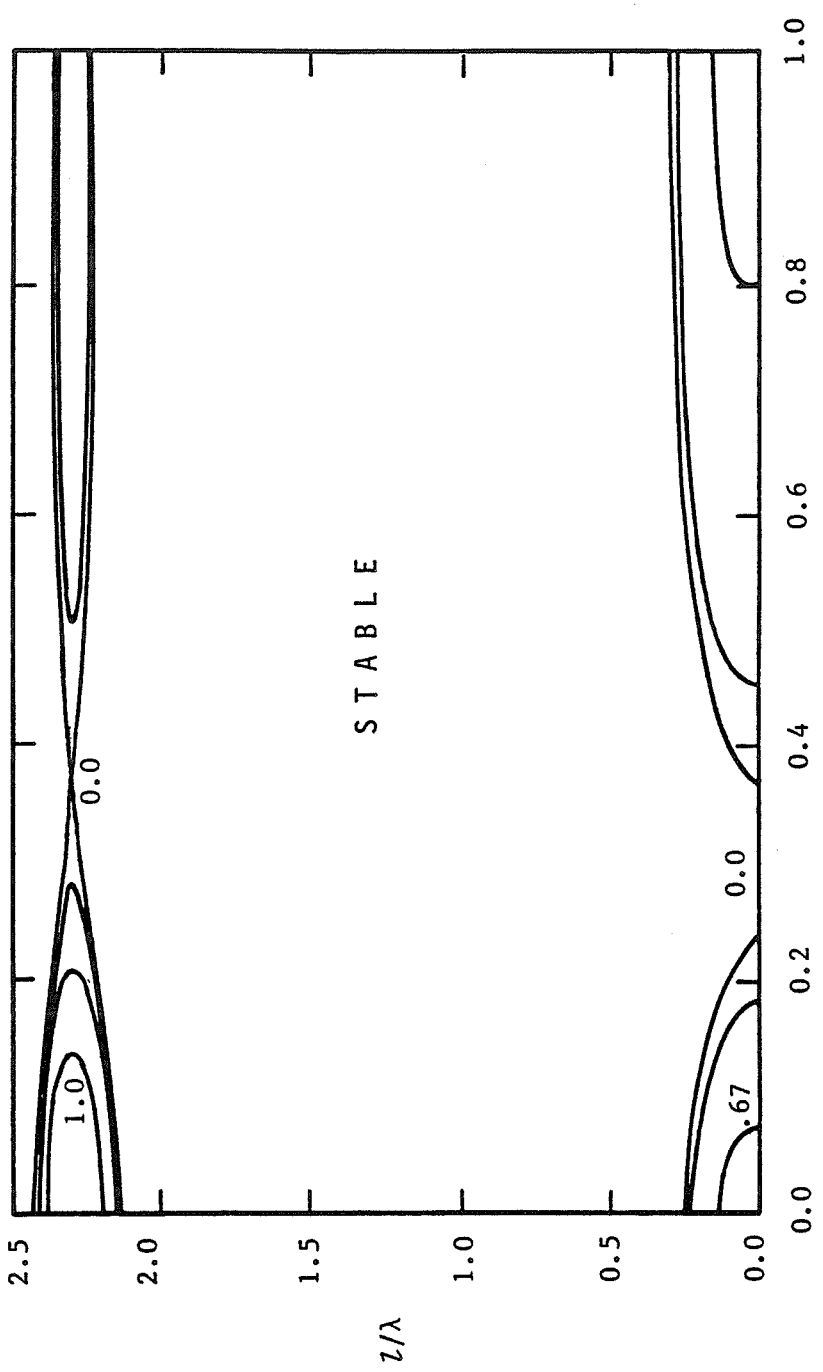

FIGURE 2.4.4 Contour plot of α_l^S in κ and l/λ for $\mu = 4.0$ and $a/l = 0.1$ in the case of the staggered double row.

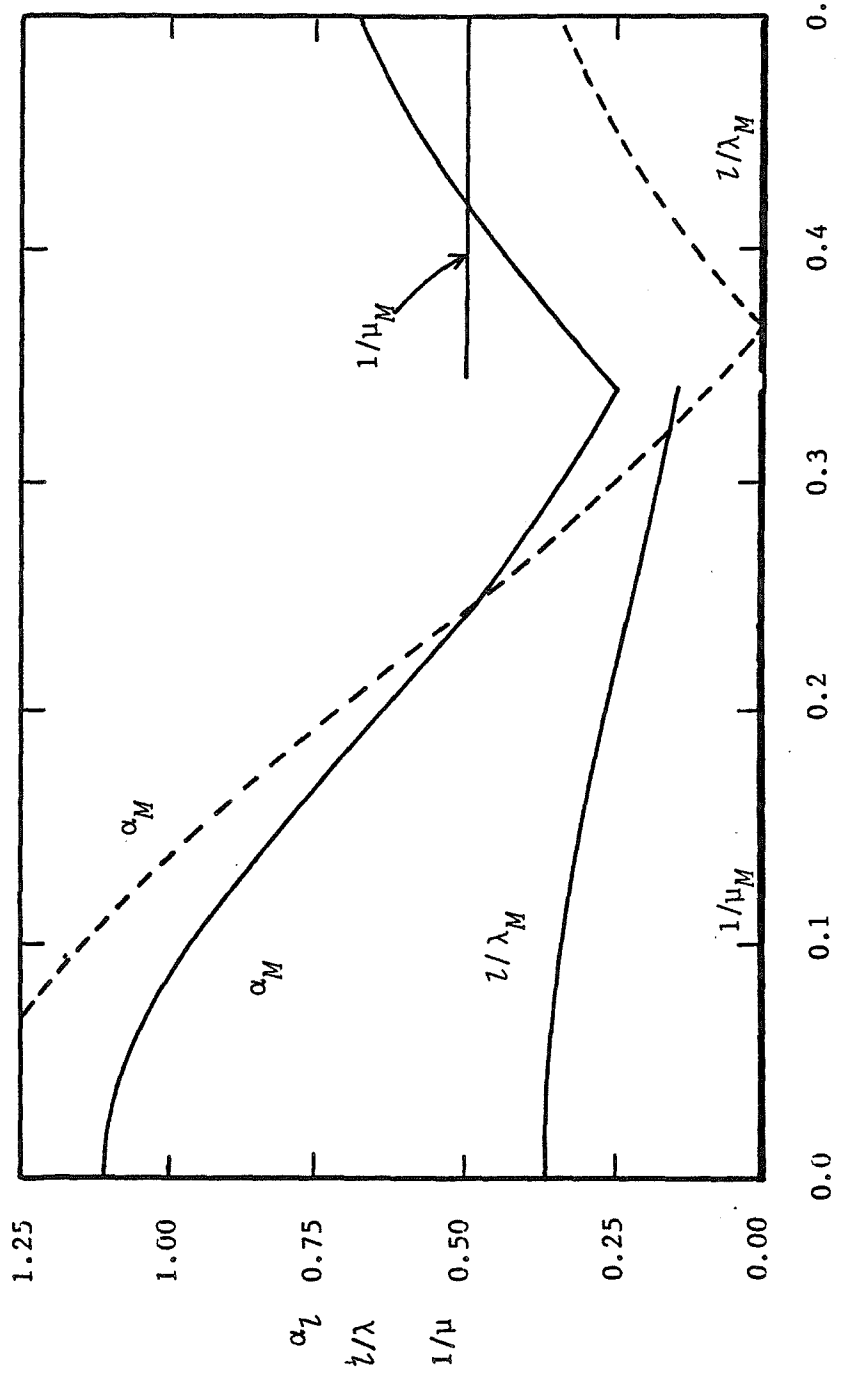

FIGURE 2.4.5 Plot of the maximum growth rate α_l^A, and corresponding l/λ and $1/\mu$ all versus κ for $a/l = 0.1$ in the case of the staggered double row. Also plotted is the short axial wavelength growth rate (dashed curve). Subscript M denotes maximum.

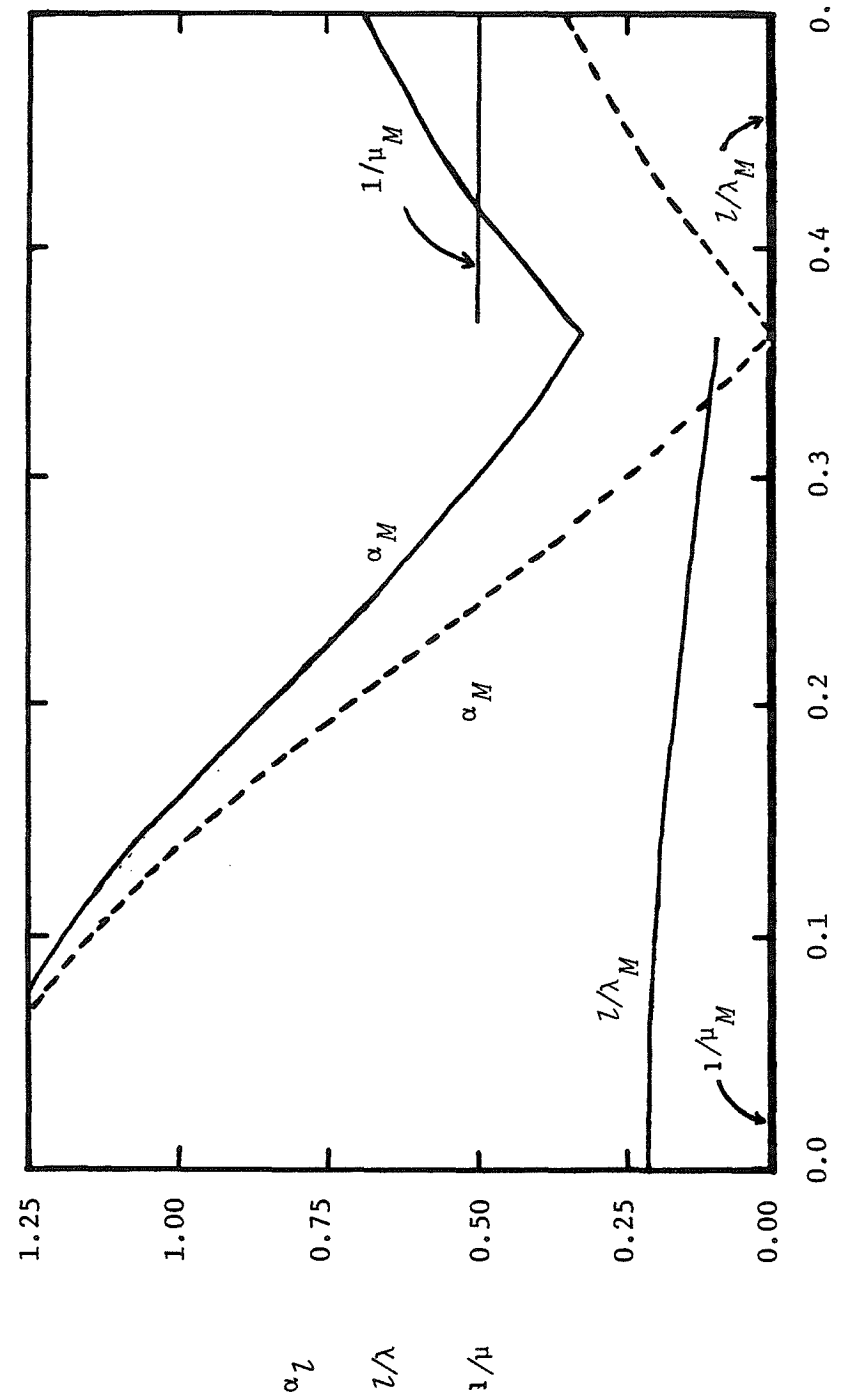

FIGURE 2.4.6 Plot of the maximum growth rate, α_ℓ^A and corresponding ℓ/λ and $1/\mu$ all versus κ for $a/\ell = 0.001$ in the case of the staggered double row. Also plotted is the short axial wavelength growth rate (dotted curve). Subscript M denotes maximum.

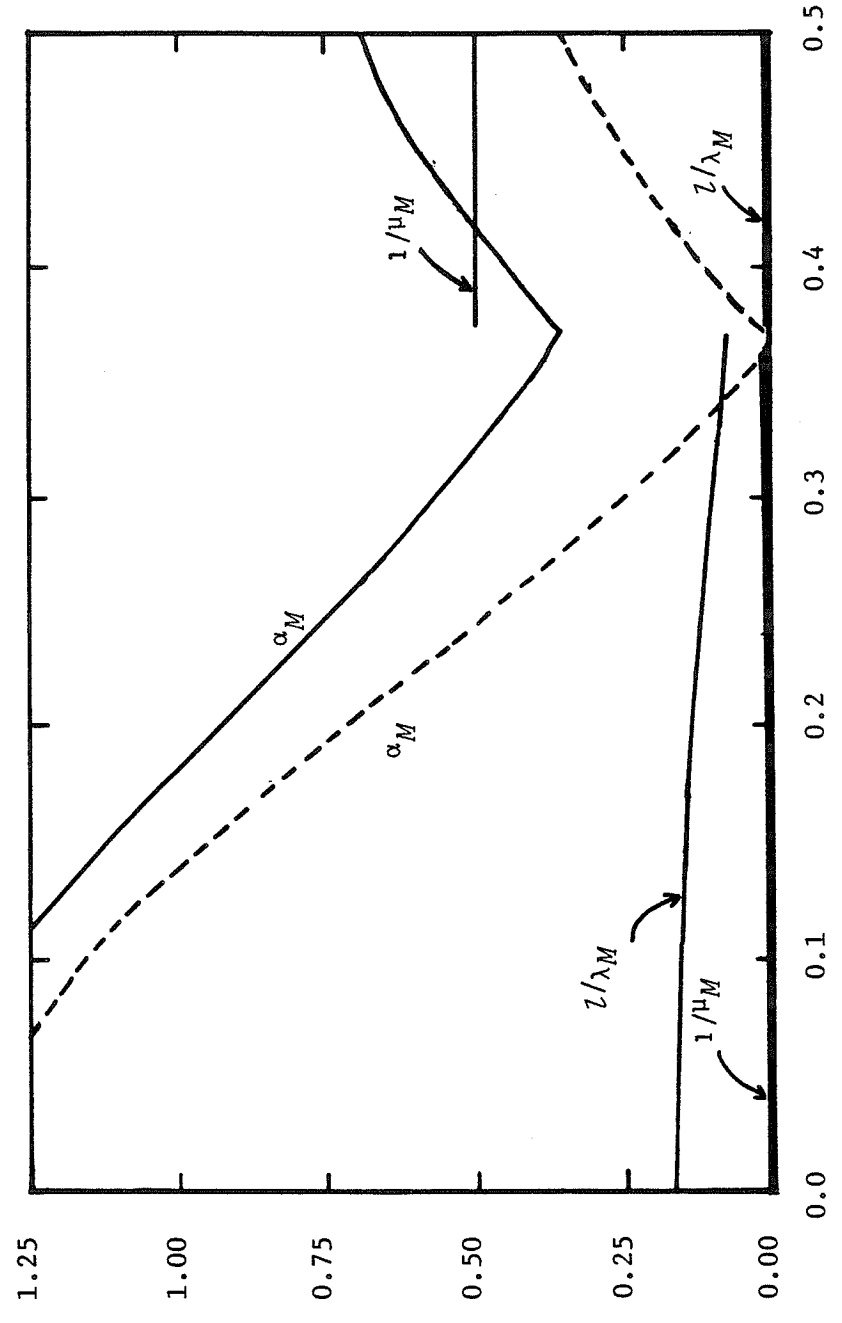

FIGURE 2.4.7 Plot of the maximum growth rate, α_ℓ^A, and corresponding ℓ/λ and $1/\mu$ all versus κ for $a/\ell = 10^{-5}$ in the case of the staggered double row. Also plotted is the short axial wavelength growth rate (dashed curve).

Subscript M denotes maximum.

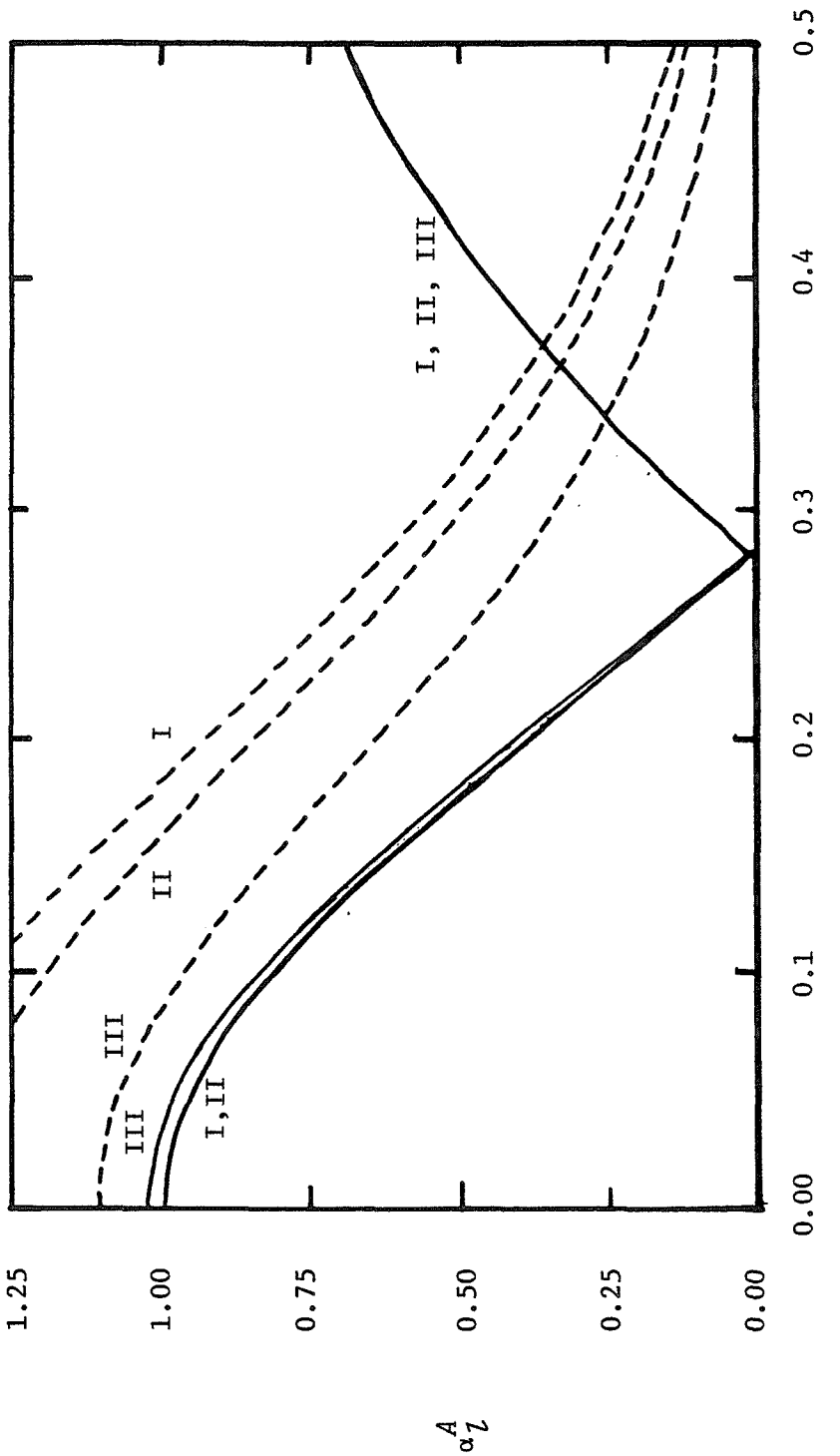

FIGURE 2.4.8 Plot of maximum growth rate, α_ℓ^A; $\mu = \infty$ (dashed lines) and $\mu = 2$ (solid lines). ($a/\ell = 10^{-5}$ (I), $a/\ell = .001$ (II), $a/\ell = .1$ (III))

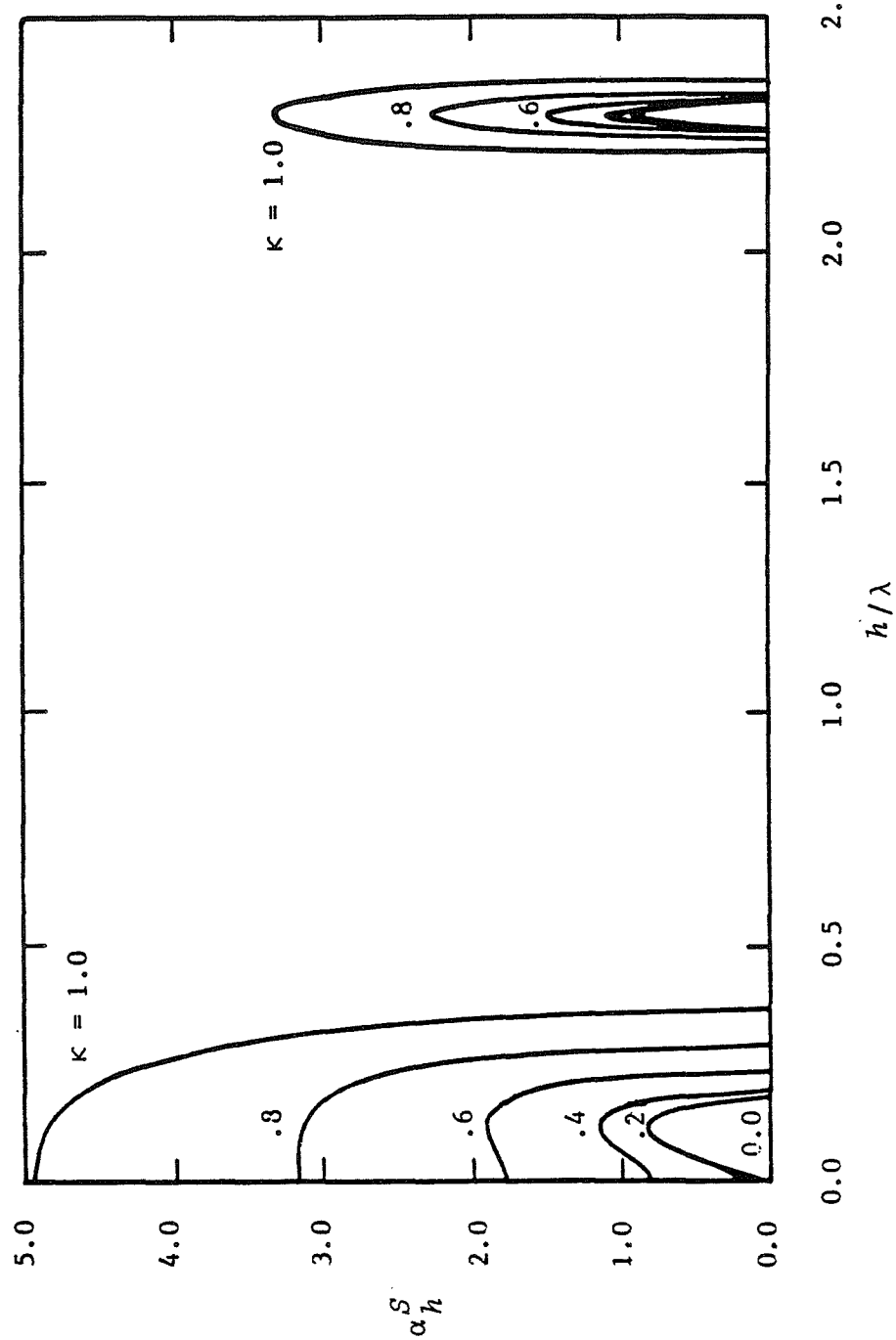

FIGURE 2.5.1 Plot of α_h^S versus h/λ for various values of κ with $\mu = 2.0$ and $\tilde{a}/h = 0.1$ in the case of the symmetric double row.

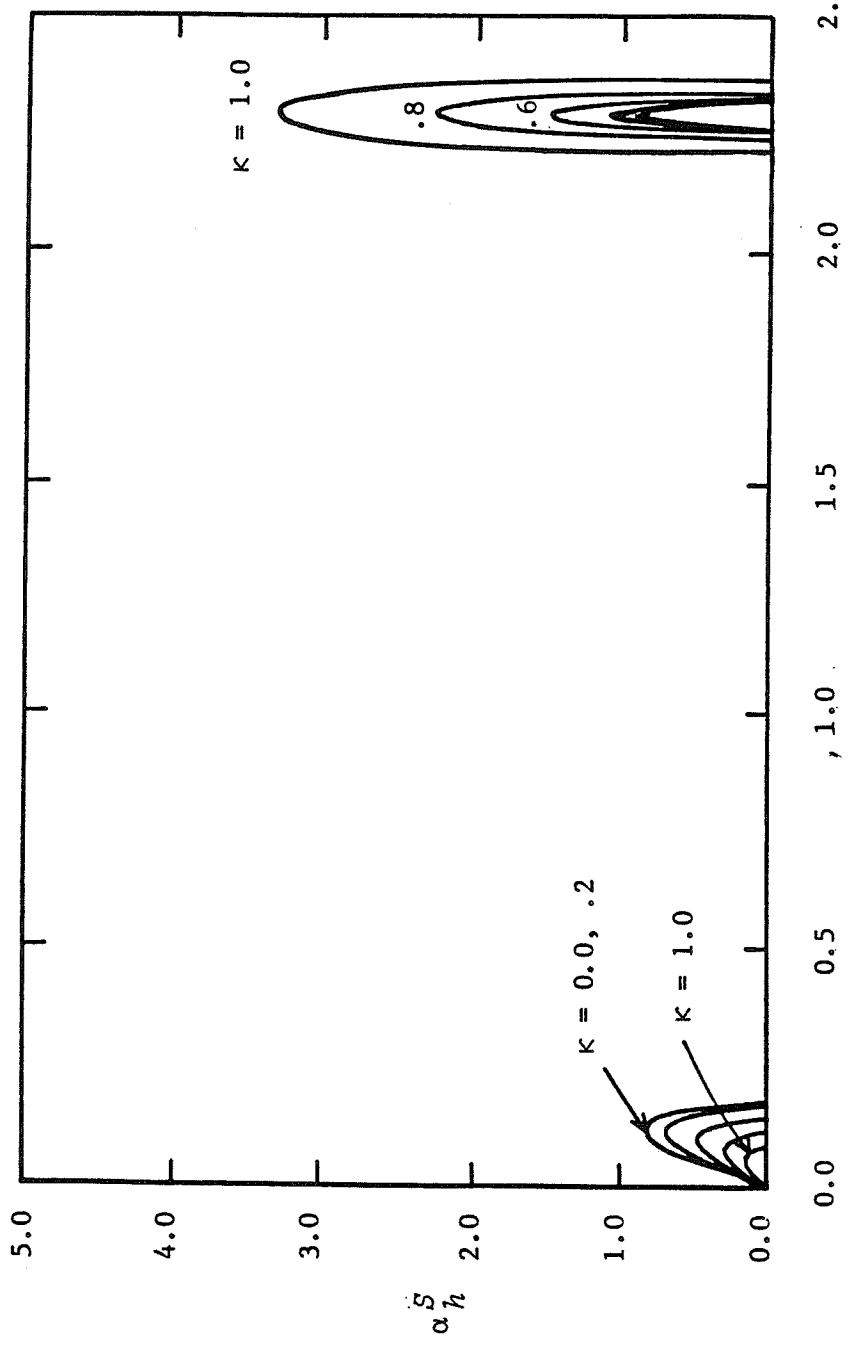

FIGURE 2.5.2 Plot of α_h^S versus h/λ for various values of κ with $\mu = \infty$ and $a/h = 0.1$ in the case of the symmetric double row.

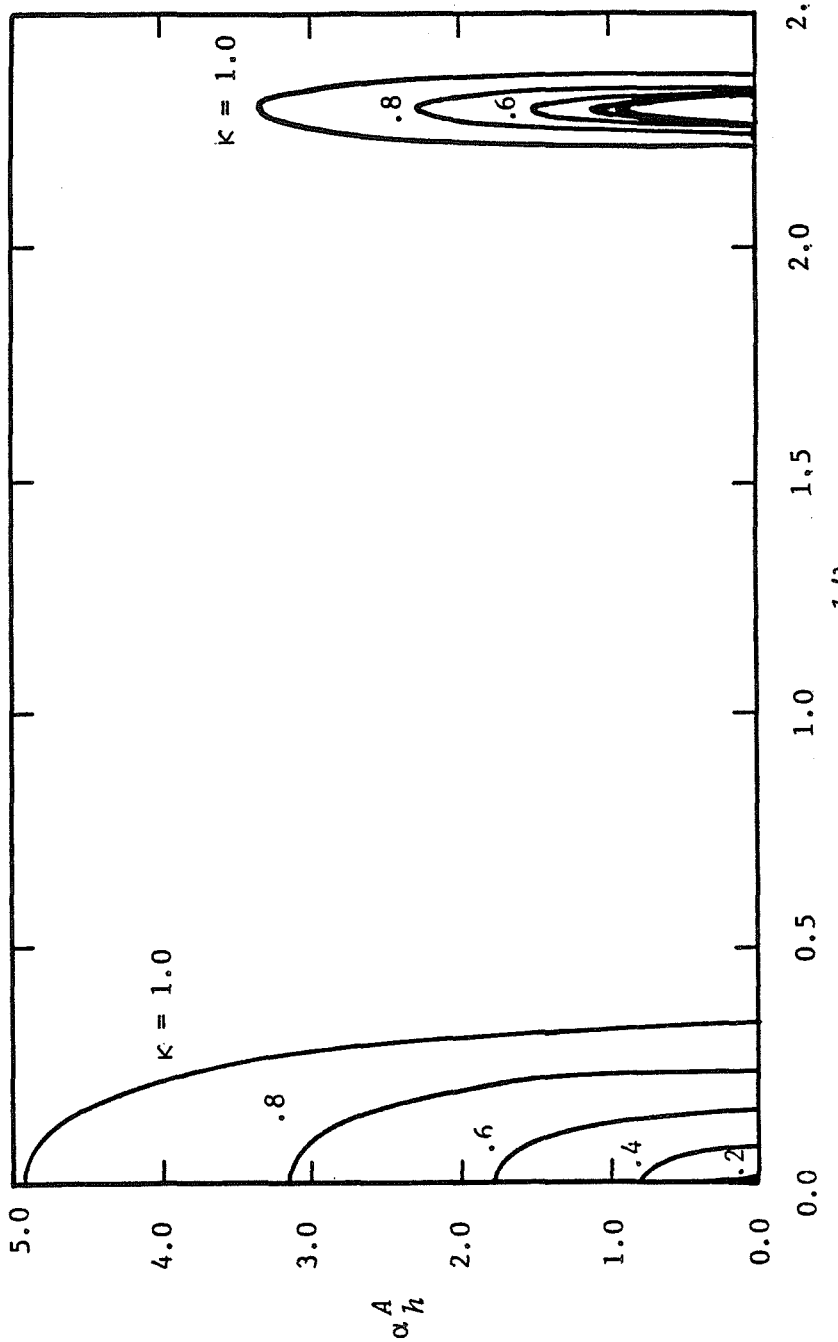

FIGURE 2.5.3 Plot of α_h^A versus h/λ for various values of κ with $\mu = 2.0$ and $a/h = 0.1$ in the case of the symmetric double row.

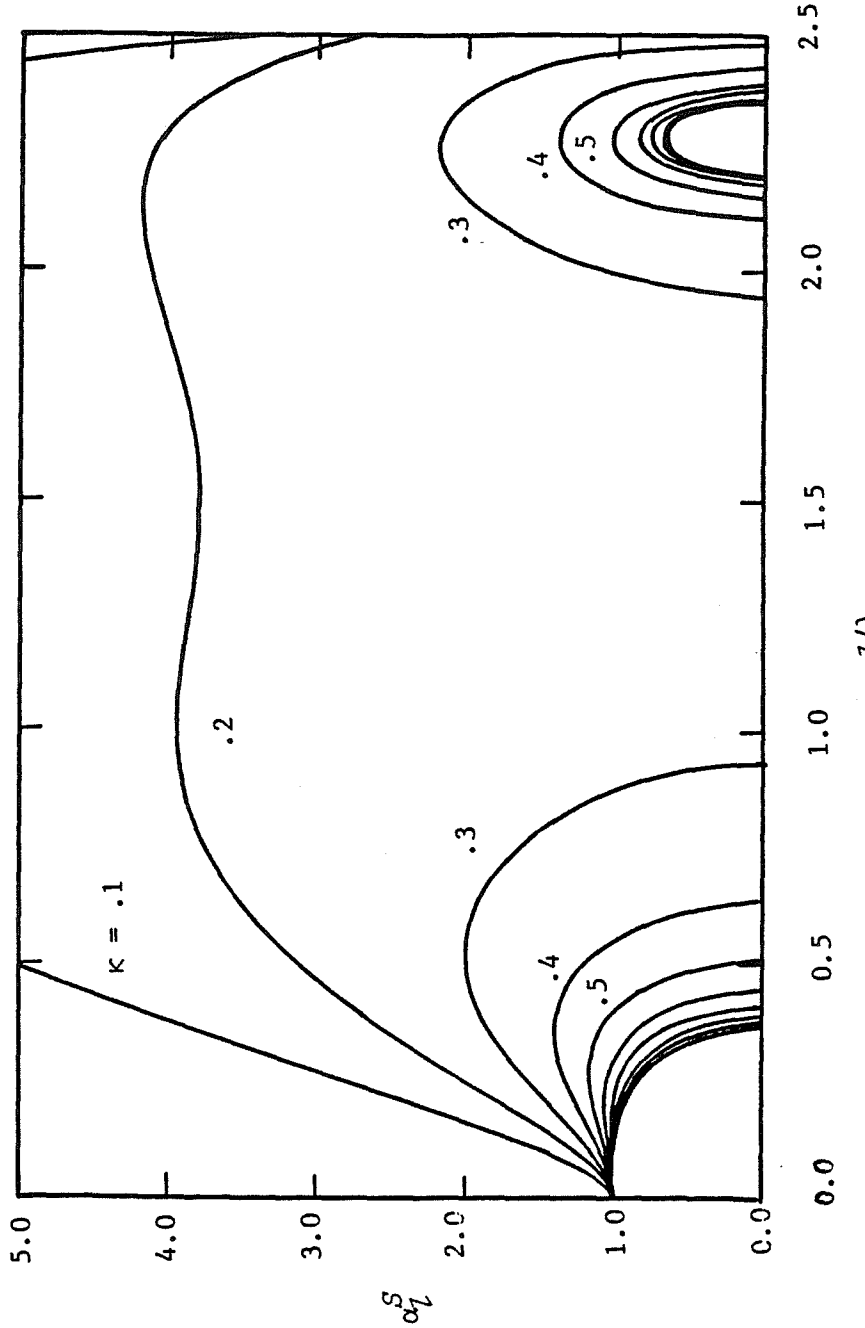

FIGURE 2.5.4 Plot of α_l^S versus l/λ for various values of κ with $\mu = 2.0$ and $a/l = 0.1$ in the case of the symmetric double row.

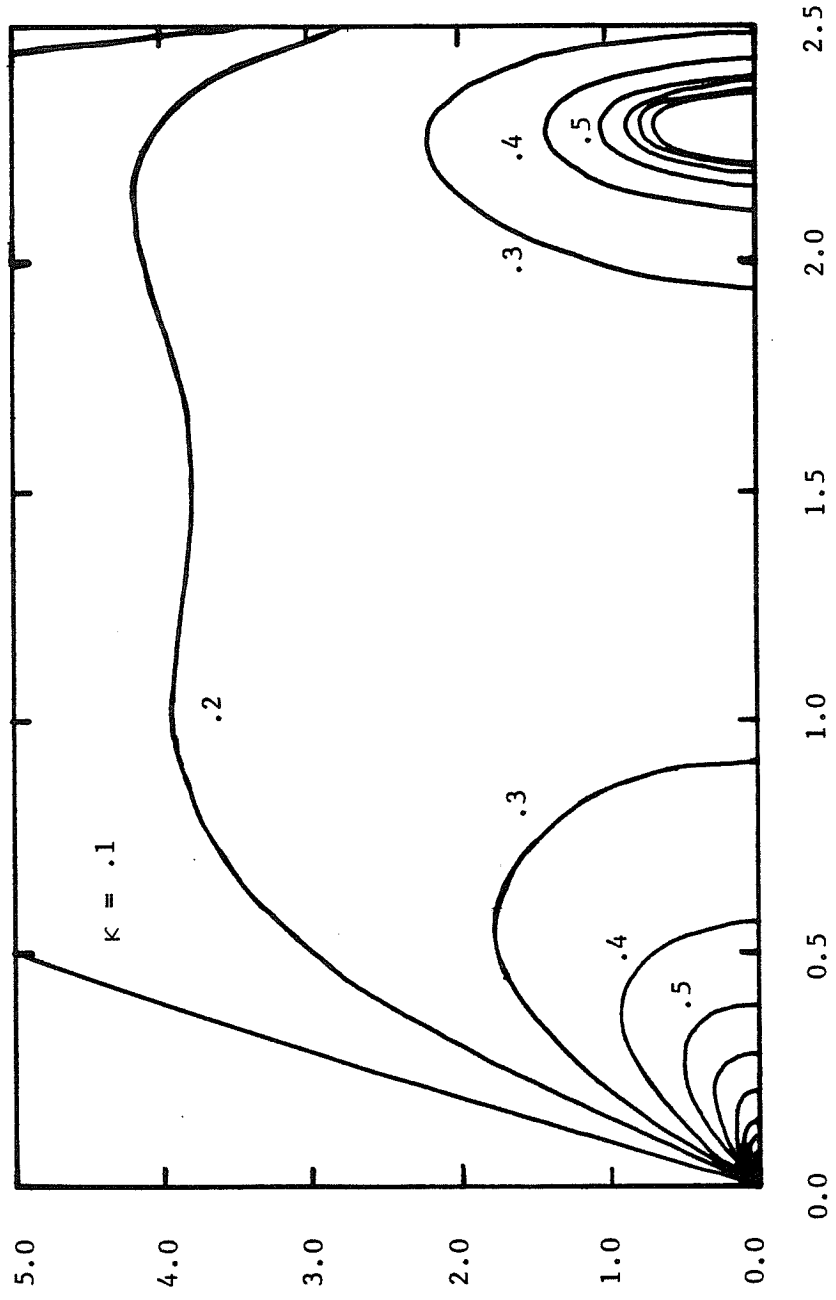

FIGURE 2.5.5 Plot of α_l^S versus l/λ for various values of κ with $\mu = \infty$ and $a/l = 0.1$ in the case of the symmetric double row.

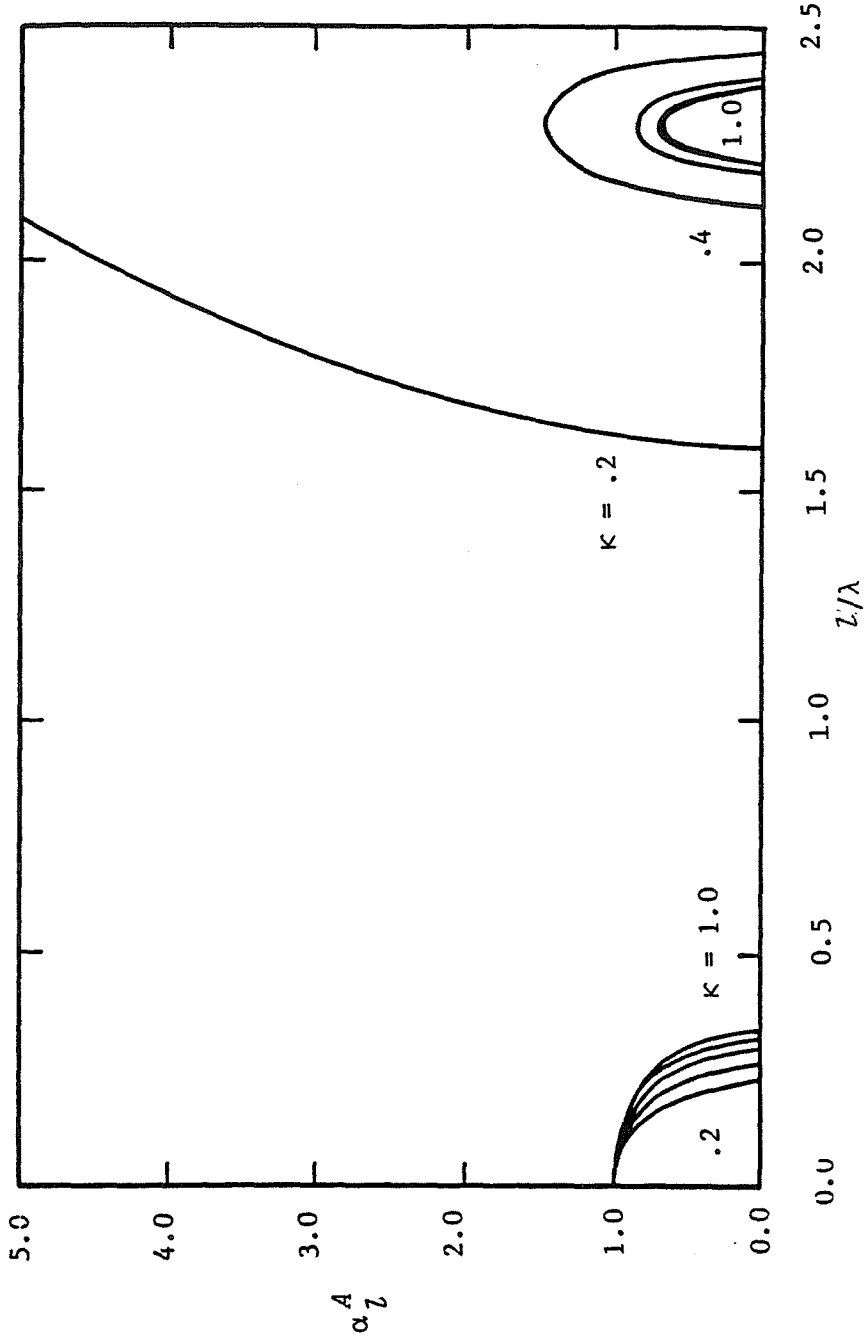

FIGURE 2.5.6 Plot of α_ℓ^A versus ℓ/λ for various values of κ with μ = 2.0 and a/ℓ = 0.1 in the case of the symmetric double row.

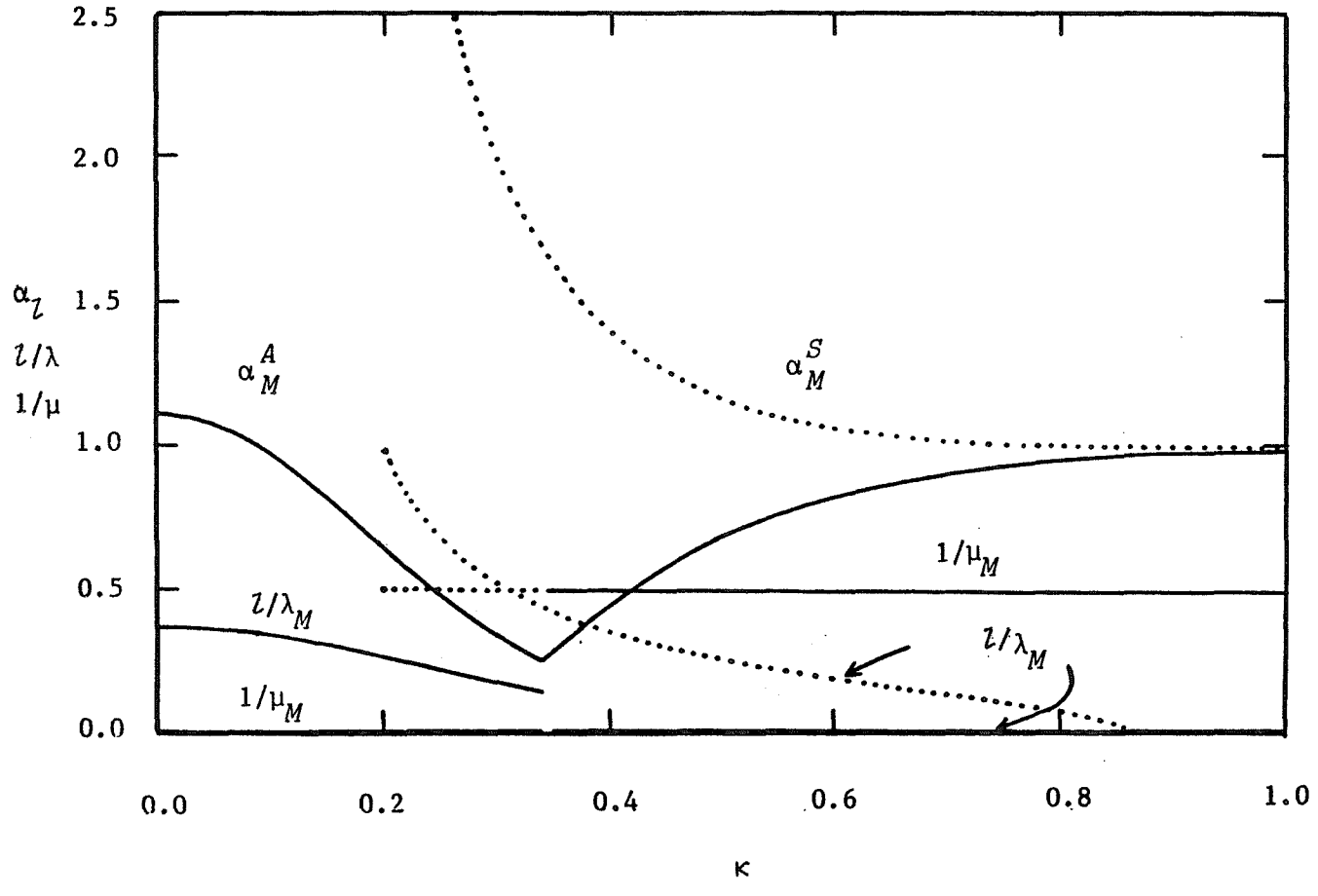

FIGURE 2.6.1 Plot of maximum α_l^A for the staggered double row and maximum α_l^S for the symmetric double row versus κ for $a/l = 0.1$. Maximum is over long axial wavelength region only. Also plotted are the values of l/λ and $1/\mu$ at which the maximum occurs. Solid lines refer to the staggered double row and dotted lines to the symmetric double row. Subscript M denotes maximum.

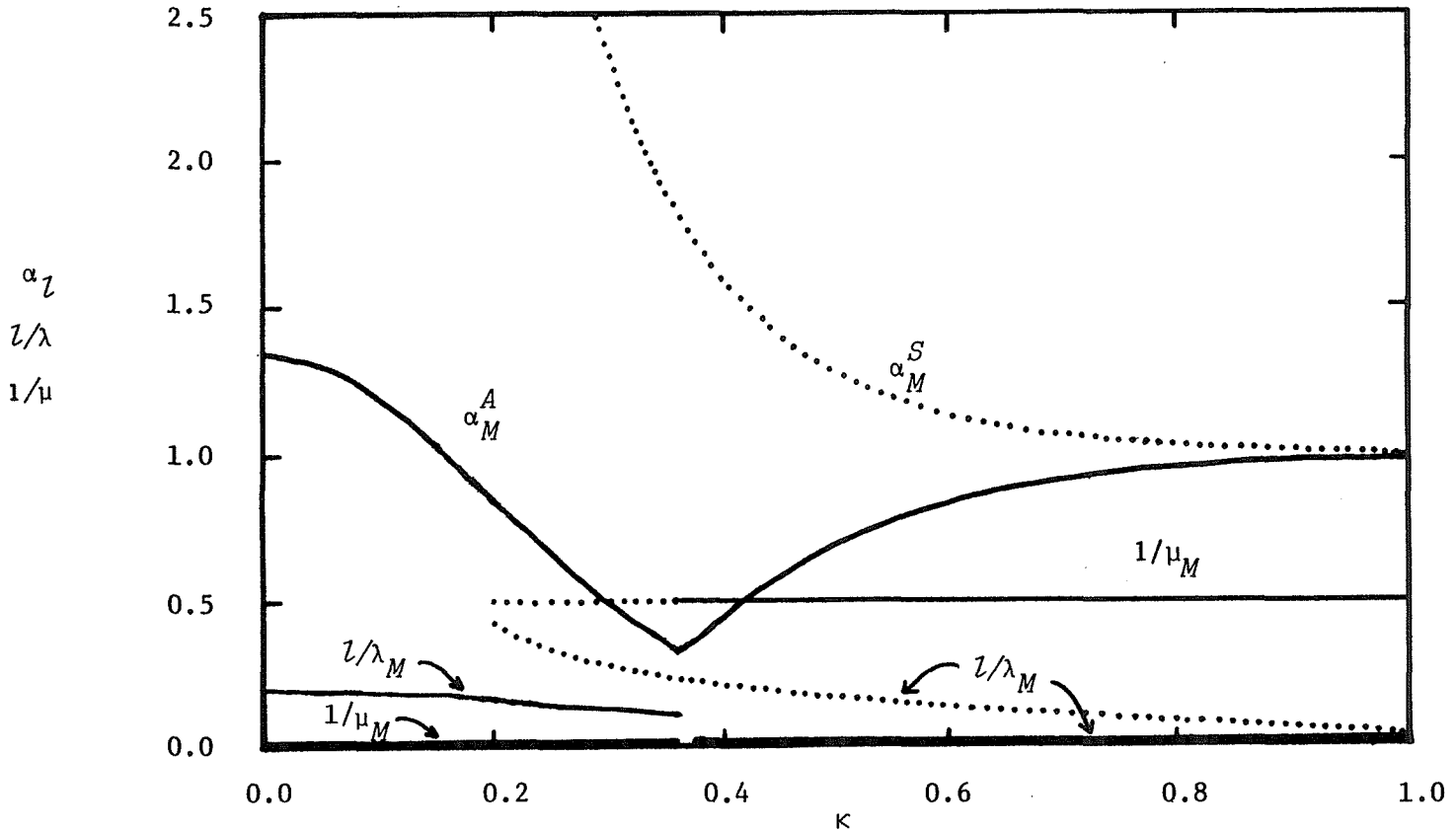

FIGURE 2.6.2 Plot of maximum α_l^A for the staggered double row and maximum α_l^S for the symmetrical double row versus κ for $a/l = 0.001$. Maximum is over long axial wavelength region only. Also plotted are the values of l/λ and $1/\mu$ at which the maximum occurs. Solid lines refer to the staggered double row and dotted lines to the symmetrical double row. Subscript M denotes maximum.

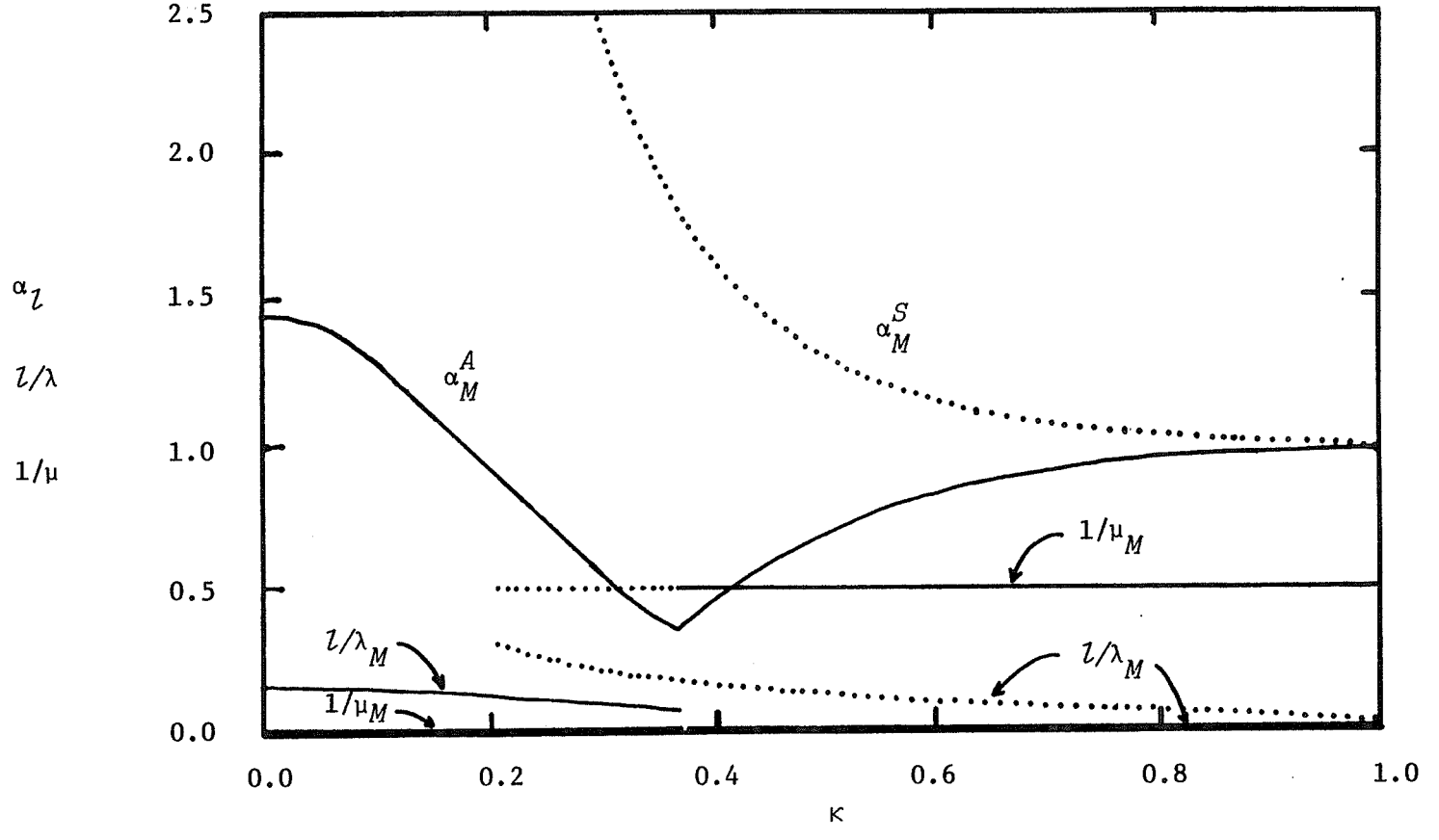

FIGURE 2.6.3 Plot of maximum α_l^A for the staggered double row and maximum α_l^S for the symmetrical double row versus κ for $a/l = 10^{-5}$. Maximum is over long axial wavelength region only. Also plotted are the values of l/λ and $1/\mu$ at which the maximum occurs. Solid lines refer to the staggered double row and dotted lines to the symmetrical double row. Subscript M denotes maximum.

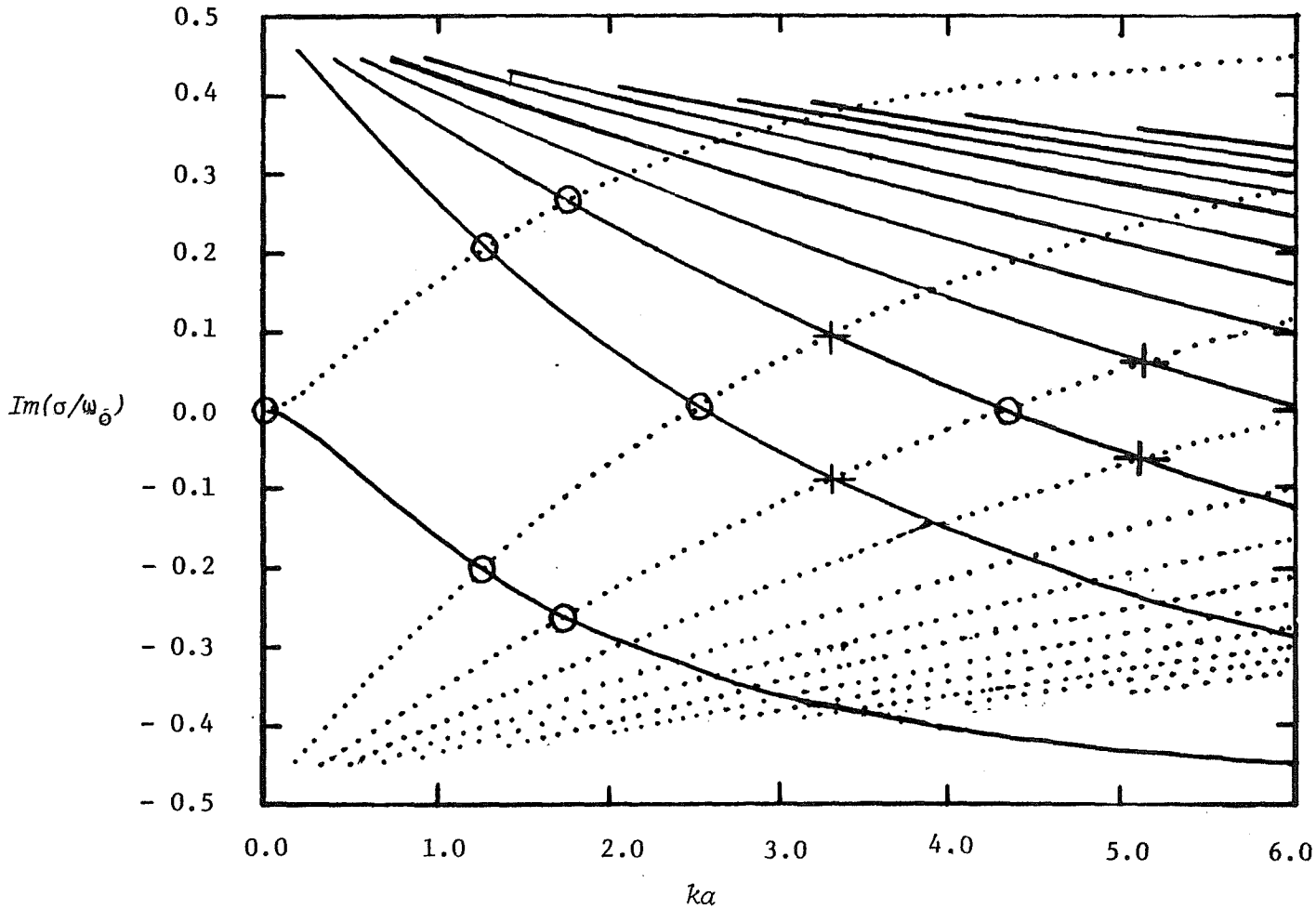

FIGURE 3.3.1 Roots of the dispersion relation for angular mode number $m = +1$ (dotted line) and $m = -1$ (solid line) for uniform circular vortex. Circles indicate unstable crossing points and crosses stable crossing points in weak strain. (After Tsai & Widnall (1976)).

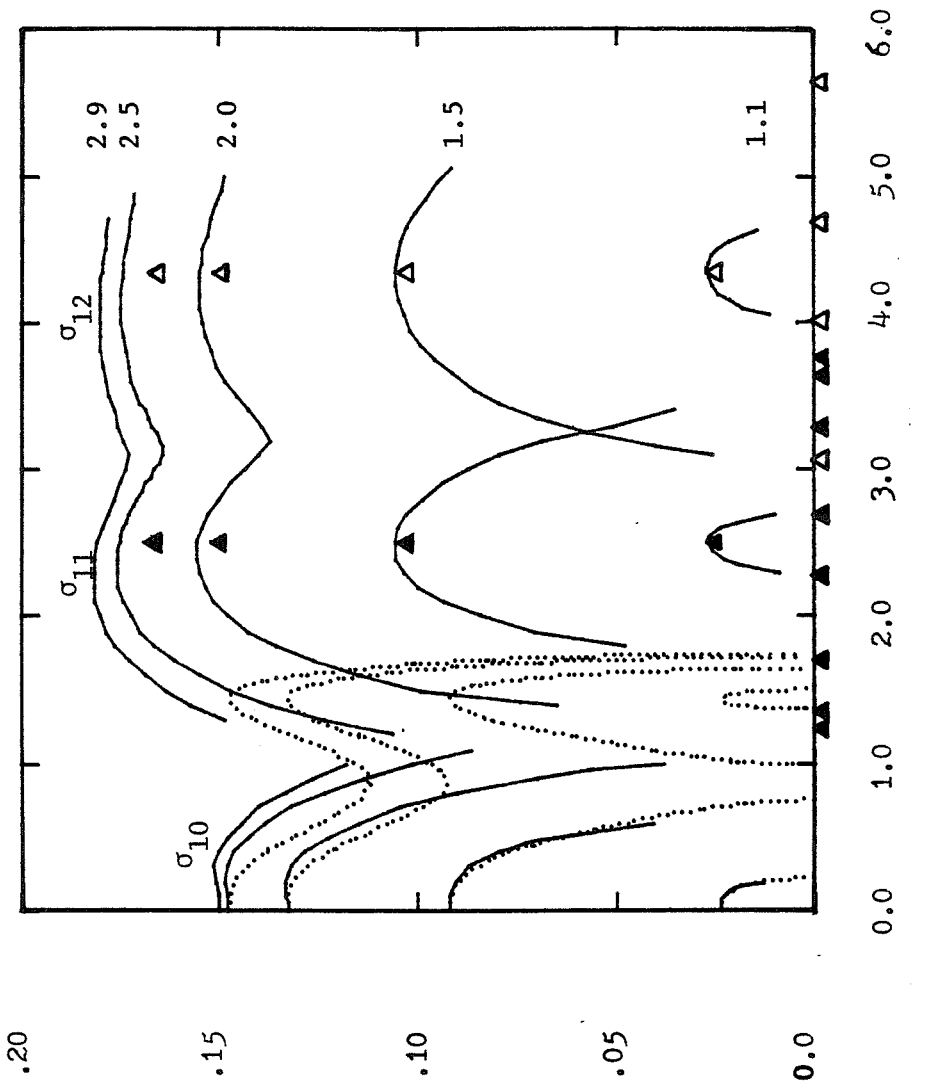

FIGURE 3.7.1 Values of σ_{10}, σ_{11} and σ_{12} versus axial wavenumber k for θ = 2.9, 2.5, 2.0, 1.5, and 1.1. Solid (open) triangles give predictions of Tsai & Widnall (1976) for magnitude and width of instability about $k\sqrt{ab} = 2.5$ (4.35). Vertex of each triangle is plotting point.

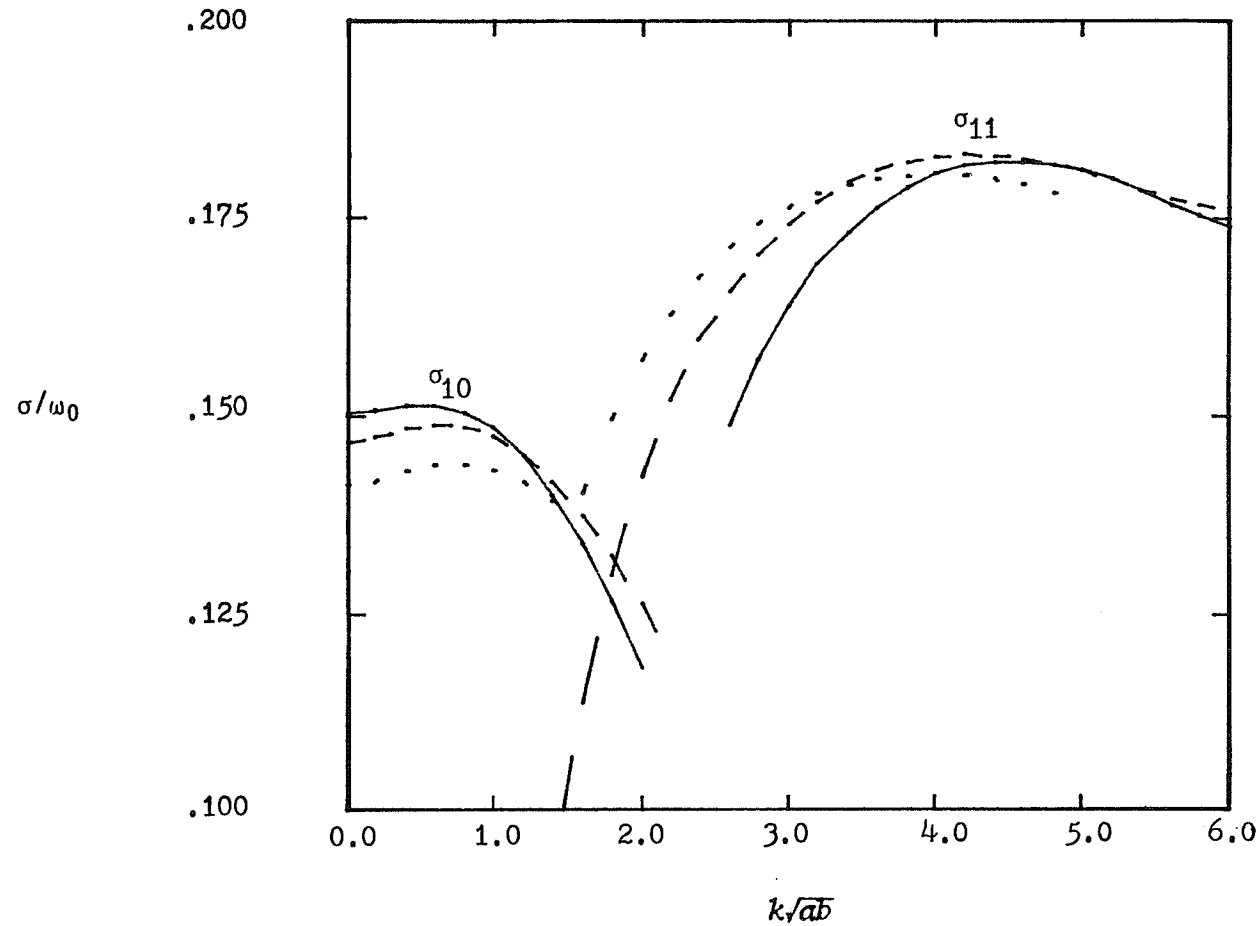

FIGURE 3.7.2 Values of σ_{10} and σ_{11} for $\theta \geq \theta_{cr}$ versus axial wavenumber k for $\theta = 2.9$ (solid) $\theta = 3.5$ (dashed) and $\theta = 4.0$ (dotted).

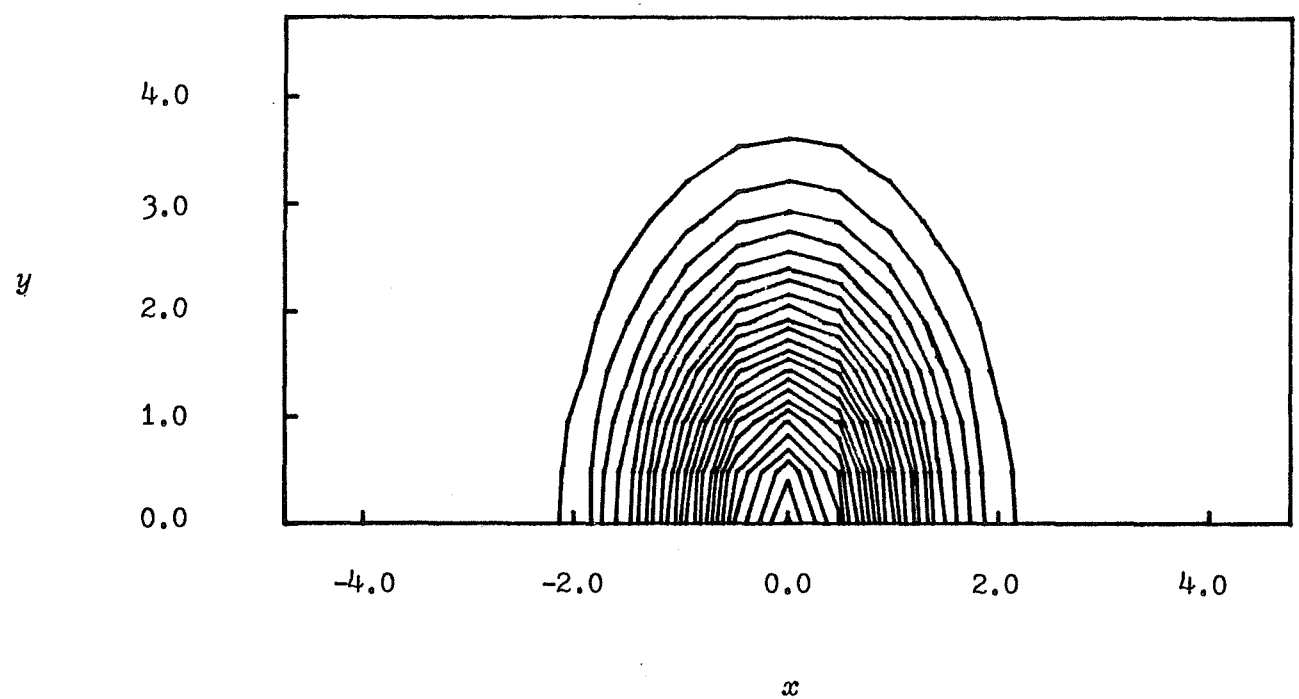

FIGURE 4.3.1 Contour plot of axial vorticity ω for $y \geq 0$ with $\varepsilon = 0.5$ and $R = 0.0$ for $M = N = 10$. Linear interpolation in contour routine shows collocation points. Plotting region is computational region. Maximum $\omega = 0.87$.

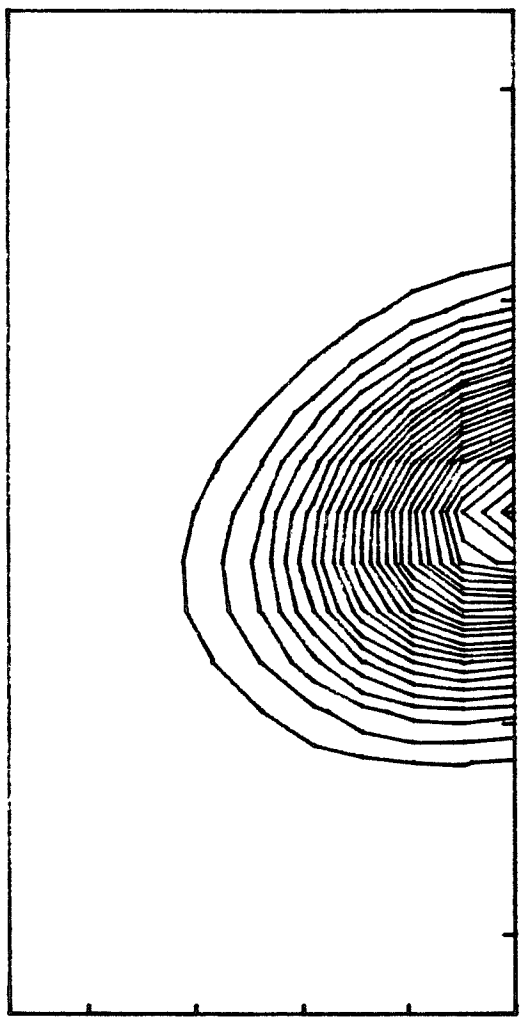

FIGURE 4.3.2 Contour plot of axial vorticity ω for $y \geq 0$ with $\varepsilon = 0.5$ and $R = 10.0$ for $M = N = 10$. Linear interpolation in contour routine shows collocation points. Plotting region is computational region. Maximum $\omega = 0.95$.

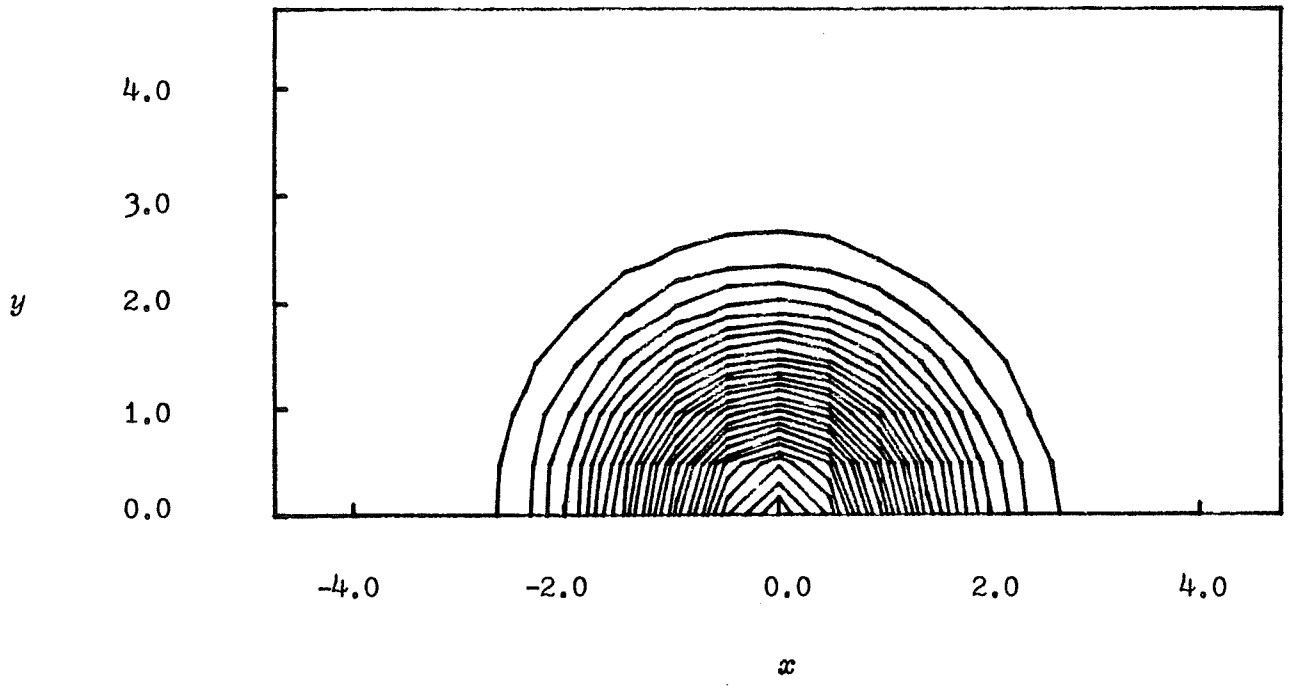

FIGURE 4.3.3 Contour plot of axial vorticity $\hat{\omega}$ for $k \geq 0$ with $\varepsilon = 0.5$ and $R = 100.0$ for $M = N = 10$. Linear interpolation in contour routine shows collocation points. Plotting region is computational region. Maximum $\omega = 1.00$.

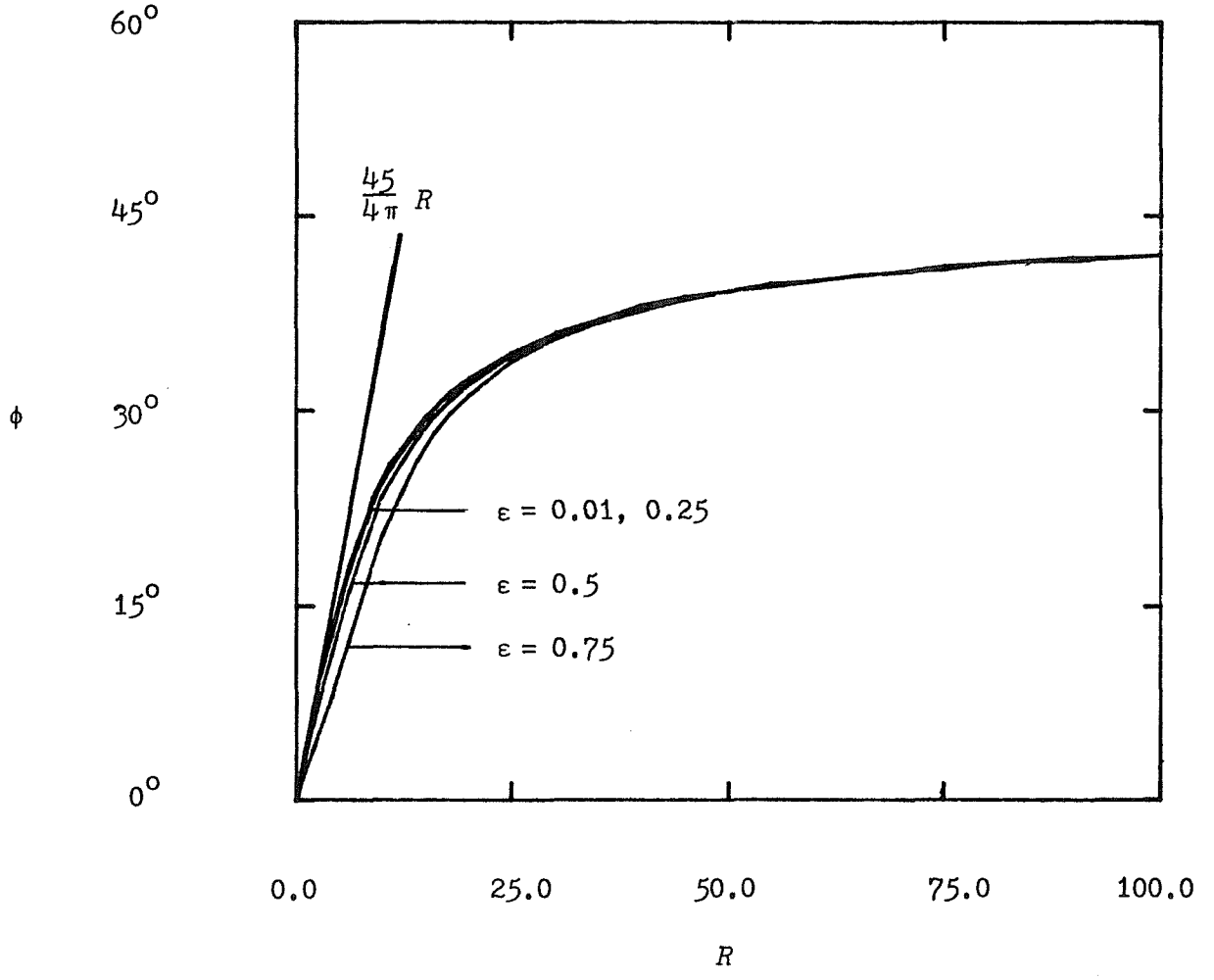

FIGURE 4.3.4 Rotation angle ϕ of coordinate axes needed so that $\sigma_{x'y'} = 0$ versus R for $\varepsilon = 0.01$, 0.25, 0.5 and 0.75. Also shown is the analytical result for $\varepsilon, R << 1$.

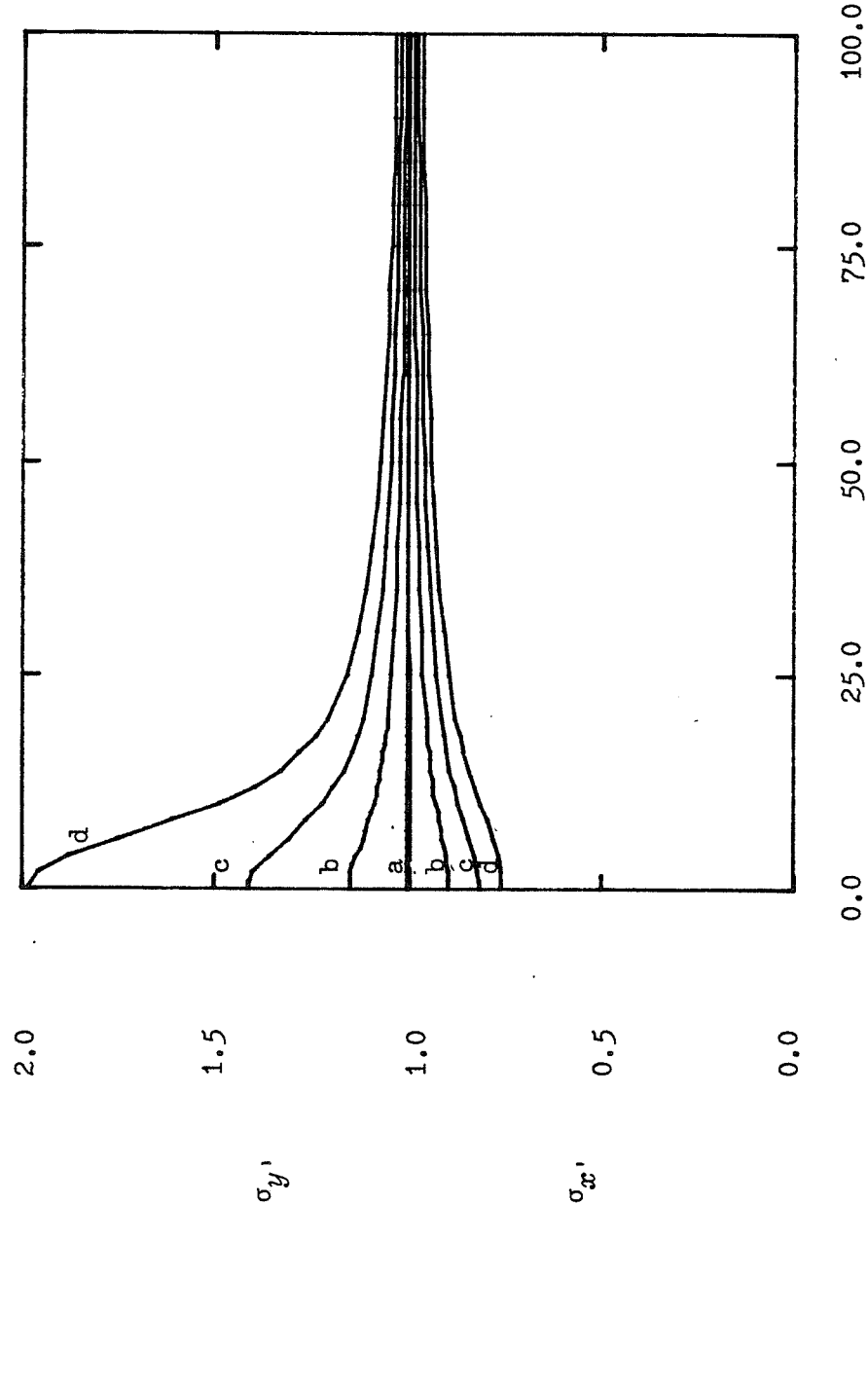

FIGURE 4.3.5 Values of $\sigma_{y'}$ (≥ 1.0) and $\sigma_{x'}$ (≤ 1.0) for ε = 0.01(a), 0.25(b), 0.5(c) and 0.75(d).

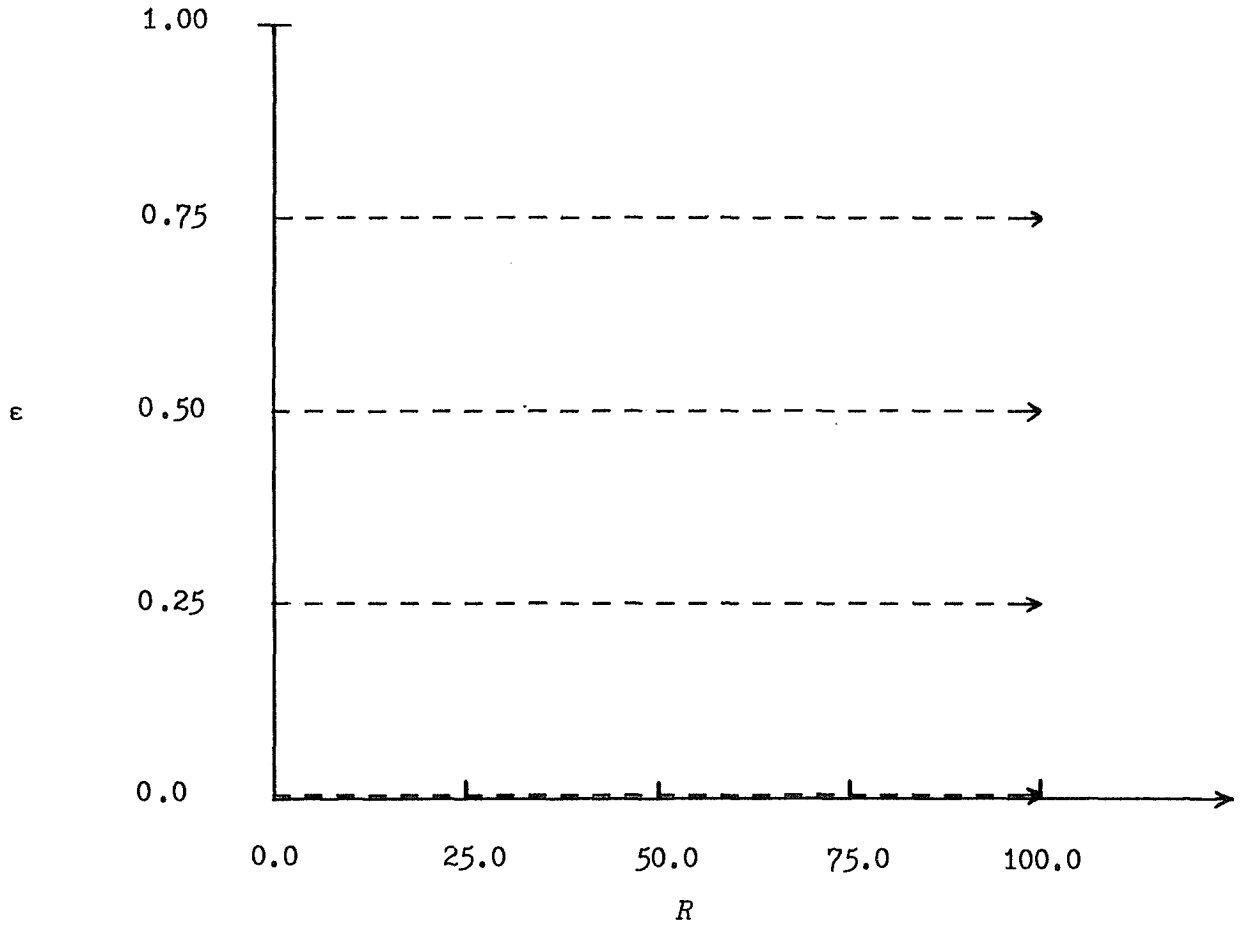

FIGURE 4.3.6 Euler-Newton continuation curves (dashed lines) in ε-R plane for non-symmetric Burgers' vortices.

n	k	μ_0	$-i\mu_1$	$\mu_2 \times 10^2$
1	0	1	0.000	0.000
1	1	3	0.125	0.144
1	2	5	0.125	0.101
1	3	7	0.117	0.054
2	0	2	0.250	0.279
2	1	4	0.250	0.428
2	2	6	0.234	0.264
3	0	3	0.375	0.851
3	1	5	0.344	0.647
4	0	4	0.438	1.303
5	0	5	0.469	1.526

TABLE 4.2.1 Values of eigenvalues $\mu(n,k) = \mu_0 + R\mu_1 + R^2\mu_2$ for $R \ll 1$ for normal modes with angular dependence n and k radial nodes.

m \ n	0	1	2	3	4	5
0	0.00000	0.00000	0.00000	0.00000	0.00000	0.00000
1	0.71401	0.28599	0.09220	0.05378	0.02724	0.02064
2	0.12652	0.18439	0.12652	0.07617	0.05040	0.03423
3	0.24939	0.16134	0.11426	0.08394	0.05966	0.04434
4	0.06275	0.10894	0.10081	0.07955	0.06275	0.04862
5	0.14987	0.10320	0.08557	0.07389	0.06077	0.05013

TABLE 4.3.1 Values of the weights $I_{m,n}$ used to compute the induced velocity at collocation points using a sinc function expansion of the vorticity.

Corrections to Thesis

Existence and Stability of Vortices and Vortex Arrays

by A. C. Robinson September 1983

p. 27 - line 18 - Replace V_η by U_η

p. 28 - (3.3.1) - Should read $\frac{\sigma^2}{{\omega_0}^2} = -\frac{1}{4}\left\{\left(\frac{2m\theta}{\theta^2+1} - 1\right)^2 - \left(\frac{\theta-1}{\theta+1}\right)^{2m}\right\}$

p. 34 - (3.5.7-3.5.8) - Replace h^2F by $\omega_0 h^2 F$

p. 45 - (4.2.6) - Replace $1 - e^{-\alpha t}$ by $1 - e^{-2\alpha t}$

p. 47 - (4.2.15) - Second equation should read $M\psi_2 = \omega_2$

p. 48 - (4.2.19) - Replace $N(k,l)$ by $N(n,l)$ in first two equations.

p. 48 - (4.2.19) - $\mu_1(n,k) = \frac{in}{N(n,k)}[F(n,k,k) + \frac{1}{2}G(n,k,k)]$

p. 48 - (4.2.23) - Replace $N(k,l)$ by $N(n,l)$

p. 51 - (4.3.7) - Replace $\nabla^2\psi = 0$ by $\nabla^2\psi = \omega$

p. 52 - (4.3.10) - ω_{00} should be ω^{00}

p. 58 - (4.3.36) - Switch x and y; replace 16 by 8

p. 59 - (4.3.37) - Switch x and y

p. 62 - [22] - Should read ... HOLMES, P. 1981 ...